UNIVERSIDADE FEDERAL DE PERNAMBUCO
CENTRO DE CIÊNCIAS EXATAS E DA NATUREZA
PROGRAMA DE PÓS-GRADUAÇÃO EM FÍSICA

Juan Carlos Chaves Capella

MODELLING OF QUANTUM MEMORIES BASED ON ATOMIC EXTERNAL DEGREES OF FREEDOM

Recife

2023

Juan Carlos Chaves Capella

MODELLING OF QUANTUM MEMORIES BASED ON ATOMIC EXTERNAL DEGREES OF FREEDOM

Tese apresentada ao Programa de Pós-Graduação em Física da Universidade Federal de Pernambuco, como requisito parcial para obtenção do título de Doutor em Física.

Área de concentração: Óptica

Orientador: Daniel Felinto Pires Barbosa

Co-orientadora: Nadja Kolb Bernardes

Recife

2023

Catalogação na fonte
Bibliotecária Nataly Soares Leite Moro, CRB4-1722

C512m Chaves Capella, Juan Carlos
Modelling of quantum memories based on atomic external degrees of freedom / Juan Carlos Chaves Capella. – 2023.
95 f.: il., fig.

Orientador: Daniel Felinto Pires Barbosa.
Tese (Doutorado) – Universidade Federal de Pernambuco. CCEN, Física, Recife, 2023.
Inclui referências e apêndice.

1. Óptica. 2. Óptica quântica. 3. Informação quântica. 4. Física atômica. 5. Imageamento quântico. I. Barbosa, Daniel Felinto Pires (orientador). II. Título.

535.2 CDD (23. ed.) UFPE- CCEN 2023 - 104

JUAN CARLOS CHAVES CAPELLA

MODELLING OF QUANTUM MEMORIES BASED ON ATOMIC EXTERNAL DEGREES OF FREEDOM

Tese apresentada ao Programa de Pós-Graduação em Física da Universidade Federal de Pernambuco, como requisito parcial para a obtenção do título de Doutor em Física.

Aprovada em: 30/06/2023.

BANCA EXAMINADORA

_____
Prof. Dr. Daniel Felinto Pires Barbosa
Orientador
Universidade Federal de Pernambuco

_____
Profa. Dra. Sandra Sampaio Vianna
Examinadora Interna
Universidade Federal de Pernambuco

_____
Prof. Dr. Fernando Roberto de Luna Parisio Filho
Examinador Interno
Universidade Federal de Pernambuco

_____
Prof. Dr. Bertúlio de Lima Bernardo
Examinador Externo
Universidade Federal da Paraíba

_____
Prof. Dr. Sebastião José Nascimento de Pádua
Examinador Externo
Universidade Federal de Minas Gerais

To nature and its weirdness.

AGRADECIMENTOS

Minha trajetória restringe meus primeiros agradecimentos bastante. De fato, não poderia deixar de primeiramente agradecer à minha namorada Lara, fundamental em todo momento do meu doutorado e para cada decisão tomada. Obrigado por me lembrar quem eu sou e me deixar confortável quando só consigo ser eu mesmo. Ainda não inventaram palavras para eu poder descrever meu amor por você, mas felizmente temos a vida toda para eu descobrir algumas. No mais, aproveito este espaço para relatar meus agradecimentos.

Ao meu orientador Daniel Felinto por ter me acolhido num grupo de pesquisa tão diferente do meu background profissional. Só tenho a agradecer sua postura destemida em me aceitar como aluno e sua orientação no sentido mais correto e abrangente da palavra.

À minha co-orientadora Nadja Bernardes que pôde me ensinar e me ajudar tanto em tão pouco tempo.

À minha família, que me apoiou desde sempre, apesar de até hoje não ter ideia em que consiste meu trabalho.

Aos inúmeros amigos e amigas, conhecidos e conhecidas que fiz ao longo de tanto tempo. Esse tempo todo vocês puderam me ensinar muito mais que física. Mantenho esse agradecimento impessoal, mas espero ter sempre deixado a relevância de cada um para mim evidente.

Agradeço também aos professores e professoras, funcionários e funcionárias do Departamento de Física da UFPE, tão fundamentais para minha formação e para o decorrer tranquilo do meu aprendizado.

Por fim, agradeço ao CNPq pelo apoio financeiro e ao povo brasileiro que custeia ciência básica no Brasil com confiança que este investimento retornará.

ABSTRACT

In this work, we present some fundamental tools in the modelling of quantum networks. We intend to develop theoretical tools such as the usage of the mixed variables density matrix formalism to model from first principles atomic experiments where external degrees of freedom play an important role, and entanglement quantification in atom-photon systems where entanglement is present in the continuous variables of the system. Namely, we first perform a detailed theoretical and experimental investigation of an atomic memory based on recoil-induced resonance in cold cesium atoms. We consider the interaction of a nearly degenerated pump and probe beams with an ensemble of two-level atoms. A full theoretical density matrix calculation in the extended Hilbert space of the internal and external atomic degrees of freedom allows us to obtain, from first principles, the transient and stationary responses determining the probe transmission and the forward four-wave mixing spectra. These two signals are generated together at the same order of perturbation with respect to the intensities of pump and probe beams. Moreover, we have investigated the storage of optical information on the spatial modes of light beams in the atomic external degrees of freedom, which provided a simple interpretation for the previously-reported non-volatile character of this memory. The retrieved signals after storage reveal the equivalent role of probe transmission and four-wave mixing, as the two signals have similar amplitudes. Probe transmission and forward four-wave-mixing spectra were then experimentally measured for both continuous excitation and after storage. The experimental observations are in good agreement with the developed theory and open a new pathway for the reversible exchange of optical information with atomic systems. Next, we review the Weisskopf-Wigner formalism for spontaneous emission considering the spatial modes of light as well as external atomic degrees of freedom which we introduce in the theory by modelling the atom as a wavepacket in momentum space with a given initial uncertainty, and perform a purity calculation in order to quantify the entanglement encoded in the momentum variables of the atom-photon system. Our purity calculations reveal two high entanglement regimes depending on the initial atomic momentum uncertainty: the Recoil entanglement regime (which arises in the small momentum uncertainty region), where recoil effects dominate the mechanisms that originate entanglement and the Doppler entanglement regime (in the large momentum uncertainty region) where homogeneous Doppler shifts in the emitted photon's frequency play the fundamental part in the build up of quantum correlations

in the system. Simplified expressions for the system's wavefunction are found for each of the entanglement regimes and physical considerations are made to explain their nature. Finally, we briefly investigate the role of entanglement in the distinguishability of two physically different quantum states that arise naturally from the theory, where we note that entanglement in the system leads to a better resolution of the two quantum states.

Keywords: quantum optics; quantum information; atomic physics; first-principles modelling; quantum imaging.

RESUMO

Neste trabalho, apresentamos algumas ferramentas fundamentais na modelagem de redes quânticas. Pretendemos desenvolver ferramentas teóricas como o uso do formalismo da matriz de densidade de variáveis mistas para modelar a partir de primeiros princípios experimentos atômicos onde os graus de liberdade externos desempenham um papel importante, e a quantificação do emaranhamento em sistemas átomo-fóton onde o emaranhamento está presente nas variáveis contínuas do sistema. Dessa forma, primeiro realizamos uma investigação teórica e experimental detalhada de uma memória atômica baseada na ressonância induzida por recuo em átomos de césio frios. Consideramos a interação de um feixe de bombeio e um feixe de prova quase degenerados com um conjunto de átomos de dois níveis. Um cálculo teórico da matriz de densidade completa no espaço de Hilbert estendido dos graus de liberdade atômicos internos e externos nos permite obter, a partir de primeiros princípios, as respostas transientes e estacionárias que determinam a transmissão do prova e os espectros de mistura de quatro ondas para frente. Esses dois sinais são gerados juntos na mesma ordem de perturbação em relação às intensidades dos feixes de bombeio e de prova. Além disso, investigamos o armazenamento de informações ópticas sobre os modos espaciais dos feixes de luz nos graus de liberdade externos atômicos, o que forneceu uma interpretação simples para o caráter não volátil relatado anteriormente dessa memória. Os sinais recuperados após o armazenamento revelam o papel equivalente da transmissão do prova e da mistura de quatro ondas, pois os dois sinais têm amplitudes semelhantes. A transmissão do prova e os espectros de mistura de quatro ondas para frente foram então medidos experimentalmente para excitação contínua e após armazenamento. As observações experimentais estão de acordo com a teoria desenvolvida e abrem um novo caminho para a troca reversível de informações ópticas com sistemas atômicos. Em seguida, revisamos o formalismo de Weisskopf-Wigner para emissão espontânea considerando os modos espaciais da luz, bem como os graus de liberdade atômicos externos, que introduzimos na teoria modelando o átomo como um pacote de onda no espaço de momento com uma dada incerteza inicial, e realizamos um cálculo de pureza para quantificar o emaranhamento codificado nas variáveis de momento do sistema átomo-fóton. Nossos cálculos de pureza revelam dois regimes de alto emaranhamento dependendo da incerteza inicial do momento atômico: o regime de emaranhamento de Recuo (que surge na região de pequena incerteza em momento), onde os efeitos de recuo dominam os mecanismos que origi-

nam o emaranhamento e o regime de emaranhamento Doppler (na região de grande incerteza em momento) onde os deslocamentos Doppler homogêneos na frequência do fóton emitido desempenham o papel fundamental na construção de correlações quânticas no sistema. Expressões simplificadas para a função de onda do sistema são encontradas para cada um dos regimes de emaranhamento e considerações físicas são feitas para explicar sua natureza. Finalmente, investigamos brevemente o papel do emaranhamento na distinguibilidade de dois estados quânticos fisicamente diferentes que surgem naturalmente da teoria, onde notamos que o emaranhamento no sistema leva a uma melhor resolução dos dois estados quânticos.

Palavras-chave: óptica quântica; informação quântica; física atômica; modelagem de primeiros princípios; imageamento quântico.

LIST OF FIGURES

CONTENTS

1 INTRODUCTION

Recent developments in quantum information science (STORZ et al., 2023; SHEN et al., 2023; MA et al., 2022; ZAPATERO et al., 2023; LAGO-RIVERA et al., 2023; MOREAU et al., 2019; HE et al., 2023; ESGUERRA et al., 2023; BJERRUM et al., 2023) have deepened the understanding that quantum computation or quantum communication presents clear potential superiority when compared to its classical counterparts. Namely, we can appreciate the vast impact of quantum information in a variety of applications ranging from quantum computation to quantum cryptography and from quantum teleportation (a quantum phenomenon with no classical counterpart) to quantum metrology (CARIOLARO, 2015).

One of the first signs that quantum computation could be superior to classical computation came with the proposal of Shor's algorithm in 1994 (SHOR, 1994), where the factorization of numbers into its prime factors could be performed by a quantum algorithm orders of magnitude faster than any known classical algorithm. Due to the fact that modern (classical) cryptography relies almost entirely on the fact that classical computers cannot perform such factorizations fast enough, it appears as though Shor's algorithm created a problem rather than a solution by (in principle) completely breaking any cryptographic key (based on the factorization problem) fast enough such that any eavesdropper could gain access to the transmitted information without being detected. However, if instead of using classical channels of communication we use quantum channels to transmit quantum information, Shor's algorithm does not pose a problem due to Quantum Key Distribution (QKD) protocols such as the BB84 (BENNETT; BRASSARD, 1984) and the Ekert91 protocol (EKERT, 1991). These protocols provide a way of transmitting cryptographic keys, and thus maintaining secure communication, via quantum channels where security is assured from a quantum principles standpoint, that is, quantum communication is as secure as quantum principles are valid physical principles.

The security shown by QKD protocols and the computational advantages presented by quantum computers lead to the envision of a *quantum network*: quantum processing nodes for the processing and storage of quantum information connected by quantum channels reliant on QKD protocols to obtain secure transmission of quantum information. Moreover, one can actually envisage the interconnection between local quantum networks, leading to a *quantum internet* (KIMBLE, 2008).

Secure transmission of quantum information does not come without any caveats. In fact,

due to the no-cloning theorem (PARK, 1970; WOOTTERS; ZUREK, 1982; DIEKS, 1982; GHIRARDI, 2013), quantum information cannot be amplified (in contrast with classical information) in order to transmit information across long distances over lossy channels, relying on *quantum repeaters* to perform such task (TAKEOKA; GUHA; WILDE, 2014; PIRANDOLA et al., 2017). In the context of quantum repeaters, atom-photon systems appear as a feasible alternative (DUAN et al., 2001; CHEN et al., 2007; SANTRA et al., 2019; WANG et al., 2021b; DHARA et al., 2022). A particularly inspiring proposal is the so-called DLCZ protocol (DUAN et al., 2001), which provides a quantum repeater protocol based on an experimentally achievable infrastructure.

Quantum repeaters and quantum processing nodes are often accompanied by *quantum memories*, that store information (usually in the form of *qubits*) for later stages of entanglement purification processes, for example, in the case of repeaters, and other computing tasks. Note that long periods of storage are necessary such that a quantum repeater finishes its entanglement purification processes or a quantum processor finishes the current processing of information before losing the information stored in the memory.

Atom-photon quantum networks are actually one of the leading approaches for scalable quantum computing (MONROE; KIM, 2013; MONROE et al., 2014; BROWN; KIM; MONROE, 2016; DEBNATH et al., 2016), combining qubit memories that can be identically replicated and remotely entangled via photonic channels (CIRAC et al., 1997; OLMSCHENK et al., 2009; MAUNZ et al., 2009; BOCK et al., 2018; KRUTYANSKIY et al., 2019; LEENT et al., 2020; STEPHENSON et al., 2020; LEENT et al., 2022), and mainly constrained by the long-lived atomic coherence times (WANG et al., 2021a). Entanglement between atoms and photons is therefore a crucial piece for quantum communication and thus have been the object of several theoretical (RZAZEWSKI; ZAKOWICZ, 1992; CHAN; LAW; EBERLY, 2002; CHAN; LAW; EBERLY, 2003; FEDOROV et al., 2005; SHI; CONG; ECKLE, 2022) and experimental investigations (PFAU et al., 1994; KURTSIEFER et al., 1997; BLINOV et al., 2004; VOLZ et al., 2006; ROSENFELD et al., 2008; CROCKER et al., 2019).

As one may already have noticed, quantum networks need a plethora of (mostly quantum) ingredients in order to work: quantum channels of communication, long-lived quantum memories, quantum processing nodes, quantum repeaters, authenticated classical channels of communication in order to perform QKD protocols, and so on. Moreover, such ingredients come in all flavors: fiber-based photonic channels of communication, free-space photonic quantum channels, quantum memories based on neutral atoms using internal or external atomic degrees of freedom, superconducting quantum computing, trapped ions quantum computing, etc.

Due to its complexity, then, research in quantum networks is often broken into smaller pieces, branching out in different directions where each branch furthers the development of one of the main ingredients of a quantum network. Our research group embarked on the pursuit of improvements in quantum memories, quantum repeaters and distribution of entanglement over a network. In relation to the present work, a step in the direction of better quantum memories was provided by the use of the so-called Recoil-Induced Resonance (RIR) phenomenon to obtain an atomic memory based on atomic external degrees of freedom (CAPELLA et al., 2022).

Similarly as light energy and momentum can be transferred to atoms altering their state of motion, the inverse process where the atomic kinetic energy and momentum are transferred to the light field can modify the light field state as well. This last process leads to the observation of various phenomena associated with laser cooled atoms as for instance the aforementioned RIR phenomenon, where the exchange of energy and momentum between two light beams is mediated by the atomic external degrees of freedom. This phenomenon was firstly predicted theoretically by Guo et al (GUO et al., 1992; GUO; BERMAN, 1993) and soon after observed experimentally (COURTOIS et al., 1994). Since then, the RIR phenomenon received considerable attention, and a number of applications associated with it has been demonstrated (TOMASZ et al., 2006). For instance, RIR was used for temperature diagnostic of cold atomic ensembles in free atoms both at stationary (MEACHER et al., 1994; FISCHER et al., 2001) and transient (GUIBAL et al., 1996) domains, and in atoms confined in optical lattices (BRZOZOWSKA et al., 2006). More recent applications of RIR for atomic thermometry can be found in Refs. (YANTING et al., 2015; WANG; DENG; WANG, 2015). The phenomenon was also used for optical switching (GORDON et al., 2010) and to probe the transient dynamic of atoms in 1D optical lattices (KOZUMA et al., 1995).

The RIR phenomenon was also employed to observe very high optical gain in an anisotropic medium (VENGALATTORE; PRENTISS, 2005) and as basis of a new type of laser, the collective atomic recoil laser (CARL), which was firstly proposed theoretically in (BONIFACIO; DESALVO, 1994) and experimentally demonstrated in (KRUSE et al., 2003). More recently, using a four-wave mixing (FWM) configuration in a degenerate two-level system of cold cesium atoms, where Zeeman coherence as well as coherence between momentum states via RIR can be excited, Lopez *et. al.* has observed a giant optical gain and self-oscillation (LOPEZ et al., 2019) through coupled cascading parametric backward- and forward-FWM (FFWM).

In the desired context of quantum memories improvements, it has been recently demonstrated the storage of information on the spatial modes of light based on the external atomic

degrees of freedom, both using the non-localized degrees of freedom associated with the RIR phenomenon (ALMEIDA et al., 2016), as well as the quantized energy levels of atoms localized in a 1D optical lattice (LOPEZ et al., 2017). This new type of memory using the atomic external degrees of freedom is particularly attractive since it is less sensitive to external magnetic and electric fields. Indeed, differently from the memories based on ground state coherences associated with the Zeeman sub levels, Almeida *et. al.* demonstrated its non volatility and robustness to the reading process, which does not destroy the stored information, so its storage time is mainly determined by the atomic motion only (ALMEIDA et al., 2016). Moreover, using the gain mechanism described in (LOPEZ et al., 2019), Lopez *et. al.* also demonstrated the operation of an atomic memory that can amplify the stored signal during the reading process (LOPEZ; MELO; TABOSA, 2020). Finally, Capella *et. al.* proposed a non-volatile atomic memory based on the RIR phenomenon exploiting the atomic external degrees of freedom in order to obtain information storage that can be retrieved through multiple modes of scattered light (CAPELLA et al., 2022), expanding the results found by (ALMEIDA et al., 2016).

On a different but completely related branch, we can also further develop the distribution of entanglement over a quantum network. Moreover, entanglement can be thought of as a *resource* for the protocols we mentioned and, therefore, quantum systems for which we can quantify, harvest, and control entanglement are desirable for implementations of quantum networks. One of the simplest systems that naturally presents entanglement in an experimentally achievable manner is an atom (previously excited) and its spontaneously emitted photon.

The problem of spontaneous emission and its associated natural linewidth was first investigated by A. Einstein in 1917 (EINSTEIN, 1917) making extensive use of rate equations. In 1927, P. A. M. Dirac presented a theory using Quantum Electrodynamics (QED) where an expression for the so-called Einstein A coefficient (related to the spontaneous emission rate) was proposed, but the calculations turned out to be very difficult (DIRAC, 1927). In 1930, however, V. Weisskopf and E. Wigner proposed a simplified version of Dirac's theory and found a work around that diminished the complexity of Dirac's expression for the calculation of natural linewidths (WEISSKOPF; WIGNER, 1930). The Weisskopf-Wigner theory for spontaneous emission then eliminated the need to introduce phenomenologically any parameters and elucidated a profound trait of the phenomenon: spontaneous emission is *not* spontaneous in the sense that no mechanism causes it, it is actually *induced* by the electromagnetic field's vacuum, being called spontaneous only due to the fact that the scientific community at the time it was named did not know of the existence of such vacuum-induced processes.

Important steps towards the control of the spontaneous emission phenomenon in various setups have already been given, ranging from the inhibition of spontaneous emission (KLEPPNER, 1981; GABRIELSE; DEHMELT, 1985) to phase and amplitude control of spontaneously emitted photons (PASPALAKIS; KNIGHT, 1998; GHAFOOR; ZHU; ZUBAIRY, 2000). Theoretical investigations also provided further understanding of spontaneous emission in different physical realizations (RZAZEWSKI; ZAKOWICZ, 1992; BONIFACIO; PREPARATA, 1970; AGARWAL, 1971; STOOP; żEWSKI, 1995; HORAK; GHERI, 1996; GUO, 2008), leading finally to the theoretical entanglement considerations (CHAN; LAW; EBERLY, 2002; CHAN; LAW; EBERLY, 2003; FEDOROV et al., 2005) we aim to extend in this thesis.

Therefore, we understand that the process of spontaneous emission is of fundamental importance in the development of the ingredients necessary to a quantum network in the sense that it provides a controllable, deeply understood source of entanglement. Although the entanglement itself does not have a clear full picture, we intend to provide some insights about the matter. Note that entanglement is a fundamental piece in any quantum processing, and therefore, the developments we intend to provide in this thesis are not only useful, but crucial to the understanding and modelling of different types of quantum networks.

In connection to the above problem, we intend to explore in this thesis theoretical tools needed for the modelling of quantum memories based on continuous variables, which provides another way of storing information in a continuous variable quantum network (NUNN et al., 2008; HOSSEINI et al., 2009; LVOVSKY; SANDERS; TITTEL, 2009; HAMMERER; SØRENSEN; POLZIK, 2010; JENSEN et al., 2011). Several results on quantum teleportation (FURUSAWA et al., 1998; SHERSON et al., 2006), Quantum Key Distribution (GROSSHANS et al., 2003), and hybrid continuous/discrete variables quantum operations (OURJOUMTSEV et al., 2007; DONG et al., 2008; TAKAHASHI et al., 2010) support the idea of a quantum network based on continuous variables as a viable option.

More precisely, we aim to provide a full first-principles theoretical model to the RIR based atomic memory described in (ALMEIDA et al., 2016; CAPELLA et al., 2022) as well as the experimental data corroborating it, and explore/quantify the entanglement encoded in the continuous variables of an atom-photon system after spontaneous decay, following the theoretical formalism developed in (WEISSKOPF; WIGNER, 1930; RZAZEWSKI; ZAKOWICZ, 1992). In order to achieve this goal, the thesis is organized as follows: on Chapter 2, we review the tools we will need in order to obtain the theoretical models we use/develop. Specifically, we review the quantum mechanics of continuous variables systems as well as the quantification of entan-

glement in discrete/continuous variables of pure bipartite systems. On Chapter 3, we develop a first-principles model for an atomic memory based on the RIR phenomenon and compare it with experimental data, where we obtain good agreement between theory and experiment. The results of this chapter were already published in (CAPELLA et al., 2022). On Chapter 4, we investigate and quantify the entanglement encoded in the momentum variables of an atom-photon system after spontaneous decay, where we reveal high entanglement regimes when we vary the atom's initial uncertainty in momentum. We also provide physically motivated discussions about the nature of such high entanglement regimes, as well as some implications of the entanglement in the distinguishability of quantum states that arise naturally from the theory. Finally, on Chapter 5, we provide the reader with a summary of the main results found as well as perspectives for future works motivated by this thesis.

2 FUNDAMENTAL CONCEPTS

In this chapter we intend to provide the reader with some fundamental concepts necessary for the understanding of this thesis. We begin with a review of quantum mechanics in the position and momentum representations. We focus on the construction of the Hilbert space associated with a continuous spectrum, the duality of the position and momentum representations, the interpretation of momentum as a generator of translation, and, finally, we discuss the corresponding wave packets. Next, we delve into the density matrix formalism for discrete, continuous and mixed systems, and focus on the time evolution of the density operator. We also define bipartite entanglement and discuss entanglement quantifiers for pure bipartite systems described by discrete and continuous Hilbert spaces.

2.1 QUANTUM MECHANICS IN THE POSITION AND MOMENTUM REPRESENTATIONS

Quantum mechanics is often associated with systems with discrete observables. As an example, we usually say that the internal energy levels on an atom are *quantized*. However, quantum mechanics is not at all limited by a discrete characteristic and, in fact, is enriched by the introduction of continuous-valued observables. Paradigmatic examples of continuous-valued observables are the x position of a particle on an axis or its corresponding linear momentum. While the 1D aspects of these examples are enough to provide an infinite dimensional Hilbert space, characteristic of a continuous-variable system, often we will consider position and momentum in its full 3D picture. Note that observables with continuous spectra are still represented by Hermitian operators, but the rigorous mathematics behind them is fundamentally more complicated than for the discrete case. Here we do not aim to provide rigorous proofs and definitions, but rather intuitive notions.

2.1.1 Continuous spectra operators and the position representation

We begin our review providing a generalization of discrete-variable quantum mechanics. Briefly, we use Latin letters to identify results for discrete-variable quantum mechanics and Greek letters for continuous-variable results. We start generalizing the eigenvalue equation for

the continuous spectrum case:

$$\hat{\xi}\,|\xi'\rangle = \xi'\,|\xi'\rangle\,, \tag{2.1}$$

where $\hat{\xi}$ is an operator and ξ' is a number. When the operator nature of the observable and numerical nature of the eigenvalue are obvious, we may sometimes drop the hat for operators. All considered operators will be Hermitian unless explicitly stated or when the non-Hermitian aspect is clear. Note that for the discrete case, the eigenvalue equation looks exactly the same:

$$\hat{A}\,|a\rangle = a\,|a\rangle\,. \tag{2.2}$$

Just as in the discrete case, for continuous spectrum Hermitian operators, eigenvectors associated with different eigenvalues are orthogonal (now with respect to a Dirac-delta distribution), and form a complete orthonormal basis. This implies in the generalizations:

$$\begin{aligned} \langle a'|a''\rangle = \delta_{a'a''} \quad &\rightarrow \quad \langle \xi'|\xi''\rangle = \delta(\xi' - \xi'') \\ \sum_{a'} |a'\rangle\langle a'| = \mathbb{1} \quad &\rightarrow \quad \int \mathrm{d}\xi' |\xi'\rangle\langle\xi'| = \mathbb{1}. \end{aligned} \tag{2.3}$$

In order to connect Hermitian operators of continuous spectra with observables, we consider the problem of detecting a particle in a position $\vec{x}$ in 3D space. We postulate the completeness of the set of eigenvectors of the position operator $\hat{\mathbf{x}}$, satisfying:

$$\hat{\mathbf{x}}|\vec{x}\rangle = \vec{x}|\vec{x}\rangle, \tag{2.4}$$

where $\vec{x}$ stands for x, y, and z. Therefore, $|\vec{x}\rangle$ is a simultaneous eigenvector of the *observables* x, y, and z. Explicitly,

$$\begin{aligned} |\vec{x}\rangle \quad &\equiv \quad |x, y, z\rangle\,, \\ \hat{x}\,|\vec{x}\rangle = x\,|\vec{x}\rangle\,, \quad \hat{y}\,|\vec{x}\rangle \quad &= \quad y\,|\vec{x}\rangle\,, \quad \hat{z}\,|\vec{x}\rangle = z\,|\vec{x}\rangle\,. \end{aligned} \tag{2.5}$$

Note that the existence of such simultaneous eigenvectors implies in the following commutation relations:

$$[\hat{x}_i, \hat{x}_j] = 0, \quad i, j = 1, 2, 3, \tag{2.6}$$

where $\hat{x}_1$, $\hat{x}_2$, and $\hat{x}_3$ stand for $\hat{x}$, $\hat{y}$, and $\hat{z}$, respectively. Orthogonality and completeness of this basis can be expressed using (2.3) by:

$$\begin{aligned} \langle \vec{x}'|\vec{x}''\rangle \quad &= \quad \delta^3(\vec{x}' - \vec{x}'')\,, \\ \int \mathrm{d}^3x\ |\vec{x}\rangle\,\langle\vec{x}| \quad &= \quad \mathbb{1}. \end{aligned} \tag{2.7}$$

Provided with the position eigenbasis, we may now expand an arbitrary quantum state (which we may assume describes a particle), $|\psi\rangle$, in this basis in an analogous manner to the discrete case:

$$|\psi\rangle = \int \mathrm{d}^3x \, |\vec{x}\rangle \underbrace{\langle \vec{x}|\psi\rangle}_{\psi(\vec{x})}, \tag{2.8}$$

where $\psi(\vec{x})$ is the commonly used wave function in the position representation (or x-representation). Note that only *external* degrees of freedom can be taken into account in this basis, internal degrees of freedom, such as spin, need to be described in an additional Hilbert space. The probability of finding such particle in a given volume d^3x around the point $\vec{x}$ is then:

$$|\psi(\vec{x})|^2 \mathrm{d}^3x = |\langle \vec{x}|\psi\rangle|^2 \mathrm{d}^3x. \tag{2.9}$$

2.1.2 Translations in Hilbert space

We introduce now the concept of translation in a Hilbert space, but we start with the simpler problem of "translating a function". We get, for a small translation of $\vec{x}'$ a shifted wave function:

$$\psi'(\vec{x}) = \psi(\vec{x}+\vec{x}') = \psi(\vec{x}) + \vec{x}' \cdot \vec{\nabla}\psi(\vec{x}) + \ldots = \underbrace{\left(1 + \frac{i}{\hbar}\vec{x}' \cdot \hat{\mathbf{P}} + \ldots\right)}_{U(\vec{x}')} \psi(\vec{x}), \tag{2.10}$$

where we introduce the translation operator $U(\vec{x})$ and its *generator*, $\hat{\mathbf{P}} = -i\hbar\vec{\nabla}$, the momentum operator. We can extend (2.10) to higher powers as follows:

$$\psi'(\vec{x}) = U(\vec{x}')\psi(\vec{x}) = \left(1 + \frac{i}{\hbar}\vec{x}' \cdot \hat{\mathbf{P}} + \frac{1}{2!}\left[\frac{i}{\hbar}\vec{x}' \cdot \hat{\mathbf{P}}\right]^2 + \frac{1}{3!}\left[\frac{i}{\hbar}\vec{x}' \cdot \hat{\mathbf{P}}\right]^3 + \ldots\right)\psi(\vec{x}), \tag{2.11}$$

which leads to the conclusion that $U(\vec{x})$ can be identified with the exponential operator $\exp\left(\frac{i}{\hbar}\vec{x} \cdot \hat{\mathbf{P}}\right)$, elucidating why we call $\hat{\mathbf{P}}$ the generator of the translation operator. Turning back to the state $|\psi\rangle$, we now have the translated ket:

$$\begin{aligned} |\psi'\rangle &= \int \mathrm{d}^3x \, \psi'(\vec{x}) \, |\vec{x}\rangle \\ &= \int \mathrm{d}^3x \, \psi(\vec{x}+\vec{x}') \, |\vec{x}\rangle \\ &= \int \mathrm{d}^3x \, \psi(\vec{x}) \, |\vec{x}-\vec{x}'\rangle \\ &= U(\vec{x}') \, |\psi\rangle \, , \end{aligned} \tag{2.12}$$

where now $U(\vec{x}')$ acts on the basis vectors $|\vec{x}\rangle$. Note also that:

$$U(-\vec{x}) = \exp\Big(-\frac{i}{\hbar}\vec{x} \cdot \hat{\mathbf{P}}\Big) = U^{-1}(\vec{x}) = U^{\dagger}(\vec{x}), \tag{2.13}$$

where in the last equality we used the fact the exponential of an Hermitian operator is an unitary operator. To prove that $U^{-1}(\vec{x}) = \exp\Big(-\frac{i}{\hbar}\vec{x}\cdot\hat{\mathbf{P}}\Big)$, we can use the Baker-Campbell-Hausdorff formula (ROSSMANN, 2006):

$$e^X e^Y = e^Z, \quad Z = X + Y + \frac{1}{2}[X,Y] + \frac{1}{12}[X,[X,Y]] - \frac{1}{12}[Y,[X,Y]] + \dots, \tag{2.14}$$

and the fact that the momentum operator components commute with each other, which can be more clearly seen in its configuration space representation $\hat{\mathbf{P}} = -i\hbar\vec{\nabla}$, due to Clairaut's theorem on the commutativity of second derivatives. More explicitly, we have the following commutation relations:

$$[\hat{P}_i, \hat{P}_j] = 0, \quad i,j = 1,2,3. \tag{2.15}$$

Therefore we can now write $U^\dagger(\vec{x}')\,|\vec{x}\rangle = |\vec{x}+\vec{x}'\rangle$. Finally, we can interpret translations in a Hilbert space as active transformations, where we transform the coordinates of the state, $\psi'(\vec{x}) = \psi(\vec{x}+\vec{x}')$, or as a passive transformation, where we transform the basis of the Hilbert space $|\vec{x}\rangle \to |\vec{x}-\vec{x}'\rangle$.

The expression: $U(\vec{x}) = \exp\Big(\frac{i}{\hbar}\vec{x}\cdot\hat{\mathbf{P}}\Big)$ needs more attention. So far, the operator nature of $\hat{\mathbf{P}}$ has been made explicit, and the $\vec{x}$ present in the formula is no more than a parameter, in the position representation we have so far worked on. In the momentum representation which we discuss next, the roles are interchanged: $\vec{p}$ becomes a parameter, while $\hat{\mathbf{x}}$ is the explicitly denoted operator.

2.1.3 The momentum representation

So far, we have worked on the position eigenbasis, but the commutation relations (2.15) have a clear parallel with (2.6). This implies in an analogous construction for the Hilbert space of a particle now in terms of eigenvectors of $\hat{\mathbf{P}}$. More explicitly,

$$\begin{aligned} \hat{\mathbf{P}}\,|\vec{p}\rangle &= \vec{p}\,|\vec{p}\rangle\,, \\ \hat{P}_x\,|\vec{p}\rangle = p_x\,|\vec{p}\rangle\,, \quad \hat{P}_y\,|\vec{p}\rangle\,, &= p_y\,|\vec{p}\rangle\,, \quad \hat{P}_z\,|\vec{p}\rangle = p_z\,|\vec{p}\rangle\,. \end{aligned} \tag{2.16}$$

We may then postulate that these eigenvectors form a complete basis (this is equivalent to assuming that the position eigenvectors form a complete basis) and write a general state $|\psi\rangle$ in this basis as follows:

$$|\psi\rangle = \int \mathrm{d}^3p\ |\vec{p}\rangle\ \underbrace{\langle\vec{p}|\psi\rangle}_{\psi_p(\vec{p})}, \tag{2.17}$$

where now we have the usual wave function ψ in the momentum representation (or p-representation), which we denote by $\psi_p(\vec{p})$. We express the orthogonality and completeness of the momentum basis as:

$$\begin{aligned} \langle \vec{p}\,'|\vec{p}\,''\rangle &= \delta^3(\vec{p}\,' - \vec{p}\,'') \\ \int \mathrm{d}^3p\, |\vec{p}\rangle\, \langle \vec{p}| &= \mathbb{1}. \end{aligned} \tag{2.18}$$

Using the completeness relation for the $\vec{x}$ basis (2.7) on the orthogonality relation of (2.18), we get:

$$\langle \vec{p}\,'|\left(\int \mathrm{d}^3x\, |\vec{x}\rangle\, \langle \vec{x}| \right)|\vec{p}\,''\rangle = \int \mathrm{d}^3x\, \langle \vec{p}\,'|\vec{x}\rangle\langle \vec{x}|\vec{p}\,''\rangle = \delta^3(\vec{p}\,' - \vec{p}\,''). \tag{2.19}$$

Comparing now with the plane-wave decomposition of the Dirac delta distribution:

$$\begin{aligned} \delta^3(\vec{p}\,' - \vec{p}\,'') &= \frac{1}{(2\pi\hbar)^3} \int \mathrm{d}^3x\, e^{i(\vec{p}\,'' - \vec{p}\,')\cdot\vec{x}/\hbar} \\ &= \int \mathrm{d}^3x\, \underbrace{\frac{1}{(2\pi\hbar)^{3/2}} e^{-i\vec{p}\,'\cdot\vec{x}/\hbar}}_{\langle \vec{p}\,'|\vec{x}\rangle} \underbrace{\frac{1}{(2\pi\hbar)^{3/2}} e^{i\vec{p}\,''\cdot\vec{x}/\hbar}}_{\langle \vec{x}|\vec{p}\,''\rangle} \\ &= \int \mathrm{d}^3x\, \langle \vec{p}\,'|\vec{x}\rangle\langle \vec{x}|\vec{p}\,''\rangle. \end{aligned} \tag{2.20}$$

That is, we have found the coordinates of any element of the $\vec{x}$ basis in the $\vec{p}$ basis (or the opposite), which allows us to exchange between both basis. We write then:

$$\langle \vec{x}|\vec{p}\rangle = \frac{1}{(2\pi\hbar)^{3/2}} e^{i\vec{p}\cdot\vec{x}/\hbar}. \tag{2.21}$$

Take now a state ket described in the momentum basis, and use the completeness relation for the $\vec{x}$ basis:

$$\begin{aligned} |\psi\rangle &= \int \mathrm{d}^3p\, |\vec{p}\rangle\, \langle \vec{p}| \int \mathrm{d}^3x\, |\vec{x}\rangle\, \langle \vec{x}|\psi\rangle \\ &= \int \mathrm{d}^3p\, |\vec{p}\rangle \underbrace{\left(\int \mathrm{d}^3x\, \frac{1}{(2\pi\hbar)^{3/2}} e^{-i\vec{p}\cdot\vec{x}/\hbar} \psi(\vec{x}) \right)}_{\psi_{\vec{p}}(\vec{p})}. \end{aligned} \tag{2.22}$$

That is,

$$\psi_{\vec{p}}(\vec{p}) = \frac{1}{(2\pi\hbar)^{3/2}} \int \mathrm{d}^3x\, e^{-i\vec{p}\cdot\vec{x}/\hbar} \psi(\vec{x}), \tag{2.23}$$

or in other words, the wave function in the momentum representation is the Fourier transform of the wave function in the position representation. Therefore, we have put the position and momentum representations on equal footing.

Finally, we use the duality between position and momentum representations to write without proof the action of the operator $e^{-i\vec{p}\cdot\hat{\mathbf{x}}/\hbar}$ (note the operator nature of $\hat{\mathbf{x}}$) on a momentum eigenket:

$$e^{-i\vec{p}'\cdot\hat{\mathbf{x}}/\hbar}\,|\vec{p}\rangle = |\vec{p}+\vec{p}'\rangle\,, \tag{2.24}$$

that is, just as the momentum operator is the generator of spatial translations, the position operator is the generator of momentum translations.

2.1.4 Wave packets in momentum and position representations

We now consider the problem of an unconfined free particle, that is, a particle whose potential energy is zero (or a constant) and is not confined to any region of space. Schrödinger's equation in the position basis for this system reads:

$$i\hbar\frac{\partial}{\partial t}\psi(\vec{x},t) = -\frac{\hbar^2}{2m}\nabla^2\psi(\vec{x},t), \tag{2.25}$$

whose solutions are of the form:

$$\psi(\vec{x},t) = A\,e^{i(\vec{p}\cdot\vec{x}-Et)/\hbar}, \tag{2.26}$$

where A is a constant and $\vec{p}$ and E satisfy the well-known classical mechanical relation for the free particle:

$$E = \frac{\vec{p}^{\,2}}{2m}. \tag{2.27}$$

Note that $|\psi(\vec{x},t)|^2 = |A|^2$, which represents an uniform distribution of probability of finding the particle throughout all space. This is a symptom of the nonphysical aspect of the plane wave as a full description of a free particle. However, the superposition principle allows us to construct solutions of (2.25) as linear combinations of plane waves which can be written as:

$$\psi(\vec{x},t) = \frac{1}{(2\pi\hbar)^{3/2}}\int \tilde{\psi}(\vec{p})e^{i(\vec{p}\cdot\vec{x}-Et)/\hbar}\mathrm{d}^3p. \tag{2.28}$$

These solutions are called *three-dimensional wave packets*, and can be used to construct square-integrable wave functions, leading to a more realistic solution to the free particle problem. Usually, we may be interested in studying the *shape* of the wave packet at a fixed time, which we may take as the origin:

$$\psi(\vec{x},0) = \psi(\vec{x}) = \frac{1}{(2\pi\hbar)^{3/2}}\int \tilde{\psi}(\vec{p})e^{i(\vec{p}\cdot\vec{x})/\hbar}\mathrm{d}^3p\,. \tag{2.29}$$

Therefore, the wave function $\psi(\vec{x})$ is given by the inverse Fourier transform of $\tilde{\psi}(\vec{p})$ or, equivalently, the coordinates of the wave packet in the momentum representation:

$$|\psi\rangle = \int \mathrm{d}^3x\, \psi(\vec{x})\, |\vec{x}\rangle = \int \mathrm{d}^3p\, \tilde{\psi}(\vec{p})\, |\vec{p}\rangle\,. \tag{2.30}$$

We may investigate then the shape of the wave packet in momentum or position space. For simplicity and in order to gain some intuition, we briefly work with a 1D wave packet. Consider a wave packet in momentum space given by:

$$\tilde{\psi}(p) = e^{-\alpha(p-p_0)^2}. \tag{2.31}$$

We can evaluate the shape of the wave packet in position space via the Fourier transform:

$$\begin{aligned}
\psi(x) &= \frac{1}{(2\pi\hbar)^{1/2}} \int_{-\infty}^{\infty} dp\, \tilde{\psi}(p)\, e^{i(p-p_0)x/\hbar} e^{ip_0x/\hbar} \\
&= \frac{1}{(2\pi\hbar)^{1/2}} e^{ip_0x/\hbar} \int_{-\infty}^{\infty} dp'\, e^{ip'x/\hbar} e^{-\alpha p'^2} \quad , \quad p' = p - p_0 \\
&= \frac{1}{(2\pi\hbar)^{1/2}} e^{ip_0x/\hbar} \int_{-\infty}^{\infty} dp'\, e^{-(x^2/4\alpha\hbar)} e^{-\alpha[p'-(ix/2\alpha\hbar)]^2} \\
&= \frac{1}{(2\pi\hbar)^{1/2}} e^{ip_0x/\hbar} e^{-(x^2/4\alpha\hbar^2)} \underbrace{\int_{-\infty}^{\infty} dq\, e^{-\alpha q^2}}_{\sqrt{\frac{\pi}{\alpha}}} \quad , \quad q = p' - (ix/2\alpha\hbar).
\end{aligned} \tag{2.32}$$

Therefore, we can write:

$$\psi(x) = \frac{1}{(2\pi\hbar)^{1/2}} \sqrt{\frac{\pi}{\alpha}} e^{ip_0x/\hbar} e^{-(x^2/4\alpha\hbar^2)}, \tag{2.33}$$

and note how $e^{ip_0x/\hbar}$ represents only a global phase, since $|e^{ip_0x/\hbar}|^2 = 1$. Hence, we obtain for the position and momentum representations:

$$\begin{aligned}
|\psi(x)|^2 &= \frac{1}{(2\pi\hbar)} \frac{\pi}{\alpha} e^{-(x^2/2\alpha\hbar^2)}\,, \\
|\tilde{\psi}(p)|^2 &= e^{-2\alpha(p-p_0)^2}.
\end{aligned} \tag{2.34}$$

Note how in position and momentum space our wave packet has a Gaussian shape and therefore is characterized by a peak centered at $x = 0$ for the position representation and $p = p_0$ in the momentum representation. In the position space, the Gaussian wave packet has a standard deviation σ_x of $\hbar\sqrt{\alpha}$ and in momentum space, a standard deviation σ_p of $1/2\sqrt{\alpha}$. This leads to a reciprocity condition: a strongly localized particle in x is broad in p, and vice-versa, in such a way that the product of both standard deviations is given by:

$$\sigma_x\sigma_p = \hbar\sqrt{\alpha} \cdot \frac{1}{2\sqrt{\alpha}} = \frac{\hbar}{2}, \tag{2.35}$$

which we note to be the lower limit of Heisenberg's uncertainty principle. It is then said that Gaussian wave packets "minimize the uncertainty relations for x and p".

2.2 DENSITY MATRICES AND ENTANGLEMENT

Any description of a quantum state arises from the result of some measurement. We can completely determine the state using simultaneous measurements of a complete set of commuting observables (LANDAU; LIFSHITZ, 1989) and the culmination of this procedure is the ability to write the state as $|\psi\rangle$, where $|\psi\rangle$ is a simultaneous eigenvector of the considered set of observables.

While the description of a system using a state vector (or equivalently, a wave function) is the most complete description for systems as the ones indicated above, there exists a class of states that do not allow such a description: subsystems of a larger, closed system. Note that due to interaction between subsystems, the state ket for the whole system $|\psi_1, \psi_2, ..., \psi_n\rangle$ relative to its n subsystems, should not be expected to be the product $|\psi_1\rangle \otimes |\psi_2\rangle \otimes \cdots \otimes |\psi_n\rangle$, and therefore, we cannot in general associate a state vector $|\psi_i\rangle$ to each of its subsystems.

There is however, a way of treating these subsystems in such a manner that when the larger closed system is composed of only one subsystem, our treatment becomes the same as the wave function one: the density matrix (or density operator) formalism. Systems that can be described by a single wave function are said to be in a *pure state* while systems that cannot are called *mixed states* or *mixture states*.

2.2.1 The density matrix formalism

Consider for example a set of spin-$1/2$ particles. Let us consider the following two possibilities: all of the spins are in a given orientation (spin-up, for example), or the set is a *statistical mixture* of spins, for example, 50% are in a spin-up $|+\rangle$ configuration while 50% are in a spin-down $|-\rangle$ orientation. This leads us to introduce the *fractional populations* or *probability weights*:

$$w_+ = 0.5 \quad w_- = 0.5, \tag{2.36}$$

for a completely random distribution of spin orientations, or an *unpolarized* ensemble of spins. For the first case, the system is in a pure state and can be described using only one state vector: $|+\rangle$. In the second case, the system is in a mixed state, and therefore cannot be described by a single state vector. Nevertheless, we can ask ourselves about the *average* orientation of the ensemble, which is expected to be zero. We can formalize this idea as follows: suppose our

system is in a statistical mixture of eigenvectors $|\alpha_i\rangle$ with fractional populations w_i of a given observable **A**. The ensemble average of the observable **A** is then:

$$\langle \mathbf{A} \rangle = \sum_i w_i \langle \alpha_i | \mathbf{A} | \alpha_i \rangle. \tag{2.37}$$

We can expand the eigenvectors $|\alpha_i\rangle$ in a complete orthonormal basis $|\phi_n\rangle$ and rewrite the ensemble average of an observable **A** as:

$$|\alpha_i\rangle = \sum_n a_i^n |\phi_n\rangle \rightarrow \langle \mathbf{A} \rangle = \sum_{i,m,n} w_i a_m^{i^*} a_n^i \langle \phi_m | \mathbf{A} | \phi_n \rangle , \tag{2.38}$$

and if we define:

$$\hat{\rho} = \sum_{i,m,n} w_i a_m^{i^*} a_n^i |\phi_n\rangle \langle \phi_m| = \sum_{m,n} \rho_{mn} |\phi_n\rangle \langle \phi_m| = \sum_i w_i |\alpha_i\rangle \langle \alpha_i| , \tag{2.39}$$

where: $\rho_{mn} = \sum_i w_i a_m^{i^*} a_n^i$, we can write:

$$\langle \mathbf{A} \rangle = \sum_{m,n} \langle \phi_n | \hat{\rho} | \phi_m \rangle \langle \phi_m | \mathbf{A} | \phi_n \rangle = \sum_n \langle \phi_n | \hat{\rho} \underbrace{\sum_m |\phi_m\rangle \langle \phi_m|}_{\mathbb{1}} \mathbf{A} | \phi_n \rangle = \sum_n \langle \phi_n | \hat{\rho} \mathbf{A} | \phi_n \rangle ,$$

therefore,

$$\langle \mathbf{A} \rangle = \mathrm{tr}(\hat{\rho} \mathbf{A}). \tag{2.40}$$

The operator defined in (2.39) is called the *density matrix* of the system and it describes pure and mixed systems. Note the notational simplification of the ensemble average of an observable. The following property gives further insight about the nature of the density operator and the fractional populations. We now prove that the trace of the density operator is equal to unity so long as the fractional populations add up to unity as well. Explicitly, note:

$$\begin{aligned} \mathrm{tr}(\hat{\rho}) &= \sum_k \langle \phi_k | \hat{\rho} | \phi_k \rangle \\ &= \sum_k \sum_{m,n} \sum_{i=1}^N w_i a_n^i a_m^{i^*} \langle \phi_k | \phi_n \rangle \langle \phi_m | \phi_k \rangle \\ &= \sum_k \sum_{i=1}^N w_i |a_k^i|^2 \\ &= \sum_{i=1}^N w_i = 1, \end{aligned} \tag{2.41}$$

since $\sum_k |a_k^i|^2 = 1$. Therefore, we can see that the fractional populations adding up to one is a direct consequence of the trace of the density operator being equal to one and vice-versa. This characterizes density matrices as *convex combinations* of $\{|\alpha_i\rangle \langle \alpha_i|\}$. From now on, we assume

this property as one of the defining properties of a density matrix. Before we generalize our results for continuous density matrices, we derive the temporal evolution of a density operator.

The temporal evolution of a state ket $|\alpha_i(t)\rangle$ is given by Schrödinger's equation:

$$i\hbar\frac{d}{dt}\,|\alpha_i(t)\rangle = \hat{H}\,|\alpha_i(t)\rangle\,, \tag{2.42}$$

and the time evolution of a bra is given by the Hermitian conjugate of the Schrödinger equation for kets:

$$-i\hbar\frac{d}{dt}\,\langle\alpha_i(t)| = \langle\alpha_i(t)|\,\hat{H}, \tag{2.43}$$

where we have explicitly used the fact that the Hamiltonian is a Hermitian operator. Therefore, using Leibniz's rule for differentiation, we obtain:

$$\begin{aligned} i\hbar\frac{d}{dt}\Big(\,|\alpha_i(t)\rangle\,\langle\alpha_i(t)|\,\Big) &= |\alpha_i(t)\rangle\,\Big(i\hbar\frac{d}{dt}\,\langle\alpha_i(t)|\,\Big) + \Big(i\hbar\frac{d}{dt}\,|\alpha_i(t)\rangle\,\Big)\,\langle\alpha_i(t)| \\ &= |\alpha_i(t)\rangle\,(-\,\langle\alpha_i(t)|\,\hat{H}) + \hat{H}\,|\alpha_i(t)\rangle\,\langle\alpha_i(t)| \\ &= \hat{H}\,|\alpha_i(t)\rangle\,\langle\alpha_i(t)| - |\alpha_i(t)\rangle\,\langle\alpha_i(t)|\,\hat{H}\,. \end{aligned} \tag{2.44}$$

Multiplying both sides by w_i and summing over i, we obtain the Liouville equation:

$$\frac{d}{dt}\,\hat{\rho}(t) = \frac{i}{\hbar}\Big[\hat{\rho}(t), \hat{H}\Big]\,, \tag{2.45}$$

We are now in position to generalize our description to encompass eigenvectors associated with Hermitian operators with continuous spectra. We perform the following generalization without proof:

$$\hat{\rho} = \sum_{m,n}\rho_{mn}\,|\phi_n\rangle\,\langle\phi_m| \;\rightarrow\; \hat{\rho} = \int \mathrm{d}\xi\mathrm{d}\xi'\,\rho(\xi,\xi')\,|\xi\rangle\,\langle\xi'|\;, \tag{2.46}$$

where $\{|\xi\rangle\}$ is a complete orthonormal basis, such as the eigenvectors of the momentum operator, which leads to a *continuous* density operator of the form:

$$\hat{\rho}(t) = \int \mathrm{d}^3p\,\mathrm{d}^3p'\,\rho(\vec{p},\vec{p}',t)\,|\vec{p}\rangle\,\langle\vec{p}'|\,. \tag{2.47}$$

As we have already discussed, such a density matrix cannot describe completely a system with internal degrees of freedom, only momenta degrees of freedom. This does not stops us, however, to define an even further generalization of the formalism. We can take into account discrete and continuous degrees of freedom defining a *mixed* (in the sense of mixed continuous and discrete variables) density operator of the form:

$$\hat{\rho} = \sum_{i,j}\int \mathrm{d}^3p\,\mathrm{d}^3p'\,\rho_{ij}(\vec{p},\vec{p}',t)\,|i\rangle\,|\vec{p}\rangle\,\langle\vec{p}'|\,\langle j|\;, \tag{2.48}$$

where i and j label discrete variables such as internal electronic states of an atom.

Let's discuss the physical interpretation of the terms $\rho_{ij}(\vec{p},\vec{p}',t)$ for a two-level atom accounting for momentum degrees of freedom. In this case, i and j assume the values 1 and 2, corresponding to the fundamental $|1\rangle$ and excited $|2\rangle$ levels, respectively. Terms such as $\rho_{11}(\vec{p},\vec{p},t)$ or $\rho_{22}(\vec{p},\vec{p},t)$, that is, terms with $i=j$ and $\vec{p}=\vec{p}'$, are referred to as *populations*, since they describe the populational occupancy of particles in the internal state $|1\rangle$ or $|2\rangle$ with momentum state $|\vec{p}\rangle$. Other terms such as $\rho_{12}(\vec{p},\vec{p},t)$ or $\rho_{11}(\vec{p},\vec{p}',t)$, that is, terms with $i\neq j$ and/or $\vec{p}\neq\vec{p}'$ are called *coherences* between internal and external states, respectively, and describe amplitudes of probabilities of transition between the states.

2.2.2 Entanglement quantification

In this thesis, we do not aim by any means to give a complete understanding of the problem of quantification of entanglement. However, in this subsection we aim to provide the reader with the tools and the physical intuition needed to understand a specific class of systems and the entanglement quantifiers suitable to it.

From the classical and quantum point of view, a pure state is as completely described as the theory allows (such as a point in phase space, in the classical case). In the quantum case, however, pure states can consist of parts which are not themselves pure states, that is, completely characterized by the theory. Such states are called entangled. A mixed state can also be entangled if it cannot be represented as a mixture of unentangled pure states (WERNER, 1989; WOOTERS, 2001). We can write the density matrix of a pure system consisting of two parts A and B, that is, a *pure bipartite system* as:

$$\begin{aligned}\hat{\rho}=|\Phi\rangle\langle\Phi| &= \sum_{i,j} c_{ij}\left|\psi_i^A\right\rangle\left|\psi_j^B\right\rangle\sum_{k,l}c_{kl}^*\left\langle\psi_l^B\right|\left\langle\psi_k^A\right| \\ &= \sum_{i,j,k,l} c_{ij}c_{kl}^*\left|\psi_i^A\right\rangle\left|\psi_j^B\right\rangle\left\langle\psi_l^B\right|\left\langle\psi_k^A\right|, \end{aligned} \tag{2.49}$$

where $\left\{\left|\psi_i^A\right\rangle\right\}$ and $\left\{\left|\psi_j^B\right\rangle\right\}$ form an orthonormal basis for the Hilbert space describing the subsystems A and B respectively.

In order to try to isolate a single component of a system (as best as we can), we define the *reduced density matrix*, $\hat{\rho}_A\left(\hat{\rho}_B\right)$, describing the subsystem $A(B)$. Note how the choice of what consists as subsystem A or B is completely arbitrary, and therefore any physically relevant conclusions or definitions must be invariant by the change of labels $A\leftrightarrow B$. The

reduced density matrix $\hat{\rho}_A$ is defined using the partial trace operation: $\hat{\rho}_A = tr_B\hat{\rho}$, while $\hat{\rho}_B = tr_A\hat{\rho}$, that is, we *trace out* the subsystem B or A to obtain a density matrix associated with subsystem A or B, alone. Explicitly, we define $\hat{\rho}_A$ and $\hat{\rho}_B$ as:

$$\begin{aligned}
\hat{\rho}_A &= tr_B\hat{\rho} = \sum_m \left\langle \psi_m^B \right| \left(\sum_{i,j,k,l} c_{ij}c_{kl}^* \left|\psi_i^A\right\rangle \left|\psi_j^B\right\rangle \left\langle \psi_l^B \right| \left\langle \psi_k^A \right| \right) \left|\psi_m^B\right\rangle \\
&= \sum_{i,k} \left(\underbrace{\sum_m c_{im}c_{km}^*}_{\rho_{ik}^A} \right) \left|\psi_i^A\right\rangle \left\langle \psi_k^A \right| \\
&= \sum_{i,k} \rho_{ik}^A \left|\psi_i^A\right\rangle \left\langle \psi_k^A \right| , \\
\hat{\rho}_B &= tr_A\hat{\rho} = \sum_m \left\langle \psi_m^A \right| \left(\sum_{i,j,k,l} c_{ij}c_{kl}^* \left|\psi_i^A\right\rangle \left|\psi_j^B\right\rangle \left\langle \psi_l^B \right| \left\langle \psi_k^A \right| \right) \left|\psi_m^A\right\rangle \\
&= \sum_{j,l} \left(\underbrace{\sum_m c_{mj}c_{ml}^*}_{\rho_{jl}^B} \right) \left|\psi_j^B\right\rangle \left\langle \psi_l^B \right| \\
&= \sum_{j,l} \rho_{jl}^B \left|\psi_j^B\right\rangle \left\langle \psi_l^B \right| . \qquad (2.50)
\end{aligned}$$

Eq. (2.50) explicits the fact that, in general, the two parts of a bipartite system "mix" together and affect each other, as we can see from the coefficients ρ_{ik}^A and ρ_{jl}^B carrying information from both parts of the system. Initially, in order to obtain generalizable results, we work with quantum systems described by discrete variables. Later, we generalize our results for mixtures of discrete and continuous variables.

The density matrix of any pure system can be written as $\hat{\rho} = |\Phi\rangle\langle\Phi|$ and, as a bipartite system, we can write the state vector $|\Phi\rangle$ as (SCHMIDT, 1906):

$$|\Phi\rangle = \sum_{i=1}^{n} c_i \left|\phi_i^A\right\rangle \otimes \left|\phi_i^B\right\rangle . \qquad (2.51)$$

This is called the Schmidt decomposition of the system. The orthonormal basis $\left\{ \left|\phi_i^A\right\rangle \right\}$ and $\left\{ \left|\phi_i^B\right\rangle \right\}$ are the Schmidt modes of the system, and the constants c_i, the Schmidt coefficients, satisfy the condition $\sum_{i=1}^{n} |c_i|^2 = 1$, which shows that each squared coefficient can be interpreted as a weight (probability) (GROBE; RZAZEWSKI; EBERLY, 1994). The question of whether this system is entangled or not now becomes a matter of counting the number of active Schmidt modes: if eq. (2.51) presents more than one Schmidt mode, the state $|\Phi\rangle$ is entangled, otherwise, $|\Phi\rangle$ is unentangled. On the other hand, we define a discrete *maximally entangled* state as having n non-zero Schmidt modes equally weighted, that is, $c_i = \frac{1}{\sqrt{n}}$.

This discussion leads to the definition of the *Schmidt rank* K: the number of active Schmidt modes, or equivalently, the number of nonzero Schmidt coefficients. Therefore, for

pure bipartite states, $K = 1$ implies in an unentangled state, while $K > 1$ indicates an entangled state, in fact, $K = n$ for a discrete maximally entangled state. The Schmidt rank then provides some information about the *degree of entanglement* present in a pure bipartite system.

The Schmidt decomposition also provides a simple form for the reduced density matrices defined in eq. (2.50), which will be useful in a later discussion. Explicitly, we can write:

$$\begin{aligned}\hat{\rho}_A &= tr_B\hat{\rho} = \sum_k \left\langle \phi_k^B \right| \left(\sum_{i,j} c_i c_j^* \left| \phi_i^A \right\rangle \left| \phi_i^B \right\rangle \otimes \left\langle \phi_j^A \right| \left\langle \phi_j^B \right| \right) \left| \phi_k^B \right\rangle = \sum_k |c_k|^2 \left| \phi_k^A \right\rangle \left\langle \phi_k^A \right| , \\ \hat{\rho}_B &= tr_A\hat{\rho} = \sum_k \left\langle \phi_k^A \right| \left(\sum_{i,j} c_i c_j^* \left| \phi_i^A \right\rangle \left| \phi_i^B \right\rangle \otimes \left\langle \phi_j^A \right| \left\langle \phi_j^B \right| \right) \left| \phi_k^A \right\rangle = \sum_k |c_k|^2 \left| \phi_k^B \right\rangle \left\langle \phi_k^B \right| .\end{aligned} \tag{2.52}$$

Our next task is to define the most widely used (and actually the only one for pure states) (PLENIO; VIRMANI, 2007; POPESCU; ROHRLICH, 1997) *entanglement quantifier*: the entropy of entanglement, and connect it to the Schmidt Rank. We now follow closely the description of Nielsen and Chuang (NIELSEN; CHUANG, 2000). A complementary view of what we discuss can be found for example in (WOOTERS, 2001).

Consider an unentangled system: $|\Phi\rangle = \left|\phi^A\right\rangle \otimes \left|\phi^B\right\rangle$. In this case, there is no uncertainty in the outcome of measurements performed on the system. When we consider an entangled state on the other hand, the multiple possible Schmidt modes introduce uncertainty in the outcome of measurements performed on the system. Therefore, a measure of the degree of uncertainty in the system should yield a measure of the degree of entanglement. This is where the concept of entropy becomes useful in the quantification of entanglement. More specifically, we now introduce the *Shannon entropy*.

Given a random variable X, a quantification of the amount of uncertainty before we obtain a certain value of X is equivalent to a quantification of the amount of information we gain after we learn the value of X. Therefore, we now turn to the problem of quantifying the amount of information gained through the process of learning a value of a random variable X. We can quantify the amount of information provided by an event E with probability p by introducing an "information function", $I(E)$, which depends solely on the event. Suppose we assume:

1) $I(E)$ is a function only of the probability of the event E, that is: $I(p)$, where $0 < p \leq 1$.

2) $I(p)$ is a smooth function of p.

3) $I(pq) = I(p) + I(q)$ for $p, q > 0$.

Note that assumption (3) is equivalent to say that the information gained from two independent events with probabilities p and q is the sum of the information gained from each event. From (3), we obtain:

$$I(p \cdot 1) = I(p) = I(p) + I(1) \quad \rightarrow \quad I(1) = 0, \tag{2.53}$$

which means that if we have an event with certainty of happening, this already tell us everything we need to know from the distribution of probability, and therefore, an event with probability 1 yields no more information than we already had. Taking the derivative in relation to q in assumption (3), and setting $q = 1$, we get:

$$p\, I'(p) = I'(1), \tag{2.54}$$

whose solution is: $I(p) = I'(1) \cdot \ln p + cte$. Imposing: $I(1) = 0$, performing the change of logarithmic basis $\ln p \rightarrow \log_2(p)$, and changing the resulting multiplicative constant to k, we finally obtain the general solution to $I(p)$ satisfying our assumptions:

$$I(p) = k \cdot \log_2(p). \tag{2.55}$$

Since $0 < p \leq 1$ and $\log_2(p) \leq 0$, we can choose the multiplicative constant to be $k = -1$, in order to obtain a positive information function. Given a random variable: X consisting of events of probabilities $\{p_1, \ldots, p_k, \ldots, p_n\}$, then, *on average*, the information obtained from the happening of one event is given by:

$$H(X) = H(p_1, \ldots, p_n) = -\sum_k p_k \log_2(p_k), \tag{2.56}$$

where $H(X)$ is the *Shannon entropy* associated with the random variable X. So far, we have not discussed the limit of: $p_k \rightarrow 0$, but since $\lim_{x \rightarrow 0} x \cdot \log_2(x) = 0$, we understand that impossible events do not contribute to the entropy, as is intuitively expected. Note how more uncertainty in a random variable X leads to more information to be gained from the occurrence of an event.

Now, we can use the Shannon entropy to develop an entanglement quantifier. First, we define the *von Neumann entropy* $S(\hat{\rho})$ of a given state $\hat{\rho}$:

$$S(\hat{\rho}) = -tr\Big(\hat{\rho} \ln \hat{\rho}\Big), \tag{2.57}$$

where we use the operator logarithm defined by:

$$\ln \hat{\rho} = -\sum_{n=1}^{\infty} \frac{(-1)^n}{n} \Big(\hat{\rho} - \mathbb{1}\Big)^n. \tag{2.58}$$

If we take a general density matrix written in its eigenbasis, $\hat{\rho} = \sum_i \eta_i \left|\Phi_i\right\rangle \left\langle\Phi_i\right|$, we can simplify the calculation of $S(\hat{\rho})$, since

$$S(\hat{\rho}) = -\sum_i \eta_i \ln \eta_i \,. \tag{2.59}$$

Therefore, we notice that $S(\hat{\rho}) = 0$ for *any* pure state, since for pure states the eigen-decomposition only has one term, $\left|\Phi\right\rangle \left\langle\Phi\right|$, and hence $\eta_1 = 1$ is the only nonzero eigenvalue. This means that the von Neumann entropy for the density matrix of the *whole* system does not discern between pure separable states and pure entangled states. In the beginning of this subsection, we identified entangled bipartite pure states as pure states consisting of two parts which are not themselves pure states. Therefore, if we can calculate the von Neumann entropy for only one of the components of our system, we can identify whether the subsystem is pure or not, that is, if the von Neumann entropy calculated over one of the subsystems is zero or not.

Now we can finally define the *entropy of entanglement* $E(\hat{\rho})$ as the von Neumann entropy of the reduced density matrices $\hat{\rho}_A$ or $\hat{\rho}_B$:

$$E(\hat{\rho}) = S(\hat{\rho}_A) = -tr_A\Big(\hat{\rho}_A \ln \hat{\rho}_A\Big) = S(\hat{\rho}_B) = -tr_B\Big(\hat{\rho}_B \ln \hat{\rho}_B\Big) = -\sum_k |c_k|^2 \ln |c_k|^2, \tag{2.60}$$

where we used the Schmidt decomposition of the reduced density matrices above. A few notes are in order: first, the entropy of entanglement calculated from $\hat{\rho}_A$ gives the same result as $\hat{\rho}_B$ and, therefore, if subsystem A is pure, so is subsystem B, and the system is unentangled; second, $E(\hat{\rho}) = 0$ means that the system is not entangled, as opposed to $S(\hat{\rho}) = 0$ which means that the system is pure; finally, note that $E(\hat{\rho}) > 0$ shows that the system is entangled and indicates a contribution of more than one active Schmidt mode (if there was only one active Schmidt mode, we would have $c_1 = 1$ as the only nonzero Schmidt coefficient, which would lead to a null entropy of entanglement, that is, a separable state).

Note that, operationally, if the Schmidt decomposition is unknown, the calculation of the entropy of entanglement can be very complicated due to the term $\ln \hat{\rho}_A$. However, if we assume that $\hat{\rho}_A$ does not diverge from the identity too much, we can approximate the logarithm in eq. (2.57) to first order, that is, $\ln \hat{\rho}_A \approx \hat{\rho}_A - \mathbb{1}$. Precisely, we can introduce the so-called Frobenius inner product of two matrices $\mathbf{A}$ and $\mathbf{B}$ as: $\langle \mathbf{A}|\mathbf{B}\rangle_F = \mathrm{Tr}\Big(\mathbf{A}^\dagger \mathbf{B}\Big)$ (HOFFMAN; KUNZE, 1971). Therefore, we can now calculate the distance $d\Big(\mathbb{1}, \hat{\rho}_A\Big)$ from the identity $\mathbb{1}$ to the reduced matrix $\hat{\rho}_A$ as:

$$d\Big(\mathbb{1}, \hat{\rho}_A\Big) = \sqrt{\mathrm{Tr}\bigg(\Big(\hat{\rho}_A - \mathbb{1}\Big)^\dagger \Big(\hat{\rho}_A - \mathbb{1}\Big)\bigg)}\,. \tag{2.61}$$

Now, if $d\Big(\mathbb{1}, \hat{\rho}_A\Big)$ is small enough (which is dictated by the level of accuracy desired for the approximation $\ln \hat{\rho}_A \approx \hat{\rho}_A - \mathbb{1}$), we can simplify the entropy of entanglement to obtain the *linear entropy* $E_L(\hat{\rho})$:

$$\begin{aligned} E_L(\hat{\rho}) &= -tr_A(\hat{\rho}_A(\hat{\rho}_A - \mathbb{1})) \\ &= tr_A(\hat{\rho}_A) - tr_A(\hat{\rho}_A^2) \\ &= 1 - P_A, \end{aligned} \tag{2.62}$$

where we used the fact that the trace of a density matrix is 1 and we defined the *purity of the reduced state* $P_A = tr_A(\hat{\rho}_A^2)$ (in this thesis, we may sometimes refer to it as *purity* when is clear that we are calculating the purity of some reduced state). We usually drop the subscript A in tr_A since we are already working with the reduced density matrix $\hat{\rho}_A$. Note that, once again, everything we use can be defined with $\hat{\rho}_B$ and yields the same results and conclusions. Linear entropy therefore also provides a quantification of the degree of entanglement present in a system, though it should be noted that it appears that for problems involving quantum phase transitions it is not as sensitive as the von Neumann entropy (PAULETTI et al., 2023). Since this is not our case, we can continue to use the linear entropy, or equivalently the purity, as an indicator of entanglement. In the Schmidt basis, once again, the calculation of purity is simplified, obtaining:

$$P_A = \sum_k |c_k|^4. \tag{2.63}$$

Note that we can identify the right hand side of eq. (2.63) as the *average* probability $|c_k|^2$. Therefore, its inverse should provide the number of nonzero probabilities, or equivalently Schmidt modes, that is, the Schmidt rank (GROBE; RZAZEWSKI; EBERLY, 1994; EBERLY; CHAN; LAW, 2003). In fact, eq. (2.63) yields $P_A = 1$ and $P_A = 1/N$ for unentangled and maximally entangled states respectively. More explicitly, we write:

$$K = \frac{1}{P_A} = \frac{1}{\sum_k |c_k|^4}. \tag{2.64}$$

Therefore, we understand now that calculating the Schmidt rank is completely equivalent to calculating the purity of the reduced state, which in turn is equivalent to the linear entropy, which, finally, gives the first order approximation to the entropy of entanglement, the paradigmatic entanglement quantifier for bipartite pure systems. In this thesis we then use these concepts interchangeably to quantify the degree of entanglement, which will be the subject of chapter 4.

Finally, we provide a brief generalization of our discussion to pure bipartite continuous-variable states, namely, written in terms of momentum eigenstates. A pure bipartite system of the form:

$$|\Phi\rangle_{AB} = \int \mathrm{d}^3p\, \mathrm{d}^3q\, C(\vec{p},\vec{q})\, |\vec{p}\rangle_A\, |\vec{q}\rangle_B\,, \tag{2.65}$$

leads to a density matrix of the form:

$$\begin{aligned} \hat{\rho}_{AB} &= |\Phi\rangle_{AB}\, \langle\Phi|_{AB} \\ &= \int \mathrm{d}^3p\, \mathrm{d}^3q\, \mathrm{d}^3p'\, \mathrm{d}^3q'\, C(\vec{p},\vec{q})C^*(\vec{p}',\vec{q}')\, |\vec{p}\rangle_A\, |\vec{q}\rangle_B\, \langle\vec{p}'|_A\, \langle\vec{q}'|_B\,, \end{aligned} \tag{2.66}$$

and a reduced density matrix $\hat{\rho}_A$:

$$\begin{aligned} \hat{\rho}_A &= tr_B\Big(\hat{\rho}_{AB}\Big) \\ &= \int \mathrm{d}^3q''\, {}_B\langle\vec{q}''|\, \hat{\rho}_{AB}\, |\vec{q}''\rangle_B \\ &= \int \mathrm{d}^3p\, \mathrm{d}^3q\, \mathrm{d}^3p'\, \mathrm{d}^3q' \underbrace{\int \mathrm{d}^3q''\delta^3(\vec{q}-\vec{q}'')\delta^3(\vec{q}'-\vec{q}'')}_{\delta^3(\vec{q}-\vec{q}')} C(\vec{p},\vec{q})C^*(\vec{p}',\vec{q}')\, |\vec{p}\rangle_A\, \langle\vec{p}'|_A \\ &= \int \mathrm{d}^3p\, \mathrm{d}^3q\, \mathrm{d}^3p'\, C(\vec{p},\vec{q})C^*(\vec{p}',\vec{q})\, |\vec{p}\rangle_A\, \langle\vec{p}'|_A\,. \end{aligned} \tag{2.67}$$

A further discussion on the purity calculation of reduced density matrices of this form and the Schmidt decomposition of continuous variable systems are given in the corresponding sections where they are needed.

3 ATOMIC MEMORY BASED ON RECOIL-INDUCED RESONANCES

In this chapter, we aim to provide a detailed theoretical investigation of the RIR phenomenon and its role in the storage of light through the modelling and observation of both the probe transmission and FFWM spectra, in the writing and reading phases, considering the simplest case of an ensemble of two-level atoms. This theoretical analysis is supported by a series of experiments performed in our group. Although the RIR effect is sometimes interpreted as Rayleigh scattering into a density grating (COURTOIS et al., 1994), we followed a different approach that we consider more amenable to model the experimental data obtained in the Cold Atoms Laboratory at DF-UFPE. Our first-principles approach models it, in the lowest order of perturbation, as Raman scattering between differently populated momentum states (GUO et al., 1992). This process creates a coherence grating between momentum states of the ground-state manifold, which later scatters the incident optical fields. Most importantly, this process does not require any dislocation of atoms in space to form density gratings, being robust with respect to the power of the excitation fields.

The model and calculation developed here allows us to obtain the transient and stationary responses of the system, and provides a simple interpretation of the non-volatility mentioned in the introduction for the RIR memory. J. P. Lopez, A. M. G. de Melo and J. W. R. Tabosa performed a thorough experimental investigation measuring simultaneously the probe transmission and FFWM excitation spectra, as well as the corresponding spectra for the retrieved signals after a specific storage time. These measurements are in good agreement with our theoretical description. This pair of signals constitute an overall quasi-phase matching process that could be explored in the future for its classical and quantum correlations.

The present chapter will be divided in 4 sections providing, in order: a brief overview of the RIR phenomenon, a theoretical model for the atomic memory developed using RIR, experimental results, and discussions comparing our theoretical model to the experimental data.

3.1 THE RIR PHENOMENON

In this section we aim to provide a brief overview of the RIR phenomenon. In order to understand the effect of the atomic/photonic recoil in the measured spectra, we may take a

pump-probe configuration as depicted in Fig. 1. It consists of two nearly degenerate coplanar fields, an excitation field with frequency ω_e and wavevector $\vec{k}_e$ and a probe field with frequency ω_p and wavevector $\vec{k}_p$ acting on an ensemble of cold two-level atoms, with a detector on the direction of the transmitted probe field.

We assume both fields to be very far from atomic resonance: $\omega_e - \omega_0 \gg \Gamma$ and $\omega_p - \omega_0 \gg \Gamma$ where ω_0 is the transition frequency between the atomic internal states and Γ is the natural line-width of the transition. This condition leads to the restriction of any dynamics to the internal ground state of the atoms, $|1\rangle$. In fact, the dynamics generated by the light beams occur on the only atomic degrees of freedom left: external (momentum) degrees of freedom. The illumination of the atomic ensemble by the fields, therefore, induces transitions between atomic momentum states, $|\vec{p}\rangle$, which we understand as Raman scattering between momentum atomic levels.

We then perform the spectroscopy by scanning the probe frequency ω_p around the excitation frequency ω_e, and measuring the transmitted probe light intensity. Note that this measurement is not background-free: we measure the resulting intensity of the sum of the incident probe field and a generated (via non-linear processes) field by the atoms.

Figure 1 – Pump-probe setup consisting of two coplanar nearly degenerate light fields, the excitation $(\vec{k}_e, \omega_e)$ and probe $(\vec{k}_p, \omega_p)$ fields illuminating an ensemble of cold two level atoms. The intensity of the transmitted probe light is monitored placing a detector along the direction of the probe field.

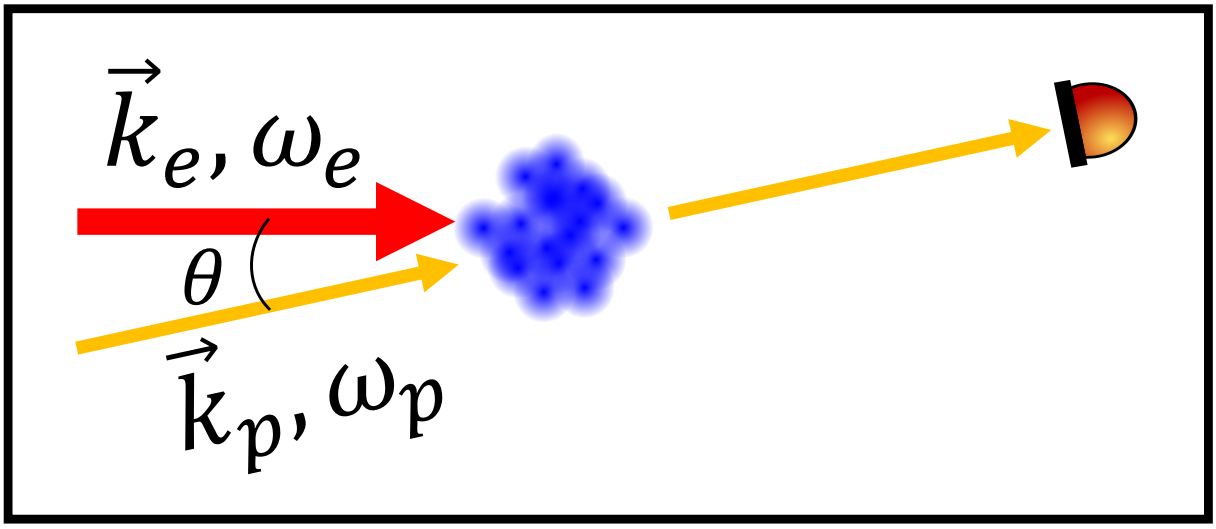

Source: The author.

In this configuration, as illustrated by Fig. 2, two main scattering processes arise: (1) the absorption of a photon from the probe field and a stimulated emission in the direction of the

excitation field (leading to attenuation of the transmitted probe field); and (2) the absorption of a photon from the excitation field and a stimulated emission in the probe direction (leading to gain in the transmitted probe field). These are Raman processes, and as such, the rate for the direct process is the same as the rate for the inverse process. Note however, that these processes connect states with different populations and therefore, processes which happen from a more populated state to a less populated state are enhanced in detriment of their inverse processes.

Since all the dynamics is restricted to momentum states, we need to model our ensemble's distribution of momenta. We assume an atomic ensemble initially at thermal equilibrium with a temperature T, which leads to a Maxwell-Boltzmann distribution of momenta of the form (up to normalization factors) $e^{-\frac{p^2}{2p_u^2}}$, with a variance of $p_u^2 = mk_BT$, where m is the atom's mass and k_B is the Boltzmann's constant, dependent on the ensemble's temperature. The two aforementioned scattering processes are represented in Fig. 2, where we depict also the ground-state manifold represented by the parabola, and the thermal distribution of momenta in green, pictorially.

Now we are in position to understand the appearance of a resonant structure in the probe transmission spectrum. Take, for example, process (1) regarding the absorption of a photon from the probe field and emission in the excitation field. This process, depicted explicitly in Fig. 2 on the left side of the energy parabola (where $\omega_p > \omega_e$) can also happen by the inverse Raman transition depicted on the right side of the parabola (where $\omega_p < \omega_e$). Due to the Maxwellian momentum distribution over the ground state, more atoms participate in the process where $\omega_p > \omega_e$, while for $\omega_p < \omega_e$, fewer atoms participate in the process. Therefore, on average, process (1) which leads to an attenuation of the transmitted probe field is greatly enhanced for $\omega_p > \omega_e$. If the probe frequency is now *much* greater than the excitation frequency, the fields would need to access higher atomic energy states, which are less populated due to the Maxwell-Boltzmann distribution. Therefore, we should observe a crescent attenuation for the probe transmitted field as we increase the probe frequency from the excitation frequency ($\omega_p > \omega_e$), a trough for a certain *resonant* frequency of attenuation ω_{att}, where a balance is achieved, and the spectrum should become flat as we keep increasing ω_p, where no gain or attenuation are observed. Note that the resonant frequency, ω_{att}, where we can send atoms between states with a large enough gradient of population while not trying to access higher energy levels, is governed directly by the width of the Maxwell-Boltzmann distribution, and therefore, the ensemble's *temperature*.

Figure 2 – Raman processes in the ground state manifold $|1,\vec{p}\rangle = |1\rangle \otimes |\vec{p}\rangle$. Depicted here are also a pictorial shape for the disposition of population in momentum states over the ground state manifold and the energy parabola representing the energies of the ground-state manifold.

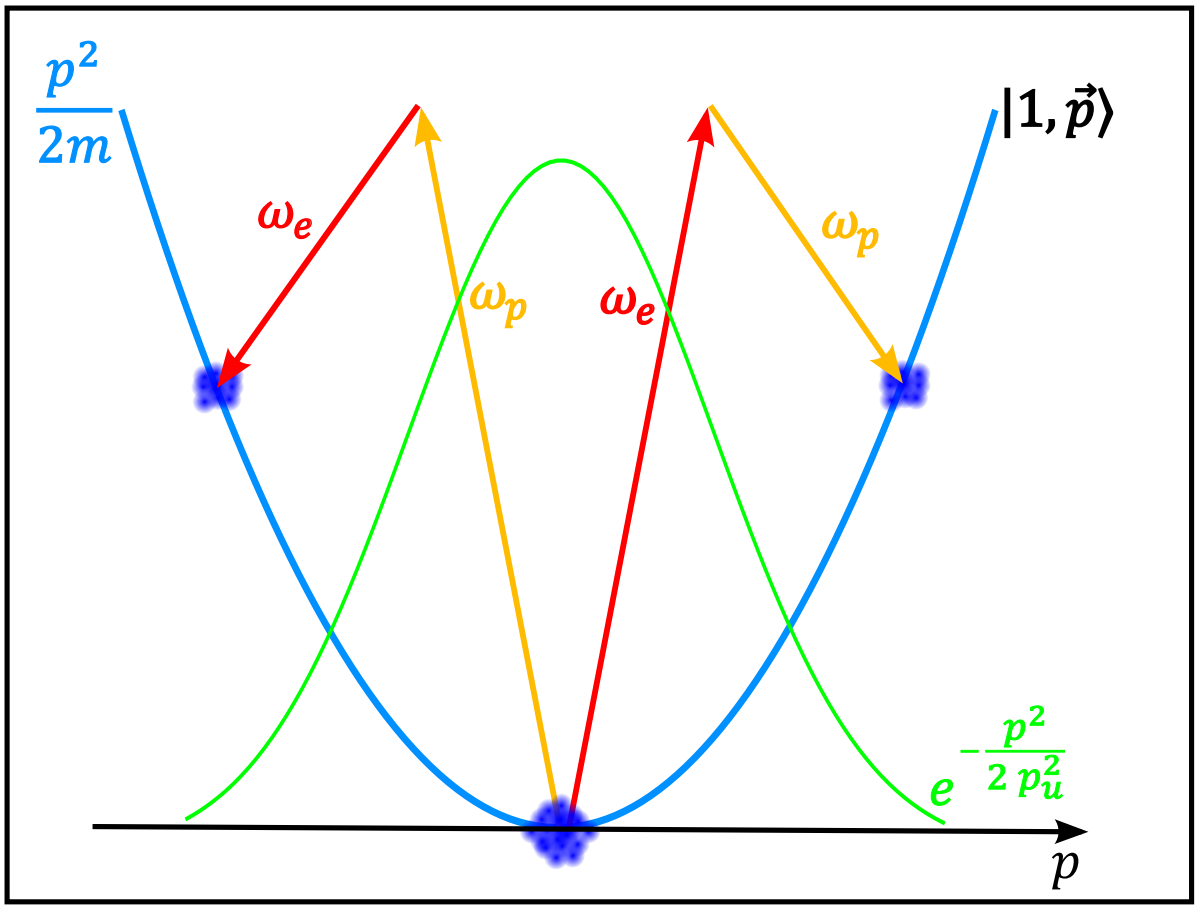

Source: The author.

On the other hand, take process (2) where the atomic ensemble absorbs a photon from the excitation field and emits another in the probe direction (leading to a gain in the transmitted probe field). Following the same steps as above, this process is greatly enhanced for $\omega_p < \omega_e$, and a balance is also achieved at a certain resonant frequency of gain, ω_{gain}, generating a peak at $\omega_p = \omega_{gain}$. This resonant frequency, by the same reasoning as before, is directly related to the ensemble's temperature.

In summary, scanning the probe frequency around the excitation frequency should lead to spectrum that presents a resonant structure at the middle with two resonant frequencies: one for the gain region ($\omega_p < \omega_e$) and one for the attenuation region ($\omega_p > \omega_e$). This *dispersive* curve has a natural width (defined as $\delta_{RIR} = \omega_{att} - \omega_{gain}$) completely dictated by the ensemble's temperature. In fact, this property lead to the use of the RIR phenomenon as an experimental tool of non-destructive temperature probing for laser cooled atoms (MEACHER et al., 1994).

3.2 THEORETICAL MODEL

In this section we present a theoretical approach to describe the non-volatile robust memory associated with the RIR phenomenon. Explicitly, we consider an initially free cold atomic cloud subjected to three subsequent processes (see Fig. 3): an interaction with excitation and probe beams (the writing phase), then a dark evolution where no fields act on the atomic cloud (dark/storage phase), and, finally, an interaction with only the excitation beam (the reading phase). We are interested in the signals generated along the probe beam and the FFWM directions. Further details of the theoretical model for each phase will be given in the respective subsections.

3.2.1 The writing phase.

For the writing phase we consider an ensemble of cold two-level atoms interacting with two fields that can be approximated by plane waves, an (strong) excitation field with wavevector $\vec{k}_e$ and frequency ω_e and a (weak) probe field with wavevector $\vec{k}_p$ and frequency ω_p:

$$\mathbf{E}(t) = \left[\mathscr{E}_e \cos\left(\vec{k}_e \cdot \hat{\mathbf{r}} - \omega_e t\right) + \mathscr{E}_p \cos\left(\vec{k}_p \cdot \hat{\mathbf{r}} - \omega_p t\right)\right] \hat{e}, \tag{3.1}$$

where $\mathscr{E}_e$ and $\mathscr{E}_p$ are the excitation and probe amplitudes, respectively, and $\hat{e}$ is the polarization vector common to both fields. The wavevector $\vec{k}_e$ points in the longitudinal z direction, and the y axis will be referred to as the transverse direction. These two define the zy plane containing both excitation and probe fields. We assume a small angle θ between the directions of the two fields, and excitation and probe frequencies with detunings from the atomic transition frequency ω_0, $\Delta_e = \omega_0 - \omega_e$ and $\Delta_p = \omega_0 - \omega_p$ much larger than the excited state natural linewidth Γ, i.e., $\Delta_e, \Delta_p >> \Gamma$. The atomic internal ground state $|1\rangle$ has energy E_1, and the internal excited state $|2\rangle$ energy E_2. The atom also has a linear momentum $\vec{p}$, associated with a state $|\vec{p}\rangle$ for its external degrees of freedom.

Considering the ground state energy $E_1 = 0$, the Hamiltonian for a single atom in the ensemble can be written as:

$$\hat{H} = \frac{\hat{\mathbf{P}}^2}{2m} + \hbar\omega_0 |2\rangle\langle 2| - e\,\hat{\mathbf{D}} \cdot \mathbf{E}(t), \tag{3.2}$$

in the dipole interaction approximation, with $\hat{\mathbf{D}}$ the atomic electric dipole operator and m the atomic mass. Using the basis of the internal states, the Hamiltonian becomes then:

Figure 3 – (a) Visualization of the three phases of the theoretical model: I) interaction with the excitation $(\vec{k}_e, \omega_e)$ and probe $(\vec{k}_p, \omega_p)$ coplanar fields; II) dark evolution of the system; III) reading phase using only the excitation field. The time duration of the dark phase is upscaled. (b) Excitation time sequence.

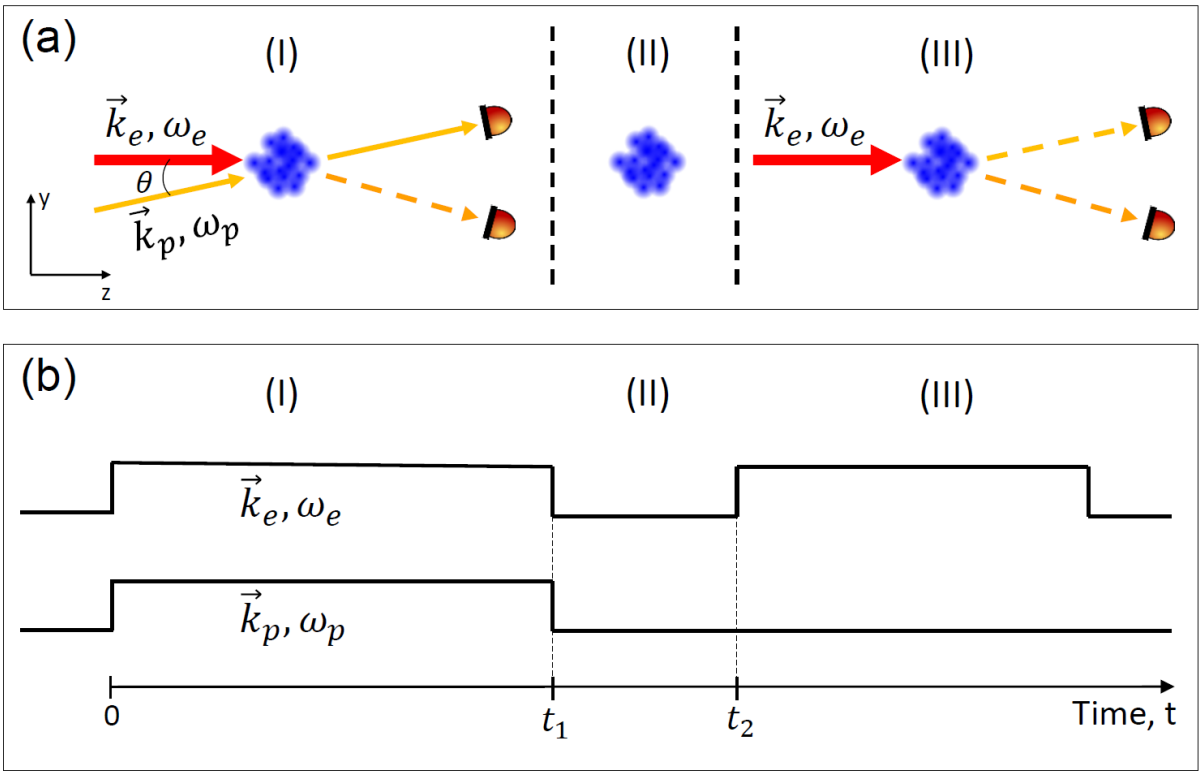

Source: (CAPELLA et al., 2022).

$$\hat{H} = \frac{\hat{\mathbf{P}}^2}{2m} + \hbar\omega_0|2\rangle\langle 2| - \left(\mu_{12}|1\rangle\langle 2| + \mu_{21}|2\rangle\langle 1|\right) \cdot \left[\mathscr{E}_e \cos\left(\vec{k}_e \cdot \hat{\mathbf{r}} - \omega_e t\right) + \mathscr{E}_p \cos\left(\vec{k}_p \cdot \hat{\mathbf{r}} - \omega_p t\right)\right], \tag{3.3}$$

with μ_{12} the dipole moment of the $|1\rangle \rightarrow |2\rangle$ transition. Following the steps from chapter 2, considering both internal and external degrees of freedom, using eq. (2.48), the mixed variables density matrix for the system is defined as:

$$\hat{\rho} = \sum_{i,j=1}^{2} \int d\vec{p} d\vec{p'}\, \rho_{ij}(\vec{p}, \vec{p}')|i\rangle|\vec{p}\rangle\langle\vec{p}'|\langle j|, \tag{3.4}$$

with $\rho_{ij}(\vec{p}, \vec{p}')$ providing the general populations and coherences in all degrees of freedom. The density matrix components can be grouped now in five different family of terms:

1. $\rho_{11}(\vec{p}, \vec{p}) \equiv$ ground-state populations;
2. $\rho_{22}(\vec{p}, \vec{p}) \equiv$ excited-state populations;
3. $\rho_{12}(\vec{p}, \vec{p}') \equiv$ optical coherences;

4. $\rho_{11}(\vec{p},\vec{p}') \equiv$ ground-state coherences ($\vec{p} \neq \vec{p}'$);

5. $\rho_{22}(\vec{p},\vec{p}') \equiv$ excited-state coherences ($\vec{p} \neq \vec{p}'$).

We anticipate that our initial state is restricted to the ground state populations (family 1) obeying a Maxwell-Boltzmann distribution in momentum. The core of the temporal dynamics, however, will unfold in the ground-state coherences (family 4) resulting in the observed traces in the light emitted by the ensemble (from the optical coherences of family 3).

The time-evolution of the density matrix components will be dictated by the Liouville equation, as seen in chapter 2:

$$\frac{d\rho_{ij}(\vec{p},\vec{p}')}{dt} = \frac{i}{\hbar}\langle\vec{p}|\langle i|[\hat{\rho},\hat{H}]|j\rangle|\vec{p}'\rangle. \tag{3.5}$$

Defining a rotating frame where $\rho_{12}(\vec{p},\vec{p}') = e^{i\omega_e t}\sigma_{12}(\vec{p},\vec{p}')$ and using the rotating wave approximation, we obtain:

$$\begin{aligned}
\frac{d\rho_{11}(\vec{p},\vec{p}',t)}{dt} &= i\Delta(\vec{p},\vec{p}')\rho_{11}(\vec{p},\vec{p}',t) - \\
&\quad - i\left[\Omega_e\sigma_{12}(\vec{p},\vec{p}'+\hbar\vec{k}_e,t) + \Omega_p\sigma_{12}(\vec{p},\vec{p}'+\hbar\vec{k}_p,t)e^{-i\delta t} - \mathrm{h.c.}\right], \\
\frac{d\sigma_{12}(\vec{p},\vec{p}',t)}{dt} &= i\left[\Delta_e + \Delta(\vec{p},\vec{p}')\right]\sigma_{12}(\vec{p},\vec{p}',t) - \\
&\quad - i\left\{\Omega_e\left[\rho_{11}(\vec{p},\vec{p}'-\hbar\vec{k}_e,t) - \rho_{22}(\vec{p}+\hbar\vec{k}_e,\vec{p}',t)\right] + \right. \\
&\quad \left. + \Omega_p e^{i\delta t}\left[\rho_{11}(\vec{p},\vec{p}'-\hbar\vec{k}_p,t) - \rho_{22}(\vec{p}+\hbar\vec{k}_p,\vec{p}',t)\right]\right\},
\end{aligned} \tag{3.6}$$

where $\Delta(\vec{p},\vec{p}') = \frac{(\vec{p}'^2-\vec{p}^2)}{2m\hbar}$ gives the difference in kinetic energy of the two states in frequency units, $\Omega_e = \mu_{12}\mathscr{E}_e/2\hbar$ and $\Omega_p = \mu_{12}\mathscr{E}_p/2\hbar$ are the Rabi frequencies associated with the excitation and probe fields, $\delta = \omega_p - \omega_e$ is the two-photon detuning, and $\mathrm{h.c.}$ stands for the hermitian conjugate. To obtain eq. (3.6), we used the fact that $e^{i\vec{p}\cdot\hat{\mathbf{x}}/\hbar}$ acts as a translation operator in momentum eigenstates. We can now express the assumption that the probe field is much weaker than the excitation field as $\Omega_p << \Omega_e$. Considering a large detuning from the excited state ($\Delta_e >> \Gamma, \delta, p^2/2\hbar m$), we can adiabatically eliminate the excited state, approximating

$$\rho_{22}(\vec{p},\vec{p}',t) \approx 0, \tag{3.7}$$

$$\frac{d\sigma_{12}(\vec{p},\vec{p}',t)}{dt} \approx 0. \tag{3.8}$$

These two conditions result in

$$\sigma_{12}(\vec{p},\vec{p}',t) \;\; = \Delta_e^{-1}\left[\Omega_e\rho_{11}(\vec{p},\vec{p}'-\hbar\vec{k}_e,t) + \Omega_p\rho_{11}(\vec{p},\vec{p}'-\hbar\vec{k}_p,t)e^{i\delta t}\right]. \tag{3.9}$$

In this way, we now only need to focus on calculating $\rho_{11}(\vec{p},\vec{p}',t)$, whose Eq. (3.6) becomes:

$$\begin{aligned}\frac{d\rho_{11}(\vec{p},\vec{p}',t)}{dt} &= i\Delta\left(\vec{p},\vec{p}'\right)\rho_{11}(\vec{p},\vec{p}',t) - \\ &- i\Omega\left[\rho_{11}(\vec{p},\vec{p}'+\hbar\Delta\vec{k},t)e^{i\delta t}+\rho_{11}(\vec{p},\vec{p}'-\hbar\Delta\vec{k},t)e^{-i\delta t}-\text{h.c.}\right], \quad (3.10)\end{aligned}$$

with $\Delta\vec{k}=\vec{k}_e-\vec{k}_p$, and $\Omega=\Omega_e\Omega_p/\Delta_e$ the two-photon Rabi frequency. Equation (3.10) generates the whole dynamics between different atomic momentum states. It is important to note that we have completely eliminated the dynamics of the internal degrees of freedom of the atom, making it explicit that the RIR phenomenon arises primarily from the dynamics of the external degrees of freedom. For perturbative calculations, a more suitable form of Eq. (3.10) is

$$\begin{aligned}\rho_{11}(\vec{p},\vec{p}',t)=\rho_{11}(\vec{p},\vec{p}',0)+i\Omega\left\{\int_0^t dt' G_0(t,t')\left[\rho_{11}(\vec{p},\vec{p}'+\hbar\Delta\vec{k},t')e^{i\delta t'}+\right.\right. \\ \left.\left.+\ \rho_{11}(\vec{p},\vec{p}'-\hbar\Delta\vec{k},t')e^{-i\delta t'}-\text{h.c.}\right]\right\}, \quad (3.11)\end{aligned}$$

where $G_0(t,t')=e^{i\Delta(\vec{p},\vec{p}')t}e^{-i\Delta(\vec{p},\vec{p}')t'}$ is a Green's function for the operator $\left[\frac{d}{dt}-i\Delta\left(\vec{p},\vec{p}'\right)\right]$, and Ω becomes the perturbation parameter.

We are interested in a first-order solution for $\rho_{11}(\vec{p},\vec{p}',t)$, which means we should substitute the 0^{th}-order solution $\rho^0_{11}(\vec{p},\vec{p}',t)=\rho_{11}(\vec{p},\vec{p}',0)$ in the integrand. At $t=0$, however, we have no coherences established between different momenta states of the atom, only populations. This condition can be expressed as:

$$\rho_{11}(\vec{p},\vec{p}',0)=\rho^0_{11}(\vec{p})\delta(\vec{p}-\vec{p}'), \quad (3.12)$$

where $\rho^0_{11}(\vec{p})$ is given by the standard Maxwell-Boltzmann distribution for the momenta of the atomic ensemble:

$$\rho^0_{11}(\vec{p})=\frac{m}{\sqrt{(2\pi)^3}\,p_u}e^{-\vec{p}^{\,2}/2p_u^2}, \quad (3.13)$$

with $p_u=\sqrt{mk_BT}$ and T the ensemble's temperature. We obtain then:

$$\begin{aligned}\rho_{11}(\vec{p},\vec{p}',t)=\rho^0_{11}(\vec{p})\delta(\vec{p}-\vec{p}')-\Omega\left\{\frac{1}{-\delta+\Delta(\vec{p},\vec{p}')}\delta(\vec{p}-\vec{p}'-\hbar\Delta\vec{k})\left[\left(e^{i\delta t}-e^{i\Delta(\vec{p},\vec{p}')t}\right)\times\right.\right. \\ \left.\times\left(\rho^0_{11}(\vec{p})-\rho^0_{11}(\vec{p}-\hbar\Delta\vec{k})\right)\right]+\frac{1}{\delta+\Delta(\vec{p},\vec{p}')}\delta(\vec{p}-\vec{p}'+\hbar\Delta\vec{k})\left[\left(e^{-i\delta t}-e^{i\Delta(\vec{p},\vec{p}')t}\right)\right. \\ \left.\left.\times\left(\rho^0_{11}(\vec{p})-\rho^0_{11}(\vec{p}+\hbar\Delta\vec{k})\right)\right]\right\}, \quad (3.14)\end{aligned}$$

which fully determines $\rho_{11}(\vec{p},\vec{p}',t)$ in first-order approximation. Note that $\rho_{11}(\vec{p},\vec{p}',t)$ represents a ground-state population for the internal degrees of freedom of the atoms, but describes

both populations and coherences of the momentum states describing the atomic external degrees of freedom. These terms act as "sources" for the optical coherences as in Eq. (3.9). In this order of perturbation, they take into account effects that depend on one single "kick" of momentum, $\hbar\Delta\vec{k}$, generating signals in different directions. If we were interested in a second-order solution for $\rho_{11}(\vec{p},\vec{p}',t)$, we would proceed in an analogous manner, substituting the first order solution we found onto the integrand of (3.11). This would lead to second-order terms taking into account now two kicks of momentum (and a correction for the "zero-kicks" solution) that would result, in the conditions considered here, in the creation of much weaker signals in other directions.

After substitution of (3.14) into (3.9), we now obtain the usual local optical coherence, given by (GUO et al., 1992):

$$\rho_{12}(\vec{r};t) = \frac{1}{(2\pi\hbar)^3}\int d\vec{p}d\vec{p}' e^{i\frac{\vec{p}\cdot\vec{r}}{\hbar}}\rho_{12}(\vec{p},\vec{p}',t)e^{-i\frac{\vec{p}'\cdot\vec{r}}{\hbar}}. \tag{3.15}$$

Since $\Omega_p << \Omega_e$, we disregard terms of order $\Omega\Omega_p$, yielding:

$$\begin{aligned}
\rho_{12}(\vec{r};t) = {} & \frac{1}{\Delta_e(2\pi\hbar)^{\frac{3}{2}}}\int d\vec{p}d\vec{p}' e^{\frac{i}{\hbar}(\vec{p}-\vec{p}')\cdot\vec{r}}\times \\
& \times\Bigg\{\Omega_p e^{i\omega_p t}\rho^0_{11}(\vec{p})\delta(\vec{p}-\vec{p}'+\hbar\vec{k_p}) + \Omega_e e^{i\omega_e t}\rho^0_{11}(\vec{p})\delta(\vec{p}-\vec{p}'+\hbar\vec{k_e}) - \\
& - \Omega\Omega_e e^{i\omega_e t}\Bigg[\frac{1}{-\delta+\Delta(\vec{p},\vec{p}'-\hbar\vec{k_e})}\delta(\vec{p}-\vec{p}'-\hbar\Delta\vec{k}+\hbar\vec{k_e})\times \\
& \times\left(e^{i\delta t}-e^{i\Delta(\vec{p},\vec{p}'-\hbar\vec{k_e})t}\right)\left(\rho^0_{11}(\vec{p})-\rho^0_{11}(\vec{p}-\hbar\Delta\vec{k})\right) + \frac{1}{\delta+\Delta(\vec{p},\vec{p}'-\hbar\vec{k_e})}\times \\
& \times\delta(\vec{p}-\vec{p}'+\hbar\Delta\vec{k}+\hbar\vec{k_e})\left(e^{-i\delta t}-e^{i\Delta(\vec{p},\vec{p}'-\hbar\vec{k_e})t}\right)\left(\rho^0_{11}(\vec{p})-\rho^0_{11}(\vec{p}+\hbar\Delta\vec{k})\right)\Bigg]\Bigg\}.
\end{aligned} \tag{3.16}$$

All observed signals originate from this equation, which deserves a closer look. The Dirac deltas express the momentum conservation required for any process. The first two terms on the right hand side give the linear response of the atomic medium, while the last two terms originate from the 3^{rd}-order non-linearity of the medium in momentum space. We turn our attention to the latter noting that the first term inside the brackets describes the gain-attenuation of the probe field, since $-\hbar\Delta\vec{k}+\hbar\vec{k_e} = \hbar\vec{k_p}$. The second term inside the brackets, on the other hand, describes a FFWM generation process. We can see that the efficiency of these processes are proportional to the difference in population of the external levels $|\vec{p}\rangle$ and $|\vec{p}\pm\hbar\Delta\vec{k}\rangle$, therefore, since $\hbar\Delta|\vec{k}|$ is small, the resonant structure is expected to be roughly as wide as the Doppler

width. Moreover, note that these two processes arise at the same order of perturbation which goes to show that a more complete understanding of the RIR phenomenon should consider both processes as equivalent.

3.2.1.1 Transmission signal.

To obtain the transmission signal, we need to look at the plane waves seeded in the $\vec{k}_p$ direction. Those arise from the terms containing $\delta(\vec{p}-\vec{p}'-\hbar\Delta\vec{k}+\hbar\vec{k}_e)=\delta(\vec{p}-\vec{p}'+\hbar\vec{k}_p)$ in (3.16). Explicitly, we have:

$$\rho_{12}^{p}(\vec{r};t)=\frac{\Omega\Omega_e e^{-(i\vec{k}_p\cdot\vec{r}-\omega_p t)}}{\Delta_e(2\pi\hbar)^{\frac{3}{2}}}\int d\vec{p}\,\frac{1}{-\delta+\Delta(\vec{p},\vec{p}-\hbar\Delta\vec{k})}\times \\ \times\left(1-e^{i(\Delta(\vec{p},\vec{p}-\hbar\Delta\vec{k})-\delta)t}\right)\left(\rho_{11}^{0}(\vec{p})-\rho_{11}^{0}(\vec{p}-\hbar\Delta\vec{k})\right). \tag{3.17}$$

Note that, using the small angle approximation, the momentum exchange only happens on the transverse y direction which implies that:

$$\Delta(\vec{p},\vec{p}-\hbar\Delta\vec{k})=\frac{\left(|\vec{p}-\hbar\Delta\vec{k}|^2-p^2\right)}{2m\hbar}\approx-\frac{p_y\Delta k}{m}+\frac{\hbar}{2m}\Delta k^2. \tag{3.18}$$

Now, if such momentum exchange is small when compared to the average momentum of atoms, we may also approximate:

$$\rho_{11}^{0}(p_y)-\rho_{11}^{0}(p_y-\hbar\Delta k)\simeq(-\hbar\Delta k)\cdot\frac{\partial\rho_{11}^{0}(p_y)}{\partial p_y}, \tag{3.19}$$

where we use the $1\mathrm{D}$ version of (3.13). The probe transmission signal is proportional to the imaginary part of the slowly-varying coherence, $\sigma_{12}^{p}(\vec{r},t)=e^{i\vec{k}_p\cdot\vec{r}+i\omega_p t}\rho_{12}^{p}(\vec{r};t)$. Using (3.18) and (3.19), we obtain then:

$$\mathrm{Im}\left[\sigma_{12}^{p}(\vec{r},t)\right]=-\frac{\Omega\Omega_e(\,m\Delta k)t}{\Delta_e(2\pi)^2\hbar^{\frac{1}{2}}p_u^2}\times\int dp_y\,\mathrm{sinc}\left[\Big(-\delta-p_y\frac{\Delta k}{m}+\frac{\hbar}{2m}\Delta k^2\Big)t\right]e^{-\frac{p_y^2}{2p_u^2}}p_y. \tag{3.20}$$

This expression for the transmission signal has already been found in the literature (GUIBAL et al., 1996) where the term of second order in Δk was discarded. Figure 4 shows the transient and stationary transmission spectra predicted by the theory using $\Delta k=1.2\times10^5\,\mathrm{m}^{-1}$, a temperature of $\mathrm{T}=500\,\mu\mathrm{K}$, and *m* as the cesium mass. Δk was calculated considering an angle $\theta=1^\circ$ between excitation and probe fields. We will use this set of parameters throughout all theoretical considerations. Note that the other parameters only amount to a global scaling factor, which is irrelevant to the discussion here presented. To obtain a rough estimate of the time τ it takes for the system to achieve a stationary state, we take the inverse

Figure 4 – Theoretical prediction for the transmission spectrum at $t \simeq 100\ \mu$s (dashed line) and at $t \gg \tau$ (solid line).

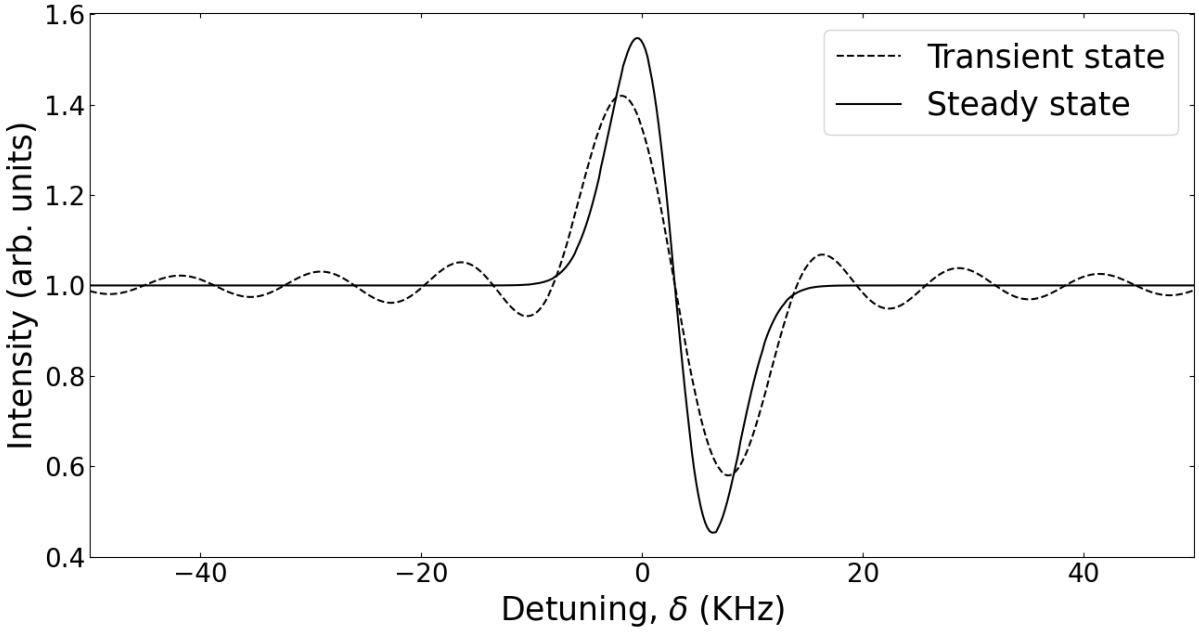

Source: (CAPELLA et al., 2022).

of the corresponding Doppler width, to find $\tau \approx 325\,\mu$s. This Doppler width is then directly responsible for the width of the stationary spectrum. Note that the RIR spectrum in Fig. 4 is broader for $t < \tau$, since it is then limited by the interaction time window itself.

We do not include any phenomenological homogeneous decay in our model, meaning that the stationary state is reached purely due to the inhomogeneous dephasing of the various atomic velocity groups. In order to highlight this property, we plot in Fig. 5 the time evolution of the transmission signal of a single velocity group (with $p_y = p_u$) versus the evolution of the ensemble of velocity groups, for a single detuning δ. The signal for a single velocity group should describe then a simple oscillation, while the signal for the ensemble reaches the usually observed stationary state.

3.2.1.2 Forward four-wave mixing.

Now, we can turn to the problem of obtaining the FFWM signal. To do so, we need to look at the contributions in the $2\vec{k}_e - \vec{k}_p$ direction. Those arise from the terms containing $\delta(\vec{p} - \vec{p}' + \hbar\Delta\vec{k} + \hbar\vec{k}_e) = \delta\Big(\vec{p} - \vec{p}' + \hbar(2\vec{k}_e - \vec{k}_p)\Big)$. Explicitly, we have:

Figure 5 – Transmission signal (black) and singled-out momentum component (upscaled) $p_y = p_u$, in orange. We use a detuning of $\delta = 200\,\mathrm{kHz}$.

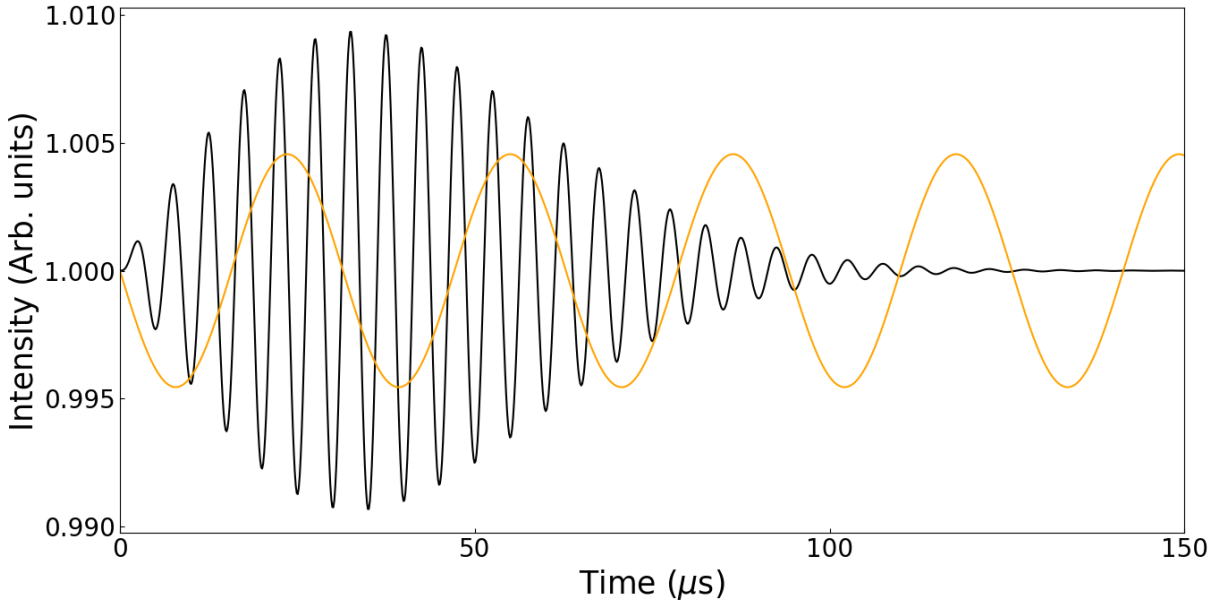

Source: (CAPELLA et al., 2022).

$$\rho_{12}^{FWM}(\vec{r},t) = \frac{\Omega\Omega_e(\hbar\, m\Delta k)}{\Delta_e(2\pi\hbar)^{\frac{3}{2}}p_u^2} e^{i\omega_e t} e^{-i(2\vec{k}_e-\vec{k}_p)\cdot\vec{r}} e^{-i\delta t} \times \int dp_y \left(1 - e^{i(\delta + p_y\frac{\Delta k}{m} + \hbar\frac{\Delta k^2}{2m})t}\right) \times \times \frac{e^{-\frac{p_y^2}{2p_u^2}} p_y}{\delta + p_y\frac{\Delta k}{m} + \hbar\frac{\Delta k^2}{2m}}. \quad (3.21)$$

The FFWM signal is then proportional to the modulus squared of $\rho_{12}^{FWM}(\vec{r},t)$, yielding the spectrum presented in Fig. 6. As we can see, the theory generates a symmetric spectrum with a peak at $\delta \approx 0$, which evolves in time. As with the structure in Fig. 4, the central peak becomes narrower as it approaches the stationary state. Fig. 6 also presents, in its inset, theoretical predictions for the FFWM signal evolution in time. These explicitly show the constructive interference resulting in the maximum of the central peak, and the oscillation coming from partial interference defining the values on the side of the peak.

The spectra shown here give the global behavior of the FFWM and transmission signals when continuously generated by the excitation and probe fields. A further study of how these spectra evolve in time will be given in Sec. 3.4. In practice, even though it is simpler to calculate and interpret the stationary states of the signals described above, it is quite common to be restricted to transient spectra in cold atoms. As the ensemble becomes colder, the times to reach the stationary state becomes longer and may become of the order of or even surpass

Figure 6 – Theoretical prediction for the FFWM spectrum at $t \simeq 100\ \mu$s (dashed line) and at $t \gg \tau$ (solid line). Inset: FFWM temporal evolution for $\delta = 0$ (black) and $\delta = \pm 8\,\mathrm{kHz}$ (orange).

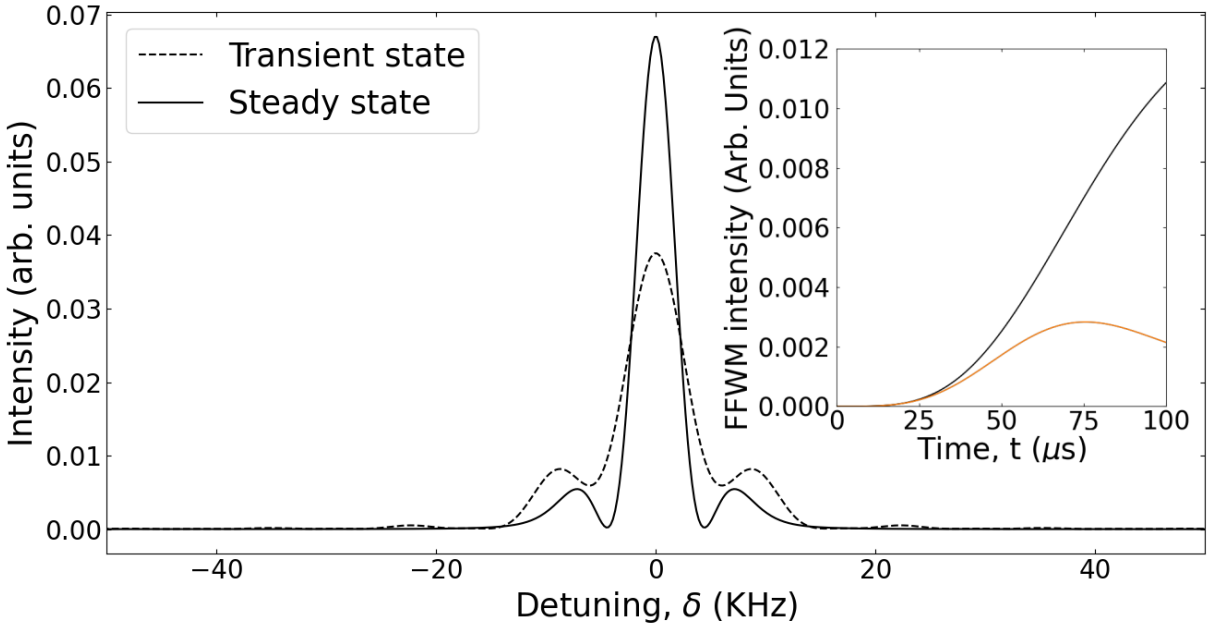

Source: (CAPELLA et al., 2022).

typical times for spurious optical pumping to any dark state in the system. This will be the case for the experiments described below.

3.2.2 The dark phase.

We now turn to the modeling of the dark phase, where no fields act on the atomic medium. From now on, we shall use $\rho^{\mathrm{I}}_{ij}(\vec{p},\vec{p}',t)$ for coherences and populations in the first (writing) phase of the theoretical model, $\rho^{\mathrm{II}}_{ij}(\vec{p},\vec{p}',t)$ for the second (dark) phase and $\rho^{\mathrm{III}}_{ij}(\vec{p},\vec{p}',t)$ for the third (reading) phase. Turning back to (3.10) and (3.9), and noting that turning off both fields means $\Omega_e = \Omega_p = \Omega = 0$, these equations simplify to:

$$\begin{aligned} \frac{d\rho^{\mathrm{II}}_{11}(\vec{p},\vec{p}',t)}{dt} &= i\Delta(\vec{p},\vec{p}')\,\rho^{\mathrm{II}}_{11}(\vec{p},\vec{p}',t)\,, \\ \sigma^{\mathrm{II}}_{12}(\vec{p},\vec{p}',t) &= 0, \end{aligned} \tag{3.22}$$

whose solution is:

$$\rho^{\mathrm{II}}_{11}(\vec{p},\vec{p}',t) = \rho^{\mathrm{I}}_{11}(\vec{p},\vec{p}',t_1)\,e^{i\Delta(\vec{p},\vec{p}')(t-t_1)}\,, \tag{3.23}$$

where we take $t = t_1$ as the instant in which the fields are turned off, and assume continuity of the solution throughout the process. We also get directly,

$$\rho^{\mathrm{II}}_{12}(\vec{p},\vec{p}',t) = 0, \tag{3.24}$$

which immediately tell us that we should expect no signals at all to be observed, as there is no optical polarisation. Although we may not be able to promptly measure it, equation (3.23) shows that in fact the information that was written in the first phase of the experiment is stored in the atomic medium, when we turn off the writing fields, in the form of coherences between different momentum states. All that is left to do now is the retrieval of this information.

Note that the model predicts that the reading results depend on the storage time because, in the dark period, the off-diagonal elements of the density matrix in the ground-state manifold all evolve with different frequencies, given by the various $\Delta(\vec{p},\vec{p}')$ when $\vec{p} \neq \vec{p}'$. Thus the evolution in the dark phase can be understood exactly as a free-induction decay, with $\Delta(\vec{p},\vec{p}')$ providing the free-evolution phases of the different energy states of the inhomogeneous system at finite temperature.

3.2.3 The reading phase.

In the reading phase, only the excitation field is turned on while the probe field stays off. This implies $\Omega_e \neq 0$ and $\Omega_p = \Omega = 0$. Equations (3.10) and (3.9) now lead to:

$$\begin{aligned} \frac{d\rho_{11}^{\mathrm{III}}(\vec{p},\vec{p}',t)}{dt} &= i\Delta(\vec{p},\vec{p}')\,\rho_{11}^{\mathrm{III}}(\vec{p},\vec{p}',t), \\ \sigma_{12}^{\mathrm{III}}(\vec{p},\vec{p}',t) &= \frac{\Omega_e}{\Delta_e}\,\rho_{11}^{\mathrm{III}}(\vec{p},\vec{p}'-\hbar\vec{k}_e,t). \end{aligned} \tag{3.25}$$

We already note that the time evolution for $\rho_{11}^{\mathrm{III}}(\vec{p},\vec{p}',t)$ does not change from the dark phase, that is, our coherences/populations seem to be unaffected by the reading process. The ground state coherences are only affected by the two-photon process, depending on Ω. This is the first sign of the robustness of the RIR based memory modeled here. We can solve for $\rho_{11}^{\mathrm{III}}(\vec{p},\vec{p}',t)$ directly, obtaining:

$$\rho_{11}^{\mathrm{III}}(\vec{p},\vec{p}',t) = \rho_{11}^{\mathrm{II}}(\vec{p},\vec{p}',t_2)e^{i\Delta(\vec{p},\vec{p}')(t-t_2)}. \tag{3.26}$$

But, note that:

$$\rho_{11}^{\mathrm{II}}(\vec{p},\vec{p}',t_2) = \rho_{11}^{\mathrm{I}}(\vec{p},\vec{p}',t_1)e^{i\Delta(\vec{p},\vec{p}')(t_2-t_1)}, \tag{3.27}$$

which then implies that:

$$\begin{aligned} \rho_{11}^{\mathrm{III}}(\vec{p},\vec{p}',t) &= \rho_{11}^{\mathrm{II}}(\vec{p},\vec{p}',t_2)e^{i\Delta(\vec{p},\vec{p}')(t-t_2)} \\ &= \rho_{11}^{\mathrm{I}}(\vec{p},\vec{p}',t_1)e^{i\Delta(\vec{p},\vec{p}')(t_2-t_1)}e^{i\Delta(\vec{p},\vec{p}')(t-t_2)} \\ &= \rho_{11}^{\mathrm{I}}(\vec{p},\vec{p}',t_1)e^{i\Delta(\vec{p},\vec{p}')(t-t_1)}. \end{aligned} \tag{3.28}$$

And consequently,

$$\sigma_{12}^{\mathrm{III}}(\vec{p},\vec{p}',t)=\frac{\Omega_e}{\Delta_e}\,\rho_{11}^{\mathrm{I}}(\vec{p},\vec{p}'-\hbar\vec{k}_e,t_1)e^{i\Delta(\vec{p},\vec{p}'-\hbar\vec{k}_e)(t-t_1)}, \tag{3.29}$$

for $t \geq t_2$. This is the main result of this section: our theoretical model shows in a very direct manner that the reading process does not destroy any information stored in the atomic medium and the retrieved signal is completely indifferent to the moment $t = t_2$ at which the reading process begins and depends only on the time frame of the writing phase, t_1. In this way, we provide a theoretical picture that explains the core experimental observations reported in (ALMEIDA et al., 2016). We now proceed to take a closer look at each mode generated from the atomic memory.

3.2.3.1 Retrieved transmission signal.

Using eq. (3.14), we may write:

$$\begin{aligned}\sigma_{12}^{\mathrm{III}}(\vec{p},\vec{p}',t)=\frac{\Omega_e}{\Delta_e}\,e^{i\Delta(\vec{p},\vec{p}'-\hbar\vec{k}_e)(t-t_1)}\Big\{&\rho_{11}^{0}(\vec{p})\delta(\vec{p}-\vec{p}'+\hbar\vec{k}_e)\\ -\Omega\Big[&\rho_{11}^{\mathrm{I(p)}}(\vec{p},\vec{p}'-\hbar\vec{k}_e,t_1)\;\delta(\vec{p}-\vec{p}'-\hbar\Delta\vec{k}+\hbar\vec{k}_e)-\\ -&\rho_{11}^{\mathrm{I(FWM)}}(\vec{p},\vec{p}'-\hbar\vec{k}_e,t_1)\;\delta(\vec{p}-\vec{p}'+\hbar\Delta\vec{k}+\hbar\vec{k}_e)\Big]\Big\},\end{aligned} \tag{3.30}$$

where we defined:

$$\begin{aligned}\rho_{11}^{\mathrm{I(p)}}(\vec{p},\vec{p}',t_1)&=\frac{1}{-\delta+\Delta(\vec{p},\vec{p}')}\times\left(e^{i\delta t_1}-e^{i\Delta(\vec{p},\vec{p}')t_1}\right)\left(\rho_{11}^{0}(\vec{p})-\rho_{11}^{0}(\vec{p}-\hbar\Delta\vec{k})\right),\\ \rho_{11}^{\mathrm{I(FWM)}}(\vec{p},\vec{p}',t_1)&=\frac{1}{\delta+\Delta(\vec{p},\vec{p}')}\times\left(e^{-i\delta t_1}-e^{i\Delta(\vec{p},\vec{p}')t_1}\right)\left(\rho_{11}^{0}(\vec{p})-\rho_{11}^{0}(\vec{p}+\hbar\Delta\vec{k})\right).\end{aligned} \tag{3.31}$$

These will generate, respectively, the retrieved signal in the direction of the probe field and in the FFWM direction. The component in the probe direction of the local optical coherence is then given by:

$$\rho_{12}^{\mathrm{III(p)}}(\vec{r},t)=-\frac{\Omega\Omega_e}{\Delta_e(2\pi\hbar)^{\frac{3}{2}}}e^{i\omega_e t}e^{-i\vec{k}_p\cdot\vec{r}}\times\int d\vec{p}\,e^{i\Delta(\vec{p},\vec{p}-\hbar\Delta\vec{k})(t-t_1)}\rho_{11}^{\mathrm{I(p)}}(\vec{p},\vec{p}-\hbar\Delta\vec{k},t_1), \tag{3.32}$$

with the measured signal being proportional to the modulus squared of $\rho_{12}^{\mathrm{III(p)}}(\vec{r},t)$. The solid curves in Fig. 7 presents the theoretical spectra (panel a) and temporal evolutions (panel b) of the retrieved probe signal. Note that the spectra of the retrieved probe beam is now a peak, similarly to the continuously-generated FFWM spectra, as they are generated from similarly excited coherences between external momentum states of the atoms. Moreover, the temporal

evolution reveals a decay much shorter than the time to reach the stationary state in the writing process for these same conditions (Fig. 4). The time of tens of microseconds for the decay is related to the diffusion time of atoms between fringes of the coherence grating printed in the ensemble, as already pointed out in (ALMEIDA et al., 2016).

3.2.3.2 Retrieved FFWM signal.

Now, it is straightforward to obtain the retrieved FFWM signal. In fact, we may write the FFWM-component of the local optical coherence as:

$$\rho_{12}^{\mathrm{III(FWM)}}(\vec{r},t) = -\frac{\Omega\Omega_e}{\Delta_e(2\pi\hbar)^{\frac{3}{2}}} e^{i\omega_e t} e^{-i(2\vec{k}_e-\vec{k}_p)\cdot\vec{r}} \times \int d\vec{p}\, e^{i\Delta(\vec{p},\vec{p}+\hbar\Delta\vec{k})(t-t_1)} \rho_{11}^{\mathrm{I(FWM)}}(\vec{p},\vec{p}+\hbar\Delta\vec{k},t_1). \tag{3.33}$$

The measured signal is then also given by the modulus squared of $\rho_{12}^{\mathrm{III(FWM)}}(\vec{r},t)$, which generates the spectrum shown by the dashed line in Fig. 7. Note the peak at $\delta \approx 0$ and it's symmetric structure, just as the spectrum in the probe direction. We may also investigate the time profile of this signal and we note again the similarities between the signals in the FFWM and probe directions. As we pointed out above, this is no coincidence: our theory shows that these signals originate from the same process and have the same behavior. The only differences we saw in the writing phase were due to the manner in which we observed each signal. In the reading phase, the measurements are performed the same way in both directions, and the differences we once observed vanish. Figure 7 explicits this behavior.

Figure 7 – (a) Theoretical spectra for the signals in the probe and FFWM direction, taken at $t = 133\,\mu s$ considering $t_1 = 102\,\mu s$ and $t_2 = 107\,\mu s$, which corresponds to a reading time of about $26\,\mu s$. (b) Theoretical time profiles for the signals in the probe and FFWM direction for (from top to bottom): $\delta \approx 0$ and $\delta \approx \pm 8\,\mathrm{kHz}$. Note that the last two are superimposed due to the symmetric nature of the spectrum.

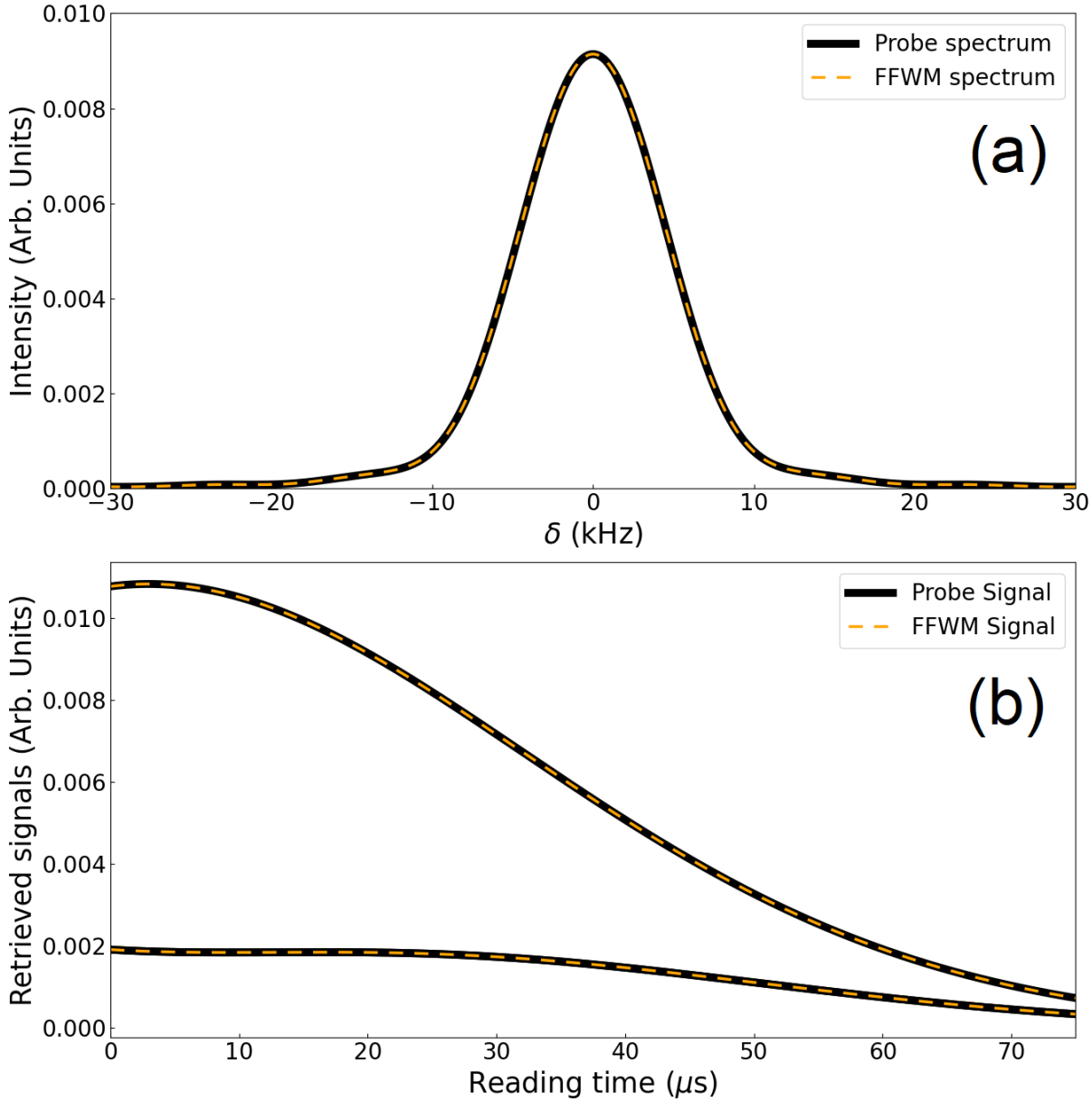

Source: (CAPELLA et al., 2022).

3.3 EXPERIMENT AND RESULTS

In order to test the validity of the previously developed theory, A. M. G. de Melo, J. P. Lopez and J. W. R. Tabosa have also investigated experimentally the probe transmission and FFWM spectra, both during the writing and reading phases, and in the transient and close to the steady state regimes. They used a cloud of cold cesium atoms with a temperature of hundreds

of μK and an on-resonance optical density of about 3, obtained from a magneto-optical trap (MOT). The experiment is performed in the absence of the trapping and repumping beams as well as the MOT quadrupole magnetic field, with the trapping beams and the quadrupole magnetic field being switched off $1\,\mathrm{ms}$ before the repumping beam in order to pump the atoms into the hyperfine $6S_{1/2}(F=4)$ ground state. The residual magnetic field is compensated by three pairs of independent Helmholtz coils, whose current is adjusted by using a microwave spectroscopic technique (ALMEIDA et al., 2016), which allows the residual field to be reduced to less than $10\,\mathrm{mG}$. The simplified experimental scheme is shown in Fig. 8(a). All the beams are provided by an external-cavity diode laser locked, using a saturated absorption signal, to the cesium closed transition $6S_{1/2}(F=4) \rightarrow 6P_{3/2}(F'=5)$. The excitation beam (E) and the probe beam (P) have the same circular polarization and their directions form a small angle of $\theta = 1$. The amplitude and frequency of beams E and P are controlled by independent acousto-optic modulators (AOMs). The frequency of the excitation beam is red-detuned by $6\Gamma \approx 30\,\mathrm{MHz}$ from the transition $(F=4) \rightarrow (F'=5)$, while the frequency of the probe beam is scanned around the frequency of the excitation beam. The probe transmission and the generated FFWM intensities are detected by fast photodetectors. The time sequence of the experiment is shown in Fig. 8(b). The excitation and probe beams are kept on for a period of $100\,\mu\mathrm{s}$ during the writing phase and then they are both turned off for a controlled period of time, $\tau_S = t_2 - t_1$. After this storage phase, the excitation beam E is turned back on to retrieve both the probe and the FFWM beams, which are detected by the same pair of photodetectors.

In the experiment, for a given excitation-probe frequency detuning δ, we record the signals propagating along the directions of the incident probe beam and the generated FFWM beam, both in the writing and reading phases. In Fig. 9 we show these signals as a function of time for excitation-probe detunings of $\delta \approx -8\,\mathrm{kHz}$, $\delta \approx 0\,\mathrm{kHz}$, and $\delta \approx +8\,\mathrm{kHz}$, respectively. In panels (a) and (c), we plot the curves for the writing period of $100\,\mu\mathrm{s}$. In panels (b) and (d), the time evolutions are plotted for a reading period of $75\,\mu\mathrm{s}$ after a storage period of $\tau_S = 5\,\mu\mathrm{s}$. The power of the excitation and probe beams are equal to $50\,\mu\mathrm{W}$ and $1\,\mu\mathrm{W}$, respectively.

First, we should note that the probe transmission signal indeed corresponds to the measurement of the imaginary part of the nonlinear susceptibility, while the FFWM signal is a measure of its squared modulus. Explicitly, consider the probe field given by the electric field E_p. For an optically thin sample, the resulting field E_{out} can be written as:

$$E_{out} = E_p + i\frac{\beta}{2c\epsilon_0}P, \tag{3.34}$$

where β is a real constant dependent on the atomic density and the length of the sample and P is the component of the complex polarization in the probe direction (CRUZ et al., 2007). The resulting intensity in the probe direction as measured by the photodetector, is then:

$$\begin{aligned}
\left|E_p + i\frac{\beta}{2c\epsilon_0}P\right|^2 &= |E_p|^2 + \frac{\beta^2}{4c^2\epsilon_0^2}|P|^2 - i\frac{\beta}{2c\epsilon_0}E_pP^* + i\frac{\beta}{2c\epsilon_0}E_p^*P \\
&= |E_p|^2 - i\frac{\beta}{2c\epsilon_0}\Big(\underbrace{E_pP^* - (E_pP^*)^*}_{2i\,\mathrm{Im}\{E_pP^*\}}\Big) \\
&= |E_p|^2 + \frac{\beta}{c\epsilon_0}\mathrm{Im}\Big\{E_pP^*\Big\} \\
&= |E_p|^2 + \frac{\beta}{c\epsilon_0}\mathrm{Im}\Big\{\Big(\mathrm{Re}\{E_p\} + i\mathrm{Im}\{E_p\}\Big)\Big(\mathrm{Re}\{P\} - i\mathrm{Im}\{P\}\Big)\Big\} \\
&= |E_p|^2 - \frac{\beta}{c\epsilon_0}\mathrm{Re}\{E_p\}\mathrm{Im}\{P\} + \frac{\beta}{c\epsilon_0}\mathrm{Im}\{E_p\}\mathrm{Re}\{P\} \\
&= |E_p|^2 - \frac{\beta}{c\epsilon_0}E_p\mathrm{Im}\{P\}, \qquad (3.35)
\end{aligned}$$

where we used the fact that $\frac{\beta^2}{4c^2\epsilon_0^2}|P|^2 \ll |E_p|^2$ and, in the last line, that the probe field is real. Therefore, the detector placed along the probe direction measures a plateau due to the term $|E_p|^2$ and any deviations from this plateau is due to the imaginary part of the polarization multiplied by the incident probe field amplitude. For the detector on the FFWM direction, however, there is no incident field other than the generated FFWM signal itself, which is due entirely to the induced polarization, and thus, the signal is proportional to the modulus squared of the component of polarization along the FFWM direction. Therefore, in the frame (a) of Fig. 9 we have normalized the measured probe transmission signal by the incident probe intensity. The retrieval of the probe and FFWM signals in the reading phase demonstrates the information on these beams have been stored in the atomic ensemble. As can be observed in panels (a) and (c), both the probe transmission and the generated FFWM signals present a transient regime strongly dependent of the excitation-probe detuning. This effect have already been observed on previous RIR experiments for the transmitted probe (GUIBAL et al., 1996). Our results show the same transient regime is also present in the generated FFWM signal. Nevertheless, all the signals reach a stationary regime even in the absence of any homogeneous decay rate as predicted by the developed theoretical model. It is also worth noting that both the retrieved signals, at the beginning of the reading phase, are always maximum for zero detuning, with their decays coming from the atomic motion, as we have already reported in (ALMEIDA et al., 2016). The amplitudes measured for the retrieved signals along the probe and FFWM directions have the same order of magnitude, but the signal in the direction of

the probe beam is still larger by a factor of four. Our theoretical analysis predicts the same amplitudes for the retrieved signals, and presently we do not fully understand this discrepancy. One possible cause could be a larger sensitivity of the FFWM signal to the phase matching conditions in the system, with beams of finite transversal dimensions.

Figure 8 – (a): Simplified experimental beams configuration to observe the RIR and the FFWM signals. (b): Time sequence specifying the writing, storage and reading phases. AOM: acousto-optic modulator; PMF: polarization maintaining fiber; PBS: polarizing beam splitter; $\lambda/2$: half waveplate; $\lambda/4$: quarter waveplate; PD: photodetector.

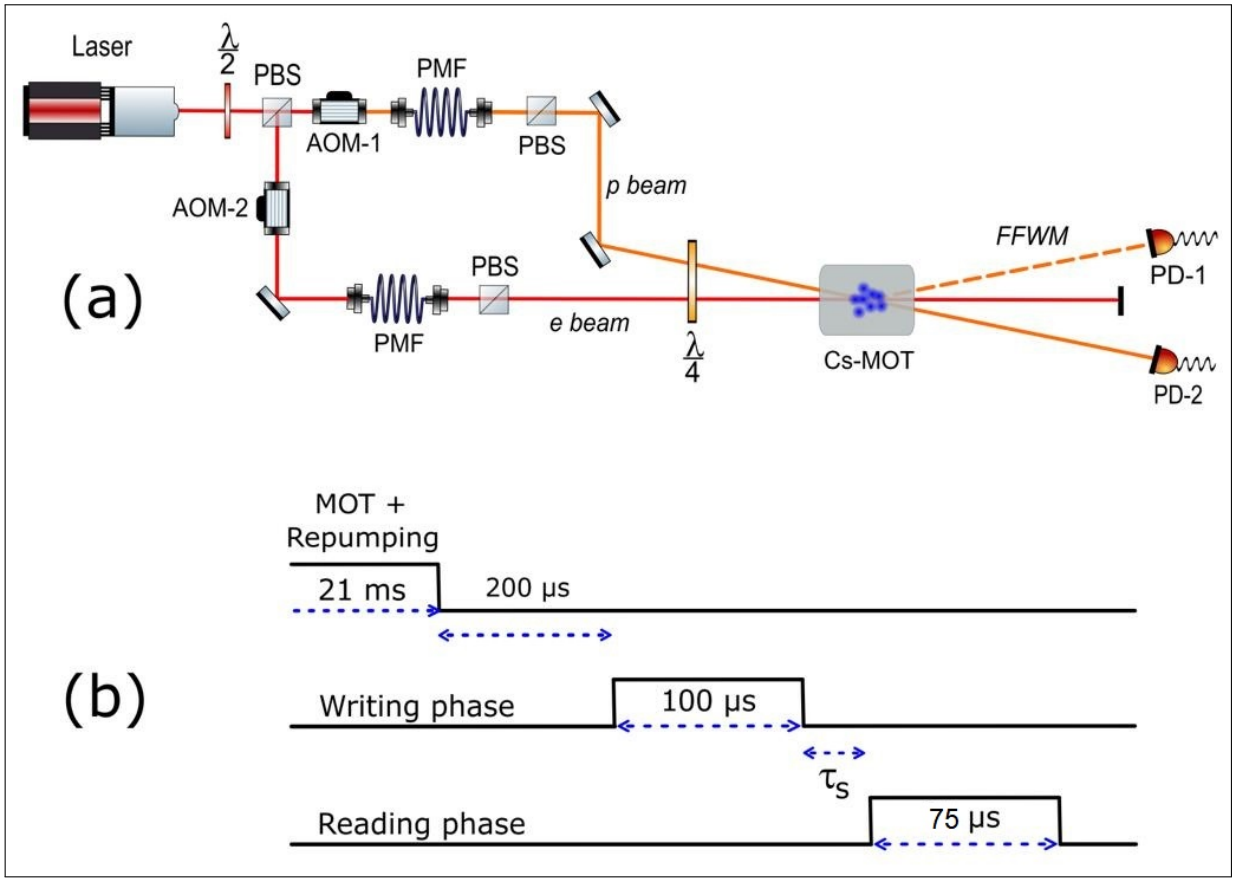

Source: (CAPELLA et al., 2022).

Figure 10 shows the measured signal intensity spectra. The intensities are measured at the end of the writing phase and at the beginning of the reading phase. We clearly see that the retrieved spectra for the signal propagating along the directions of the probe and the FFWM beams have essentially the same spectral width as the corresponding signals in the writing phase, which evidentiates they are determined by the same physical mechanism. We may also note the similar structure of the spectra predicted by the theoretical model introduced in section II.

Figure 9 – Time evolution of the probe transmission and the generated FFWM beams during the writing, (a) and (c), and the reading, (b) and (d), phases for $\delta \approx -8\,\mathrm{kHz}$ (orange), $\delta \approx 0\,\mathrm{kHz}$ (black) and $\delta \approx +8\,\mathrm{kHz}$ (red). In (a) we have normalized the associated signal by the intensity of the incident probe, as explained in the text.

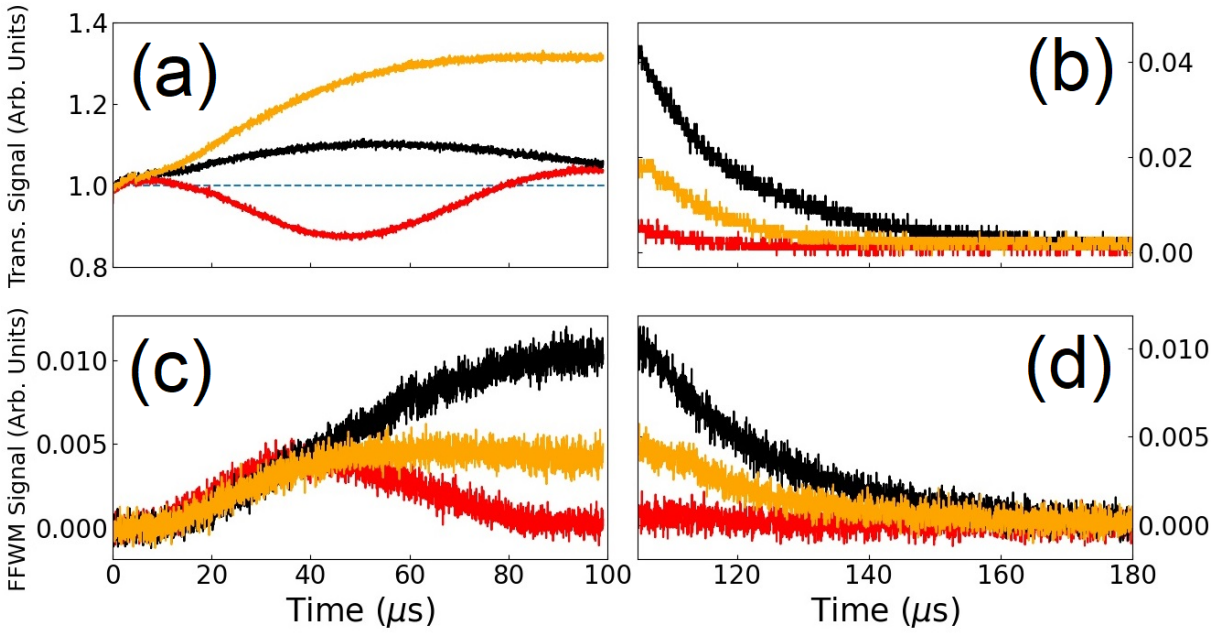

Source: (CAPELLA et al., 2022).

Figure 10 – Measured spectra for the probe transmission in (a) the end of the writing phase and (b) the beginning of the reading phase, and corresponding spectra for the FFWM in the (c) writing and (d) reading phases.

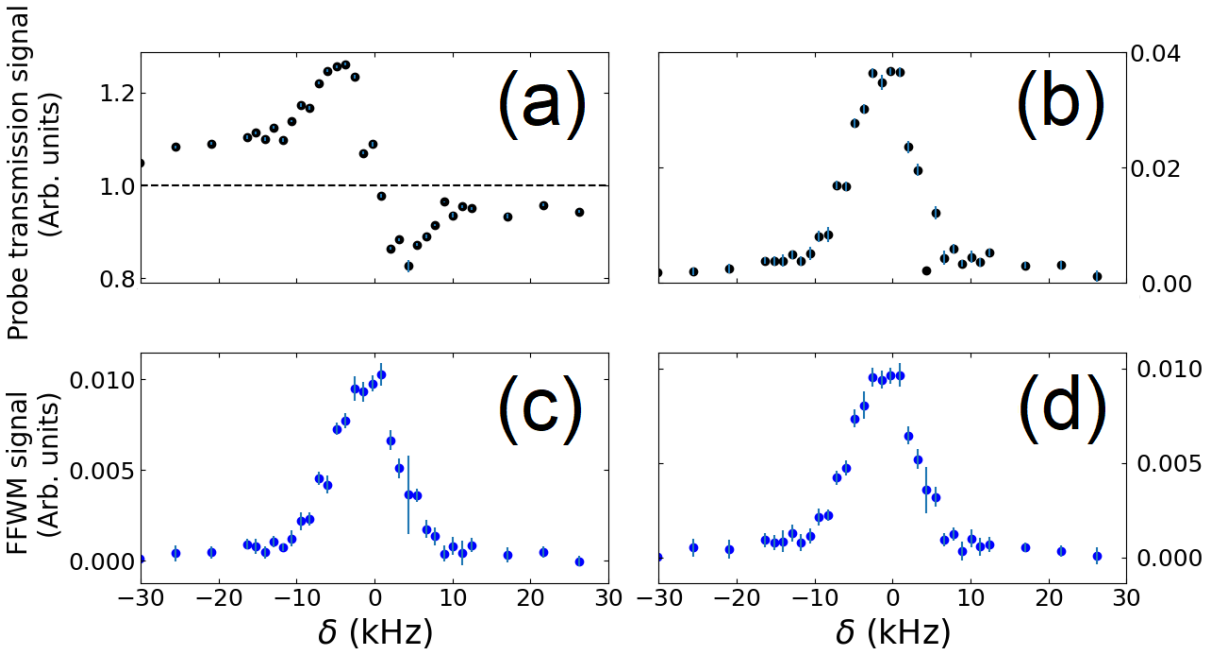

Source: (CAPELLA et al., 2022).

3.4 DISCUSSIONS

In this section, we aim to provide at first a global comparison between the theoretical model predictions and the experimental results. Secondly, we study the time profiles of these signals and delve into the limits of our theoretical model. During the writing phase of the experiment, we expect a progressive establishment of coherence between different momentum states which translates into a transient dynamics of the measured spectra that converges to a stationary shape. During the reading phase, the loss of coherence due to atomic motion implies that the shape of the measured spectra is only slightly time-dependent. In order to achieve the first goal of this section, we obtain the time evolution of the linewidths of each signal (for the writing and reading phases). The signal's linewidths (for the probe transmission signal the linewidth is defined as the frequency separation between the gain and attenuation peaks $\delta_{RIR} = \omega_{att} - \omega_{gains}$) in the writing phase are strongly dependent on the time we perform the measurement. For very short times, the widths are large and Fourier limited, evolving to stationary values for long times. This behavior was verified experimentally as shown in Fig 11(a) and is in reasonable agreement with the predictions of the developed theory as shown in Fig. 11(b). We note that the build up of coherence makes the measured spectra sharper in time. As it was demonstrated previously in (MEACHER et al., 1994) the stationary value of the probe transmission signal linewidth is determined by the temperature of the atomic ensemble. Therefore, our results suggest a new way to measure the temperature of the atoms through the measurement of the linewidth of the FFWM signal, which is background free. Figures 11(c) and 11(d) show the experimental and theoretical time evolutions for the retrieved linewidths, which theoretically get larger in time. One should note that an experimental observation of this dynamics becomes very limited by noise for longer times. Despite the good global agreement, the theoretical model does not show any difference between the probe and FFWM linewidths in the reading phase, even though the experiment shows a slight difference of about $1\,\mathrm{kHz}$.

A closer look at the theoretical time profiles of the signals provided in Fig. 12 shows some limitations of our model. In fact, comparing Figs. 9(a) and 9(c) to Figs. 12(a) and 12(c), for example, we note that the experimental signals are noticeably more asymmetric than the theoretical ones. More importantly, Figures 9(b) and 9(d) show experimental decay times lower than the ones predicted by our theory, and the shape of the experimental signal follows a more exponential-like decay than a Gaussian-like one, as given by our theoretical model. In Ref. (ALMEIDA et al., 2016), however, the authors had previously reported a curve correspon-

Figure 11 – (a): Experimental temporal evolution of the spectral width of the probe transmission spectrum (frequency separation between the gain peak and the attenuation trough $\delta_{RIR} = \omega_{att} - \omega_{gain}$) and the full width at half maximum of the generated FFWM spectrum measured in the writing phase. (b): Theoretical curves corresponding to (a). (c): Experimental temporal evolution of the spectral full width at half maximum of the retrieved FFWM and transmission spectrum measured in the reading phase. (d): Theoretical curves corresponding to (c).

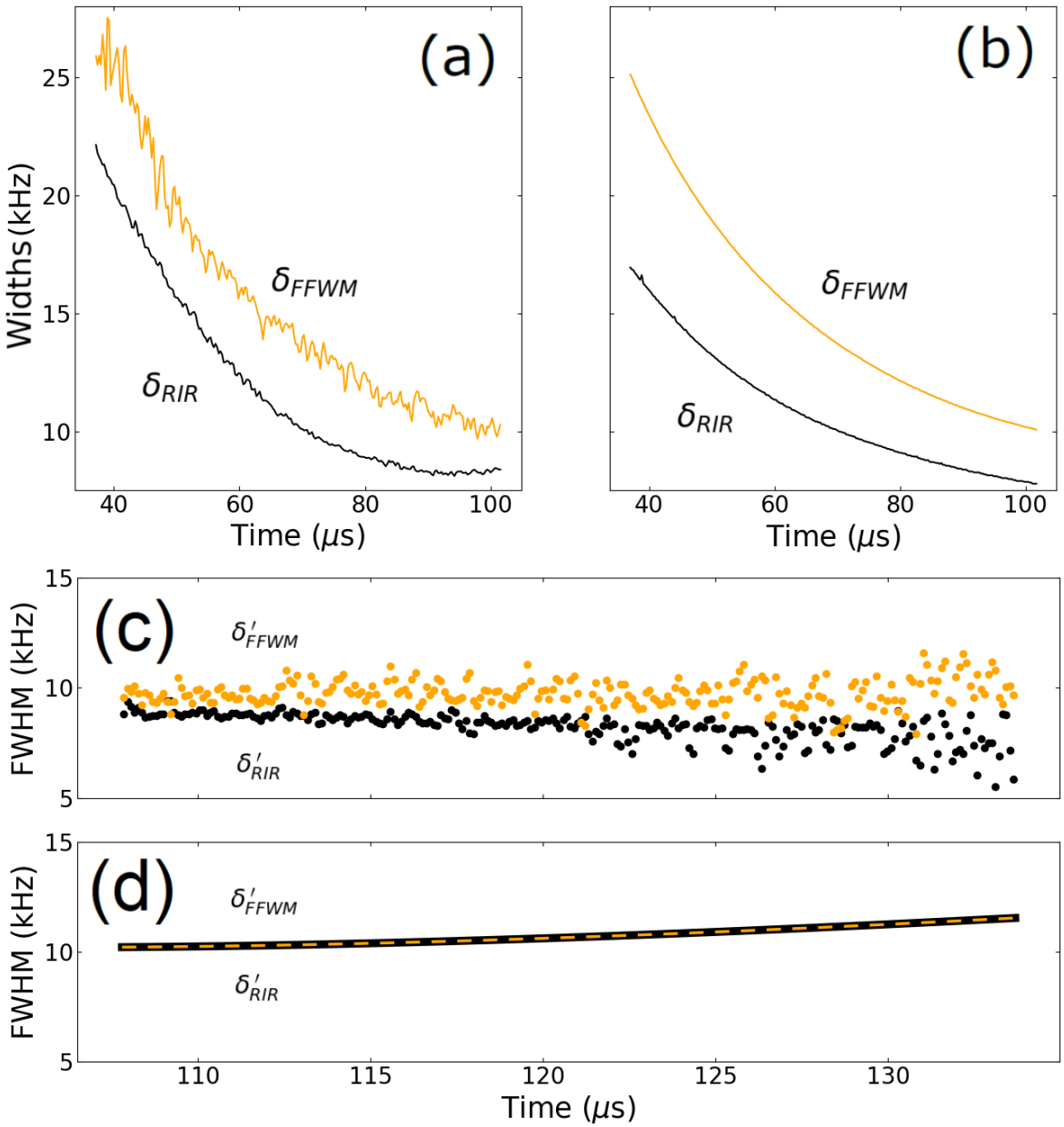

Source: (CAPELLA et al., 2022).

ding to Fig. 9(b) that followed more a Gaussian-like shape. In our view, this discrepancy may result from different structures of the residual magnetic field in the experimental apparatus. For example, if the residual field contains a larger component perpendicular to the propagation direction, it may remove more frequently atoms from the cycling transition. We could then introduce this mechanism as a simple exponentially decaying depletion of atoms that partici-

pate in the process. In this chapter, however, we opted not to introduce any phenomenological modification of the theory, in order to highlight the limits of our first-principles approach. Additional effects such as induced heating of the atomic ensemble by the interacting fields are also not included in our theoretical model but could play a role in the time dynamics, as already pointed out in (ALMEIDA et al., 2016).

Figure 12 – Theoretical time evolution of the probe transmission signal in the (a) writing and (b) reading phases. Generated FFWM signals during the (c) writing and (d) reading phases for: $\delta \approx -8\,\mathrm{kHz}$ (orange), $\delta \approx 0\,\mathrm{kHz}$ (black) and $\delta \approx 8\,\mathrm{kHz}$ (red).

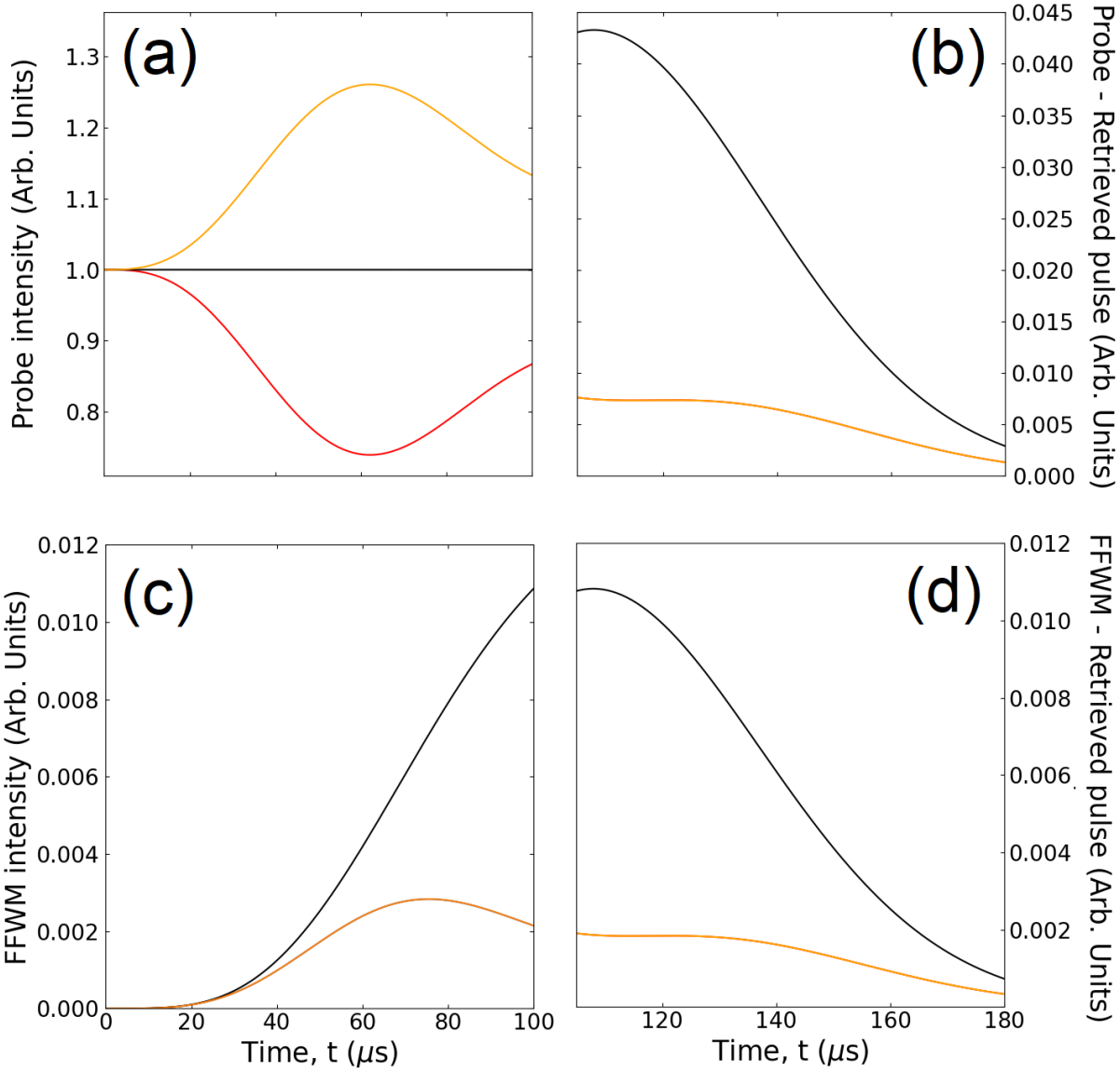

Source: (CAPELLA et al., 2022).

4 ENTANGLEMENT IN WEISSKOPF-WIGNER THEORY OF SPONTANEOUS DECAY

In the present chapter, we aim to use the Weisskopf-Wigner theory for spontaneous emission to understand how entanglement arises and how it can be minimized by a suitable choice of atomic momentum uncertainty. Moreover, we investigate the physical mechanisms behind the creation of entanglement and briefly discuss its physical implications in the distinguishability of two paradigmatic quantum states that arise from the theory.

4.1 WEISSKOPF-WIGNER THEORY FOR SPONTANEUS EMISSION

In this section we summarize the Weisskopf-Wigner model for spontaneous decay (WEISSKOPF; WIGNER, 1930) following the theoretical picture proposed by (RZAZEWSKI; ZAKOWICZ, 1992) which takes into account the atomic external degrees of freedom. More precisely, we model the atom as a wave-packet in momentum space.

Consider a two-level atom initially excited, interacting with the vacuum of the electromagnetic field. The Hamiltonian of the system may be written as

$$\hat{H} = \hat{H}_A + \hat{H}_F + \hat{V}_I, \tag{4.1}$$

where $\hat{H}_A, \hat{H}_F$, and $\hat{V}_I$ refer to the free Hamiltonian of the atom, the free Hamiltonian of the electromagnetic field, and the interaction potential, respectively. Explicitly, we have for the free Hamiltonians:

$$\begin{aligned} \hat{H}_A &= \frac{\hat{\mathbf{P}}^2}{2m} + \sum_{j=1}^{2} E_j \left|j\right\rangle\!\left\langle j\right| = \frac{\hat{\mathbf{P}}^2}{2m} + \frac{\hbar\omega_0}{2}\hat{\sigma}_z, \\ \hat{H}_F &= \sum_l \hbar\omega_{\vec{k}} \left(\hat{a}_l^\dagger \hat{a}_l + \frac{\mathbb{1}}{2}\right), \end{aligned} \tag{4.2}$$

where $\hat{\mathbf{P}}$ is the linear momentum operator of the atom, $E_j = \pm\frac{\hbar\omega_0}{2}$ are the energies associated with the atomic internal degrees of freedom, $\{|1\rangle, |2\rangle\}$, $l = (s, \vec{k})$ accounts simultaneously for the polarization and wave vector variables, $\hat{a}_l$ denotes the annihilation operator of a $(s, \vec{k})$ mode of the electromagnetic field with angular frequency $\omega_{\vec{k}}$, and $\hat{\sigma}_+$ is the raising operator in the internal atomic degrees of freedom. The interaction potential reads:

$$\hat{V}_I = \hbar \sum_l g_l^{ab} e^{i\vec{k}\cdot\hat{\mathbf{r}}}\, \hat{a}_l\, \hat{\sigma}_+ + h.c.\,, \tag{4.3}$$

where g_l^{ab} is the coupling constant given by:

$$g_l^{ab} = -\frac{i}{\hbar}\sqrt{\frac{\hbar\omega_k}{2\epsilon_0 V}}\vec{\mu}_{ab}\cdot\hat{e}_l\, e^{i\vec{k}_l\cdot\vec{r}_0}, \tag{4.4}$$

with $\vec{\mu}_{ab} = \langle a|e\hat{\mathbf{r}}|b\rangle$ the dipole moment of the interaction. In order to simplify the time evolution of our system, we can use the interaction Hamiltonian in the interaction picture:

$$\hat{V}_I' = e^{i\hat{H}_0 t/\hbar}\hat{V}_I e^{-i\hat{H}_0 t/\hbar}, \tag{4.5}$$

where $\hat{H}_0$ corresponds to the free Hamiltonian contributions of the atom and the field $\hat{H}_0 = \hat{H}_A + \hat{H}_F$:

$$\hat{H}_0 = \frac{\hat{\mathbf{P}}^2}{2m} + \frac{\hbar\omega_0}{2}\hat{\sigma}_z + \sum_l \hbar\omega_{\vec{k}}\hat{a}_l^\dagger\hat{a}_l, \tag{4.6}$$

where we neglected the zero-point energy of the electromagnetic field. After extensive use of the Baker-Campbell-Hausdorff formula (2.14), the interaction Hamiltonian reads:

$$\hat{V}_I' = \hbar\sum_l g_l^{ab} e^{i\frac{\hat{p}^2}{2m\hbar}t} e^{i\vec{k}\cdot\hat{\mathbf{r}}} e^{-i\frac{\hat{p}^2}{2m\hbar}t}\hat{a}_l e^{-i\omega_{\vec{k}}t} e^{i\omega_0 t}\hat{\sigma}_+ + h.c.\,. \tag{4.7}$$

For the sake of simplicity, from now on we omit the prime symbol. Nevertheless, unless explicitly mentioned, we are still treating our problem in the interaction picture. It is reasonable to assume the following form for the state of the system throughout time evolution:

$$|\psi(t)\rangle = \int \mathrm{d}\vec{p}\; c_0(\vec{p},t)\,|1\rangle_A\,|\vec{p}\rangle_E\,|0\rangle_F + \sum_l \int \mathrm{d}\vec{p}\; c_l(\vec{p},t)\,|0\rangle_A\,|\vec{p}\rangle_E\,|1_l\rangle_F\,, \tag{4.8}$$

where $|j\rangle_A$ indicates the atomic internal j-th eigen-state, $|\vec{p}\rangle_E$ the linear momentum state associated with the atom and $|m_l\rangle_F$, the Fock state related to the $\vec{k}$ mode of the electromagnetic field (note that we momentarily disregard the polarization of the photon, but it will return in a later discussion). Now we turn our attention to calculate the coefficients $c_0(\vec{p},t)$ and $c_l(\vec{p},t)$, which represent respectively the amplitude of probability of the atom *not* emitting a photon and the atom emitting a photon with state $l = (\vec{k},s)$. First of all, let's find a reduced form for the exponentials involving position and momentum operators in eq.(4.7). We can write:

$$e^{i\frac{\hat{p}^2}{2m\hbar}t} e^{i\vec{k}\cdot\hat{\mathbf{r}}} e^{-i\frac{\hat{p}^2}{2m\hbar}t} = \int \mathrm{d}\vec{p}\; e^{\frac{i}{2m\hbar}\left(\left|\vec{p}+\hbar\vec{k}\right|^2-|\vec{p}|^2\right)t}\left|\vec{p}+\hbar\vec{k}\right\rangle\!\left\langle\vec{p}\,\right|, \tag{4.9}$$

where we used the fact that: $e^{i\vec{p}_1\cdot\hat{\mathbf{r}}/\hbar}\,|\vec{p}_2\rangle = |\vec{p}_1+\vec{p}_2\rangle$. The interaction Hamiltonian then reduces to:

$$\hat{V}_I = \hbar\sum_l \int \mathrm{d}\vec{p}\; g_l^{ab} e^{i(\omega_0-\omega_{\vec{k}})t} e^{\frac{i}{2m\hbar}\left(\left|\vec{p}+\hbar\vec{k}\right|^2-|\vec{p}|^2\right)t}\hat{\sigma}_+\hat{a}_l\left|\vec{p}+\hbar\vec{k}\right\rangle\!\left\langle\vec{p}\,\right| + h.c.\,. \tag{4.10}$$

In this expression we can see the effect of the interaction: as the atom decays to the ground state, a quanta is created in the mode $\vec{k}$ of the electromagnetic field (energy conservation) and the atom suffers a recoil in the opposite direction of the emitted photon (linear momentum conservation). We are now in a good position to begin considering the time evolution of our system. Schrödinger's equation in the interaction picture (that is, the time evolution of a ket in the interaction picture $|\psi(t)\rangle_I$), is given by:

$$i\hbar\frac{\partial}{\partial t}|\psi(t)\rangle_I = \hat{V}_I|\psi(t)\rangle_I \ , \tag{4.11}$$

where we will drop the subscript "I" for the state ket and assume that (4.8) is written in the interaction picture. We now look at each side of eq.(4.11) separately and note that we can write the right hand side (RHS) of eq.(4.11) as:

$$\begin{aligned}\hat{V}_I|\psi(t)\rangle &= \hbar\sum_l\int \mathrm{d}\vec{p}\ g_l^{ab}e^{i(\omega_0-\omega_{\vec{k}})t}e^{\frac{i}{2m\hbar}\left(\left|\vec{p}+\hbar\vec{k}\right|^2-|\vec{p}|^2\right)t}\ c_l(\vec{p},t)\,|1\rangle_A\left|\vec{p}+\hbar\vec{k}\right\rangle_E|0\rangle_F + \\ &+ \hbar\sum_l\int \mathrm{d}\vec{p}\ g_l^{ab*}e^{-i(\omega_0-\omega_{\vec{k}})t}e^{\frac{i}{2m\hbar}\left(\left|\vec{p}-\hbar\vec{k}\right|^2-|\vec{p}|^2\right)t}\ c_0(\vec{p'},t)\,|0\rangle_A\left|\vec{p}-\hbar\vec{k}\right\rangle_E|1_l\rangle_F\,.\end{aligned} \tag{4.12}$$

On the other hand, the left hand side (LHS) reads:

$$\frac{\partial}{\partial t}|\psi(t)\rangle = \int \mathrm{d}\vec{p}\ \frac{\partial c_0(\vec{p},t)}{\partial t}|1\rangle_A|\vec{p}\rangle_E|0\rangle_F + \sum_l\int \mathrm{d}\vec{p}\ \frac{\partial c_l(\vec{p},t)}{\partial t}|0\rangle_A|\vec{p}\rangle_E|1_l\rangle_F\,. \tag{4.13}$$

Therefore, the time evolution of the state of the system is given by:

$$\begin{aligned}&i\int \mathrm{d}\vec{p}\ \frac{\partial c_0(\vec{p},t)}{\partial t}|1\rangle_A|\vec{p}\rangle_E|0\rangle_F + i\sum_l\int \mathrm{d}\vec{p}\ \frac{\partial c_l(\vec{p},t)}{\partial t}|0\rangle_A|\vec{p}\rangle_E|1_l\rangle_F = \\ &\quad= \sum_l\int \mathrm{d}\vec{p}\ g_l^{ab}e^{i(\omega_0-\omega_{\vec{k}})t}e^{\frac{i}{2m\hbar}\left(\left|\vec{p}+\hbar\vec{k}\right|^2-|\vec{p}|^2\right)t}\ c_l(\vec{p},t)\,|1\rangle_A\left|\vec{p}+\hbar\vec{k}\right\rangle_E|0\rangle_F + \\ &\quad+\sum_l\int \mathrm{d}\vec{p}\ g_l^{ab*}e^{-i(\omega_0-\omega_{\vec{k}})t}e^{\frac{i}{2m\hbar}\left(\left|\vec{p}-\hbar\vec{k}\right|^2-|\vec{p}|^2\right)t}\ c_0(\vec{p'},t)\,|0\rangle_A\left|\vec{p}-\hbar\vec{k}\right\rangle_E|1_l\rangle_F\,.\end{aligned} \tag{4.14}$$

Projecting eq.(4.14) onto $\langle 1|_A\langle\vec{p}\,|_E\langle 0|_F$, we get:

$$i\ \frac{\partial c_0(\vec{p},t)}{\partial t} = \sum_l\ g_l^{ab}e^{i(\omega_0-\omega_{\vec{k}})t}e^{\frac{i}{2m\hbar}\left(|\vec{p}|^2-\left|\vec{p}-\hbar\vec{k}\right|^2\right)t}\ c_l(\vec{p}-\hbar\vec{k},t). \tag{4.15}$$

Now we proceed to project eq.(4.14) onto $\langle 0|_A\left\langle\vec{p}-\hbar\vec{k}\ \right|_E\langle 1_l|_F$, obtaining:

$$i\ \frac{\partial c_l(\vec{p}-\hbar\vec{k},t)}{\partial t} = g_l^{ab*}e^{-i(\omega_0-\omega_{\vec{k}})t}e^{\frac{i}{2m\hbar}\left(\left|\vec{p}-\hbar\vec{k}\right|^2-|\vec{p}|^2\right)t}\ c_0(\vec{p},t). \tag{4.16}$$

Thus by solving Eqs. 4.15 and 4.16, we get a complete description about the state of the system, $|\psi(t)\rangle$. Let us define the function $F_l(\vec{p},t)$ as:

$$F_l(\vec{p},t) = ig_l^{ab} e^{i(\omega_0-\omega_{\vec{k}})t} e^{\frac{i}{2m\hbar}\left(|\vec{p}|^2-\left|\vec{p}-\hbar\vec{k}\right|^2\right)t}, \tag{4.17}$$

we can rewrite Eqs. 4.15 and 4.16 as:

$$\frac{\partial c_0(\vec{p},t)}{\partial t} = -\sum_l F_l(\vec{p},t)\ c_l(\vec{p}-\hbar\vec{k},t), \tag{4.18}$$

$$\frac{\partial c_l(\vec{p}-\hbar\vec{k},t)}{\partial t} = F_l^*(\vec{p},t)\ c_0(\vec{p},t), \tag{4.19}$$

subject to the following initial state:

$$|\psi(t)\rangle = \int \mathrm{d}\vec{p}\,\varphi(\vec{p})\,|1\rangle_A\,|\vec{p}\rangle_E\,|0\rangle_F\ , \tag{4.20}$$

which is equivalent to the initial conditions:

$$\begin{cases} c_0(\vec{p},t=0) = \varphi(\vec{p}) \\ c_l(\vec{p},t=0) = 0, \end{cases}$$

where $\varphi(\vec{p})$ corresponds to the linear momentum distribution of the atom before the decay process. Integrating eq.(4.19) in time we get:

$$c_l(\vec{p}-\hbar\vec{k},t) = \int_0^t \mathrm{d}t' F_l^*(\vec{p},t')\ c_0(\vec{p},t'). \tag{4.21}$$

Substituting $c_l(\vec{p}-\hbar\vec{k},t)$ in eq.(4.18):

$$\frac{\partial c_0(\vec{p},t)}{\partial t} = -\sum_l \int_0^t \mathrm{d}t' F_l(\vec{p},t) F_l^*(\vec{p},t') c_0(\vec{p},t'). \tag{4.22}$$

In order to facilitate the calculations, let us decompose the sum over l into an integration in $\vec{k}$ and a sum in the polarization variable s. For this we must take into account the density of states in the space of wave-vectors $\vec{k}$, $\rho_{\vec{k}} = V/(2\pi)^3$, where V is the volume involved in the quantization process. Such a correspondence among integration and sum in $\vec{k}$ reads:

$$\sum_l \to \sum_{s=1}^{2} \int \mathrm{d}\vec{k} \frac{V}{(2\pi)^3}, \tag{4.23}$$

then, we can write:

$$\frac{\partial c_0(\vec{p},t)}{\partial t} = -\frac{V}{(2\pi)^3} \sum_{s=1}^{2} \int \mathrm{d}\vec{k} \int_0^t \mathrm{d}t' F_{s,\vec{k}}(\vec{p},t) F_{s,\vec{k}}^*(\vec{p},t') c_0(\vec{p},t'). \tag{4.24}$$

On the other hand,

$$F_{s,\vec{k}}(\vec{p},t)F^{*}_{s,\vec{k}}(\vec{p},t') = \left|g^{ab}_{s,\vec{k}}\right|^2 e^{i\left(\omega_0-\omega_{\vec{k}}+\frac{|\vec{p}|^2}{2m\hbar}-\frac{|\vec{p}-\hbar\vec{k}|^2}{2m\hbar}\right)(t-t')}, \tag{4.25}$$

and therefore:

$$\frac{\partial c_0(\vec{p},t)}{\partial t} = -\frac{V}{(2\pi)^3}\int \mathrm{d}\vec{k}\int_0^t \mathrm{d}t' c_0(\vec{p},t') e^{i\left(\omega_0-\omega_{\vec{k}}+\frac{|\vec{p}|^2}{2m\hbar}-\frac{|\vec{p}-\hbar\vec{k}|^2}{2m\hbar}\right)(t-t')}\sum_{s=1}^{2}\left|g^{ab}_{s,\vec{k}}\right|^2. \tag{4.26}$$

Let us express the vector $\vec{k}$ in spherical coordinates $\vec{k}=(k,\theta_k,\varphi_k)$, thus $\mathrm{d}\vec{k} = k^2\,\mathrm{d}k\,\mathrm{d}\theta_k\,\mathrm{d}\varphi_k$. In addition it is more convenient to deal with the frequency associated with the mode with wave-vector amplitude k, $\omega_{\vec{k}}=\omega_k=kc$, thus $\mathrm{d}\vec{k}=\omega_k^2/c^3\,\mathrm{d}\omega_k\,\mathrm{d}\theta_k\,\mathrm{d}\varphi_k$. On the other hand, recalling the definition of the coupling constant g_l^{mn} (eq.(4.4)), we have

$$\left|g^{ab}_{l}\right|^2 = \frac{1}{\hbar^2}\frac{\hbar\omega_k}{2\epsilon_0 V}\left(\vec{\mu}_{ab}\cdot\hat{e}_l\right)^2, \tag{4.27}$$

and we can rewrite eq.(4.26), as:

$$\begin{aligned}\frac{\partial c_0(\vec{p},t)}{\partial t} &= -\frac{1}{(2\pi)^3c^3}\frac{1}{2\hbar\epsilon_0}\int_0^\infty \mathrm{d}\omega_k\,\omega_k^3\int_0^\pi \mathrm{d}\theta_k\sin\theta_k\int_0^{2\pi}\mathrm{d}\varphi_k\int_0^t \mathrm{d}t' c_0(\vec{p},t')\times\\ &\times\ e^{i\left(\omega_0-\omega_{\vec{k}}+\frac{|\vec{p}|^2}{2m\hbar}-\frac{|\vec{p}-\hbar\vec{k}|^2}{2m\hbar}\right)(t-t')}\sum_{s=1}^{2}\left(\vec{\mu}_{ab}\cdot\hat{e}_l\right)^2,\end{aligned} \tag{4.28}$$

Let's calculate the term: $\sum_{s=1}^{2}\left(\vec{\mu}_{ab}\cdot\hat{e}_l\right)^2$. Given that the wave propagates in the direction of the wave-vector, $\hat{k}=\vec{k}/\left|\vec{k}\right|$, we can define two unitary vectors $\hat{i}$ and $\hat{j}$ mutually orthogonal to $\hat{k}$, such that:

$$\vec{\mu}_{ab} = \left(\vec{\mu}_{ab}\cdot\hat{i}\right)\hat{i} + \left(\vec{\mu}_{ab}\cdot\hat{j}\right)\hat{j} + \left(\vec{\mu}_{ab}\cdot\hat{k}\right)\hat{k}. \tag{4.29}$$

Then, if $\hat{i}$ and $\hat{j}$ are aligned with the polarization directions $\hat{e}_1$ and $\hat{e}_2$, it is easy to see that

$$\sum_{s=1}^{2}\left(\vec{\mu}_{ab}\cdot\hat{e}_l\right)^2 = \left(\vec{\mu}_{ab}\cdot\hat{i}\right)^2 + \left(\vec{\mu}_{ab}\cdot\hat{j}\right)^2 = \left|\vec{\mu}_{ab}\right|^2 - \left(\vec{\mu}_{ab}\cdot\hat{k}\right)^2. \tag{4.30}$$

Without loss of generality, we can assume the vector $\vec{\mu}_{ab}$ parallel to the z-axis, in this way

$$\sum_{s=1}^{2}\left(\vec{\mu}_{ab}\cdot\hat{e}_l\right)^2 = \left|\vec{\mu}_{ab}\right|^2\left(1-\cos^2\theta_k\right) = \left|\vec{\mu}_{ab}\right|^2\sin^2\theta_k. \tag{4.31}$$

Substituting the last result in eq.(4.28) we have

$$\begin{aligned}\frac{\partial c_0(\vec{p},t)}{\partial t} &= -\frac{1}{(2\pi)^2c^3}\frac{\left|\vec{\mu}_{ab}\right|^2}{2\hbar\epsilon_0}\int_0^\infty \mathrm{d}\omega_k\omega_k^3\int_0^\pi \mathrm{d}\theta_k\sin^3\theta_k\int_0^t \mathrm{d}t' c_0(\vec{p},t')\times\\ &\times\ e^{i\left(\omega_0-\omega_{\vec{k}}+\frac{|\vec{p}|^2}{2m\hbar}-\frac{|\vec{p}-\hbar\vec{k}|^2}{2m\hbar}\right)(t-t')}.\end{aligned} \tag{4.32}$$

Let us analyse the frequency in the argument of the exponential term:

$$\begin{aligned}\omega_0 - \omega_{\vec{k}} + \frac{|\vec{p}|^2}{2m\hbar} - \frac{\left|\vec{p} - \hbar\vec{k}\right|^2}{2m\hbar} &= \omega_0 - \omega_{\vec{k}} + \frac{\vec{p}\cdot\vec{k}}{m} - \frac{\hbar}{2m}\left|\vec{k}\right|^2 \\ &= \omega_0 - \omega_{\vec{k}} + \frac{k}{m}\vec{p}\cdot\hat{k} - \frac{\hbar k^2}{2m} \\ &= \omega_0 - \omega_{\vec{k}}\left(1 - \frac{\vec{p}\cdot\hat{k}}{mc} + \frac{1}{2}\frac{\hbar\omega_{\vec{k}}}{mc^2}\right), \end{aligned} \tag{4.33}$$

where k corresponds to the module of the wave-vector $\vec{k}$. At this point we need to take into account several approximations in order to facilitate the calculations:

- The atom possesses a low initial linear momentum,

$$|\vec{p}| \ll mc. \tag{4.34}$$

- The energy of the emitted photon is negligible in comparison with the energy of the atom at rest

$$\hbar\omega_{\vec{k}} \ll mc^2. \tag{4.35}$$

- Under the last two approximations, the frequency in the exponential argument reduces to $\omega_0 - \omega_{\vec{k}}$, in this case the integration in t' is not zero only in a region around $\omega_{\vec{k}} \approx \omega_0$, thus it is reasonable to take the term $\omega_{\vec{k}}^3$ out of the integration as ω_0^3. In general terms, we can approximate

$$\omega_{\vec{k}}^{\alpha} \approx \omega_0^{\alpha}, \tag{4.36}$$

  with $\alpha \geq 1$.

After taking into account all the considerations above, eq.(4.32) reduces to:

$$\begin{aligned}\frac{\partial c_0(\vec{p},t)}{\partial t} &= -\frac{2|\vec{\mu}_{ab}|^2\omega_0^3}{3(2\pi)^2c^3\hbar\epsilon_0}\int_0^{\infty}\mathrm{d}\omega_k\int_0^t \mathrm{d}t' c_0(\vec{p},t')e^{i\left(\omega_0-\omega_{\vec{k}}\right)(t-t')}, \\ &= -\frac{|\vec{\mu}_{ab}|^2\omega_0^3}{6\pi^2c^3\hbar\epsilon_0}\int_0^t \mathrm{d}t' c_0(\vec{p},t')\int_0^{\infty}\mathrm{d}\omega_k e^{i\left(\omega_0-\omega_{\vec{k}}\right)(t-t')}, \\ &= -\frac{|\vec{\mu}_{ab}|^2\omega_0^3}{6\pi^2c^3\hbar\epsilon_0}\int_0^t \mathrm{d}t' c_0(\vec{p},t')\int_{-\infty}^{\infty}\mathrm{d}\omega_k e^{i\left(\omega_0-\omega_{\vec{k}}\right)(t-t')}, \\ &= -\frac{|\vec{\mu}_{ab}|^2\omega_0^3}{6\pi^2c^3\hbar\epsilon_0}\int_0^t \mathrm{d}t' c_0(\vec{p},t')2\pi\delta\left(t-t'\right), \\ &= -\frac{|\vec{\mu}_{ab}|^2\omega_0^3}{3\pi c^3\hbar\epsilon_0}c_0(\vec{p},t). \\ &= -\frac{1}{4\pi\epsilon_0}\frac{4|\vec{\mu}_{ab}|^2\omega_0^3}{3\hbar c^3}c_0(\vec{p},t). \\ &= -\frac{\Gamma}{2}c_0(\vec{p},t), \end{aligned} \tag{4.37}$$

where we obtain the spontaneous decay rate $\Gamma = \frac{1}{4\pi\epsilon_0}\frac{4|\vec{\mu}_{ab}|^2\omega_0^3}{3\hbar c^3}$. The solution to eq.(4.37) can be easily found and is equal to:

$$c_0(\vec{p},t) = \varphi(\vec{p})\ e^{-\frac{\Gamma}{2}t}, \tag{4.38}$$

which explicits the exponential decay nature of the spontaneous emission process. This is the extension of the main result of the original paper (WEISSKOPF; WIGNER, 1930) to wave packets: an initially excited two-level atom modelled by a wave packet in momentum space when interacting with the electromagnetic vacuum spontaneously decay with a characteristic rate Γ (RZAZEWSKI; ZAKOWICZ, 1992).

Back to Equation (4.19), we can now easily find the coefficients $c_l(\vec{p}-\hbar\vec{k},t)$:

$$\begin{aligned}\frac{\partial c_l(\vec{p}-\hbar\vec{k},t)}{\partial t} &= F_l^*(\vec{p},t)\ c_0(\vec{p},t)\\ &= F_l^*(\vec{p},t)\ c_0(\vec{p},t)\\ &= g_l^{ab*}\varphi(\vec{p})\ e^{-\frac{\Gamma}{2}t}e^{-i\left(\omega_0-\omega_{\vec{k}}+\frac{|\vec{p}|^2}{2m\hbar}-\frac{|\vec{p}-\hbar\vec{k}|^2}{2m\hbar}\right)t}.\end{aligned} \tag{4.39}$$

Integrating in time and using the corresponding initial condition, we obtain:

$$c_l(\vec{p}-\hbar\vec{k},t) = g_l^{ab*}\varphi(\vec{p})\ \frac{1-e^{-\frac{\Gamma}{2}t}e^{-i\left(\omega_0-\omega_{\vec{k}}+\frac{|\vec{p}|^2}{2m\hbar}-\frac{|\vec{p}-\hbar\vec{k}|^2}{2m\hbar}\right)t}}{\omega_{\vec{k}}-\omega_0+\frac{\left|\vec{p}-\hbar\vec{k}\right|^2}{2m\hbar}-\frac{|\vec{p}|^2}{2m\hbar}+i\frac{\Gamma}{2}}. \tag{4.40}$$

Finally, we obtain the solution of eq.(4.11):

$$|\psi(t)\rangle \;=\; \int \mathrm{d}\vec{p}\ c_0(\vec{p},t)\,|1\rangle_A\,|\vec{p}\rangle_E\,|0\rangle_F + \sum_l \int \mathrm{d}\vec{p}\ c_l(\vec{p}-\hbar\vec{k},t)\,|0\rangle_A\left|\vec{p}-\hbar\vec{k}\right\rangle_E|1_l\rangle_F\,, \tag{4.41}$$

where the coefficients $c_0(\vec{p},t)$ and $c_l(\vec{p}-\hbar\vec{k},t)$ are given by Eqs. (4.38) and (4.40) respectively.

4.2 QUANTUM STATE AFTER THE EMISSION PROCESS

We are interested in the entanglement that arises between photon and atom after the decay process. Therefore, we need to guarantee that the spontaneous emission happened, and we then use the asymptotic behavior of eq.(4.41) in the limit $\Gamma t \gg 1$. Since for long times, $c_0(\vec{p},t)\to 0$, after dropping the subscript E for the atomic external degrees of freedom, we obtain:

$$|\psi\rangle \approx \sum_{\vec{k},s}\int \mathrm{d}\vec{p}\ c_{\vec{k},s}(\vec{p}-\hbar\vec{k})\,|0\rangle_A\left|\vec{p}-\hbar\vec{k}\right\rangle\left|1_{\vec{k},s}\right\rangle, \tag{4.42}$$

where the $c_{\vec{k},s}(\vec{p}-\hbar\vec{k})$ are given by eq.(4.40). Notice that, since we are restrained to the 1-photon subspace of the Fock space associated with the electromagnetic field, we can write the ket associated with the state of the photon $\left|1_{\vec{k},s}\right\rangle$ as $\left|\vec{k},s\right\rangle$. In order to write the state in a more treatable way, we use the relations between sum and integration of the variable $\vec{k}$ in two cases:

a) sum involving a ket:

$$\sum_k (\dots)\,|k\rangle \to \left(\frac{L}{2\pi}\right)^{3/2} \int \mathrm{d}^3k\ (\dots)\left|\vec{k}\right\rangle, \tag{4.43}$$

b) sum not involving a ket:

$$\sum_k (\dots) \to \left(\frac{L}{2\pi}\right)^{3} \int \mathrm{d}^3k\ (\dots), \tag{4.44}$$

where the coefficient $\left(\frac{L}{2\pi}\right)$ corresponds to the density of states in the reciprocal space. In this limit, we are in the subspace corresponding to the atomic internal ground state, and therefore we can ignore the atomic internal degrees of freedom, and write the atom-photon state as:

$$|\psi\rangle = \frac{V^{1/2}}{(2\pi)^{3/2}} \sum_s \int \mathrm{d}\vec{k} \int \mathrm{d}\vec{p}\ c_{\vec{k},s}(\vec{p}-\hbar\vec{k})\left|\vec{p}-\hbar\vec{k}\right\rangle_{at}\left|\vec{k},s\right\rangle_{ph}, \tag{4.45}$$

where the subscripts at and ph refer to the atomic and photonic subsystems respectively and $V = L^3$. Now we turn our attention to the coefficient $C(\vec{p},\vec{k},s) \equiv \frac{V^{1/2}}{(2\pi)^{3/2}} c_{\vec{k},s}(\vec{p}-\hbar\vec{k})$. Note that we can write it as:

$$\begin{aligned} C(\vec{p},\vec{k},s) &= \frac{V^{1/2}}{(2\pi)^{3/2}} \frac{\frac{i}{\hbar}\sqrt{\frac{\hbar\omega_k}{2\epsilon_0 V}}\ \vec{\mu}_{ab}\cdot\hat{e}_{\vec{k},s}\ e^{-i\vec{k}\cdot\vec{r}_0}\varphi(\vec{p})}{\omega_{\vec{k}} - \omega_0 + \frac{\left|\vec{p}-\hbar\vec{k}\right|^2}{2m\hbar} - \frac{|\vec{p}|^2}{2m\hbar} + i\frac{\Gamma}{2}} \\ &= \frac{2i}{(2\pi)^{3/2}\Gamma}\sqrt{\frac{\omega_k}{2\hbar\epsilon_0}} \frac{\vec{\mu}_{ab}\cdot\hat{e}_{\vec{k},s}\ e^{-i\vec{k}\cdot\vec{r}_0}\varphi(\vec{p})}{2\frac{\omega_{\vec{k}}-\omega_0}{\Gamma} + \frac{\hbar^2\left|\vec{k}\right|^2 - 2\hbar\vec{k}\cdot\vec{p}}{m\hbar\Gamma} + i}. \end{aligned} \tag{4.46}$$

Without loss of generality we can fix the vector $\vec{\mu}_{ab} = |\vec{\mu}_{ab}|\hat{n}_3$ and the set of orthogonal vectors $\{\vec{k},\hat{e}_{\vec{k},1},\hat{e}_{\vec{k},2}\}$ as

$$\begin{aligned} \vec{k} &= k\sin\theta_k\cos\phi_k\hat{n}_1 + k\sin\theta_k\sin\phi_k\hat{n}_2 + k\cos\theta_k\hat{n}_3, \\ \hat{e}_{\vec{k},1} &= \cos\theta_k\cos\phi_k\hat{n}_1 + \cos\theta_k\sin\phi_k\hat{n}_2 - \sin\theta_k\hat{n}_3, \\ \hat{e}_{\vec{k},2} &= -\sin\phi_k\hat{n}_1 + \cos\phi_k\hat{n}_2\,, \end{aligned} \tag{4.47}$$

where $\{\hat{n}_1,\hat{n}_2,\hat{n}_3\}$ is a rotated orthonormal basis which aligns $\vec{\mu}_{ab}$ to $\hat{n}_3$. Thus, $\vec{\mu}_{ab}\cdot\hat{e}_{\vec{k},1} = -|\vec{\mu}_{ab}|\sin\theta_k$ and $\vec{\mu}_{ab}\cdot\hat{e}_{\vec{k},2} = 0$. Therefore, the coefficient $C(\vec{p},\vec{k},s)$ reduces to:

$$C(\vec{p},\vec{k},s) = \frac{-2i}{(2\pi)^{3/2}\Gamma}\sqrt{\frac{\omega_k}{2\hbar\epsilon_0}}\ \delta_{s,1}\frac{|\vec{\mu}_{ab}|\sin\theta_k\ e^{-i\vec{k}\cdot\vec{r}_0}\varphi(\vec{p})}{2\frac{\omega_{\vec{k}}-\omega_0}{\Gamma} + \frac{\hbar^2\left|\vec{k}\right|^2 - 2\hbar\vec{k}\cdot\vec{p}}{m\hbar\Gamma} + i}, \tag{4.48}$$

which implies in $C(\vec{p},\vec{k},2)=0$, and:

$$C(\vec{p},\vec{k},1)=\frac{-2i}{(2\pi)^{3/2}\Gamma}\sqrt{\frac{\omega_k}{2\hbar\epsilon_0}}\frac{|\vec{\mu}_{ab}|\sin\theta_k\ e^{-i\vec{k}\cdot\vec{r}_0}\varphi(\vec{p})}{2\frac{\omega_{\vec{k}}-\omega_0}{\Gamma}+\frac{\hbar^2\left|\vec{k}\right|^2-2\hbar\vec{k}\cdot\vec{p}}{m\hbar\Gamma}+i}. \tag{4.49}$$

This illustrates the fact that the photon can only be emitted in a single polarization. For the sake of simplicity, from now on we refer to the coefficient $C(\vec{p},\vec{k},1)$ as $C(\vec{p},\vec{k})$. After some steps, the above expression is reduced to:

$$C(\vec{p},\vec{k})=-\frac{i}{2\pi}\left(\frac{3\omega_k c^3}{\Gamma\omega_0^3}\right)^{1/2}\frac{\sin\theta_k\ e^{-i\vec{k}\cdot\vec{r}_0}\varphi(\vec{p})}{2\frac{\omega_{\vec{k}}-\omega_0}{\Gamma}+\frac{\hbar^2\left|\vec{k}\right|^2-2\hbar\vec{k}\cdot\vec{p}}{m\hbar\Gamma}+i}. \tag{4.50}$$

In summary, we can write the state of the atom-photon system asymptotically as:

$$|\psi\rangle\approx\int \mathrm{d}\vec{k}\int \mathrm{d}\vec{p}\ C(\vec{p},\vec{k})\left|\vec{p}-\hbar\vec{k}\right\rangle_{at}\left|\vec{k}\right\rangle_{ph}, \tag{4.51}$$

where $C(\vec{p},\vec{k})$ is given by eq.(4.50). We note directly that the amplitude $C(\vec{p},\vec{k})$ mixes atomic and photonic momentum variables in a non-separable manner; this is where most of the literature stops and argues that this implies in the existence of entanglement in the system and no further discussion arises. We departure from this point of view and look more closely at the atom-photon state.

4.3 QUANTIFICATION OF ENTANGLEMENT ENCODED IN THE MOMENTUM VARIABLES

As already discussed in Chapter 2, in section 2.2.2, one of the ways we can assess the presence of entanglement in a pure bipartite quantum state is by evaluating the purity of the reduced state of one of the components. From eq.(4.51) it is straightforward to show that the reduced state associated with the atomic subsystem can be written as:

$$\begin{aligned}\rho_a&=\mathrm{tr}_{ph}\left(|\psi\rangle\langle\psi|\right)\\&=\int \mathrm{d}\vec{k}\ \mathrm{d}\vec{p}\ \mathrm{d}\vec{p'}\ C(\vec{p},\vec{k})C^*(\vec{p'},\vec{k})\left|\vec{p}-\hbar\vec{k}\right\rangle\!\left\langle\vec{p'}-\hbar\vec{k}\right|.\end{aligned} \tag{4.52}$$

Therefore, the purity of the reduced state of the atom reads:

$$\begin{aligned}P_a&=\mathrm{tr}\left(\rho_a^2\right)\\&=\int \mathrm{d}\vec{k}\ \mathrm{d}\vec{k'}\ \mathrm{d}\vec{q}\ \mathrm{d}\vec{q'}\ C(\vec{q}+\hbar\vec{k},\vec{k})C^*(\vec{q}+\hbar\vec{k'},\vec{k'})C(\vec{q'}+\hbar\vec{k'},\vec{k'})C^*(\vec{q'}+\hbar\vec{k},\vec{k}),\end{aligned} \tag{4.53}$$

with $C(\vec{q}+\hbar\vec{k},\vec{k})$ given by eq.(4.50). Note that in the expressions above we have employed the variable associated with the *final* momentum of the atom, $\vec{q}$, instead of the initial one, $\vec{p}$.

In order to proceed with the purity calculation we need to provide an explicit form for $\varphi(\vec{p})$, that is, a given shape for the initial distribution of atomic momenta. Experimentally, we can trap an excited atom in a minimum of a given potential, which can be approximated as a harmonic potential (HENSON et al., 2022) leading to an atomic state corresponding to the ground state of a quantum harmonic oscillator for its external degrees of freedom, that is, a Gaussian wave-packet in momentum. Therefore, we use this experimental picture to assume a Gaussian wave-packet as our initial distribution of atomic momenta. Explicitly, we assume:

$$\varphi(\vec{p}) = \left(\frac{1}{\pi\Delta p^2}\right)^{3/4} e^{-\frac{\vec{p}^2}{2\Delta p^2}}. \tag{4.54}$$

Now, we can calculate the purity of the reduced atomic state for a few physical realizations of the spontaneous emission process as we have modelled it, considering different spectral lines for various atoms. Note that for theses systems, every parameter such as Γ, ω_0 and m are fixed by the considered spectral line of the given atom. Nonetheless, there is still a free parameter embedded in our model: Δp, the initial atomic momentum uncertainty. Therefore, we shall study the dependence of the purity on Δp.

Since $\Delta p > 0$, we can reparametrize our problem to a more suitable quantity which will make the comparison to atomic scales easier, by defining the effective energy, ε_e, as:

$$\varepsilon_e = \frac{\Delta p^2}{2m} = k_B T_e, \tag{4.55}$$

where we also define the effective temperature T_e, and we may use energy or temperature interchangeably. This allows us to map variations in momentum uncertainty to variations in an energy scale, which in turn, allows us to compare the effective energies or temperatures to Doppler and Recoil energies or temperatures, $\varepsilon_D\,(\text{or}\,T_D)$ and $\varepsilon_R\,(\text{or}\,T_R)$, respectively, which are defined by:

$$\begin{aligned} \varepsilon_D &= k_B T_D = \frac{\hbar\Gamma}{2} \\ \varepsilon_R &= k_B T_R = \frac{\hbar^2\omega_0^2}{mc^2}. \end{aligned} \tag{4.56}$$

As is to be expected, the 12-D integral in eq.(4.53) cannot be put into an analytical form. Therefore, we perform a numerical integration (using the quasi-Monte Carlo method of integration embedded into the Mathematica® version 11.2 software) to obtain the scattered

points in Fig. 13 for the different spectral lines considered in Table 1. This particular choice of spectral lines gives a sizeable range of Doppler and recoil temperatures and in fact, a good range for the quantity T_D/T_R, which as we can see from Fig. 13 yields different behaviors to each of the lines.

One characteristic that is common to all the considered spectral lines is the presence of two high entanglement regimes for small ε_e and large ε_e, illustrated by the decrease in purity shown in Fig. 13 on the edges of each line. Some spectral lines, such as the $\mathrm{Cs}-\mathrm{D}_2$ line and the $\mathrm{K}-\mathrm{D}_2$ line separate these high entanglement regimes quite well with a region of purity near 1 in the middle, while others, such as the Sr - Narrow line, do not, presenting a lot of entanglement in all effective energies considered.

Table 1 – Recoil and Doppler temperatures for the different spectral lines considered.

	$\mathrm{Cs}-\mathrm{D}_2$ Line	$\mathrm{K}-\mathrm{D}_2$ Line	$\mathrm{Li}-\mathrm{D}_2$ Line	K - Narrow Line	Li - Narrow Line	Sr - Narrow Line
$T_R(\mu K)$	0.20	0.82	6.36	2.95	27.48	0.46
$T_D(\mu K)$	124.84	144.26	140.37	28.44	18.02	0.18

Source: (STECK, 2003).

The next subsections are dedicated to understanding these two regimes in an analytical manner expliciting the non-separability of the state from a simplification of the amplitude $C(\vec{p}+\hbar\vec{k},\vec{k})$ and a physically driven interpretation of the observed increase in entanglement.

4.3.1 Simplification of the amplitude $C(\vec{q}+\hbar\vec{k},\vec{k})$ near resonance.

The state's amplitude $C(\vec{q}+\hbar\vec{k},\vec{k})$ is roughly comprised of two competing distributions: a Gaussian distribution (originating from the Maxwellian distribution of atomic momentum) and a distribution that resembles a Lorentzian distribution (originating from the natural spectral distribution of the emitted photon while altered by the atomic recoil). Both of these distributions are characterized by a prominent peak, therefore, most of the dynamics we observe should be concentrated near this resonance.

The aim of the present subsection is then to use this fact to our advantage, simplifying the expression for the amplitude to use it later to obtain even simpler expressions valid for each entanglement regime. We begin by writing (4.50) as:

Figure 13 – Purity as a function of $\varepsilon_e/\varepsilon_R$ for the different atomic spectral lines considered in table 1. The scattered points represent the full computation of the purity using the amplitude given by (4.50), while the solid curves gives the product of the purities, P_p, calculated using the small Δp and large Δp approximations given respectively by (4.66) and (4.67).

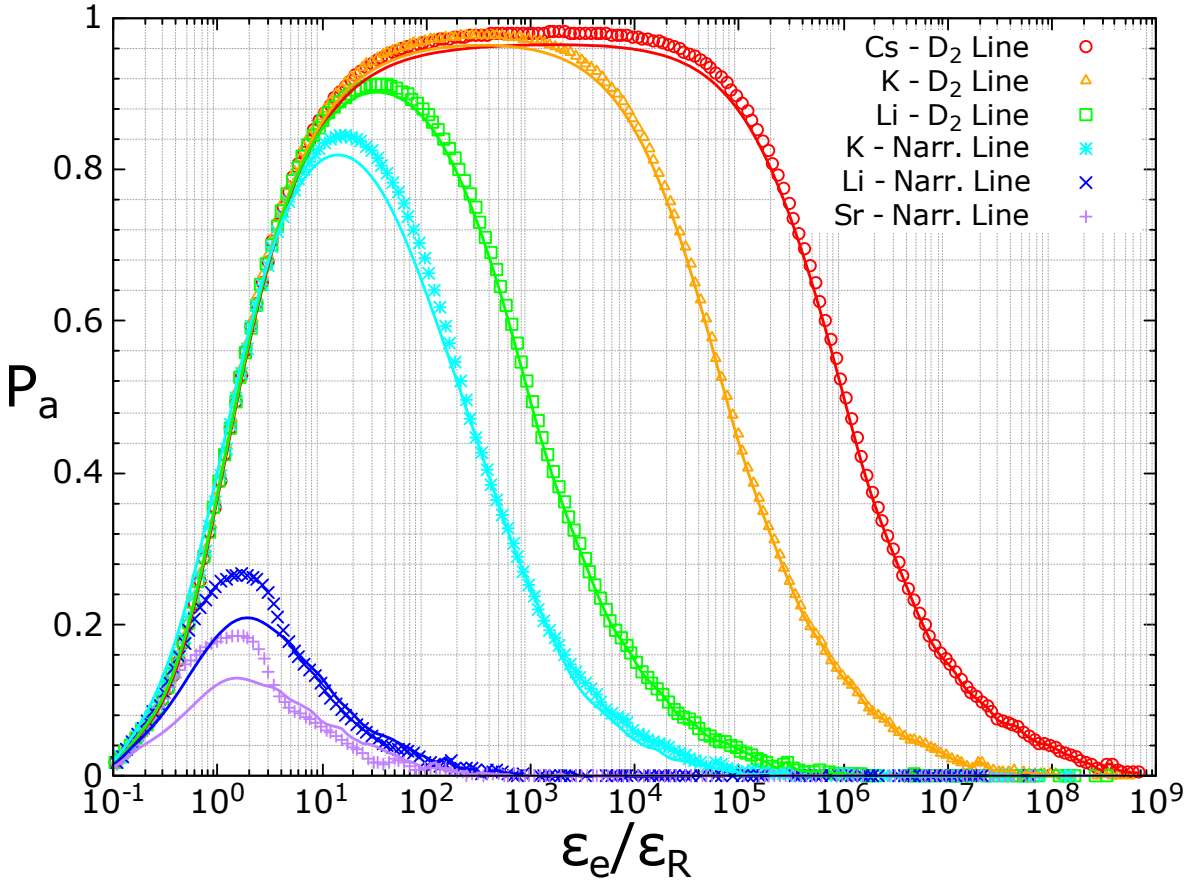

Source: The author.

$$C(\vec{q}+\vec{k}^{(\mathrm{II})},\,\vec{k}^{(\mathrm{II})}) = iA\frac{\sin\theta_{k^{\mathrm{II}}}\;\varphi(\vec{q}+\vec{k}^{(\mathrm{II})})}{-\frac{1}{m\hbar\Gamma}\left(k^{\mathrm{II}}\right)^2+\left(\frac{2c}{\Gamma\hbar}-\frac{2}{m\hbar\Gamma}q\cos\gamma_1\right)k^{\mathrm{II}}+i-\frac{2\omega_0}{\Gamma}}\,, \tag{4.57}$$

where $A=-\frac{1}{2\pi}\left(\frac{3c^3}{\omega_0^2\Gamma}\right)^{1/2}$, $\vec{k}^{(\mathrm{II})}=\hbar\vec{k}$ and γ_1 is the angle between $\vec{q}$ and $\vec{k}$. Note that this angle does not change when we perform this change of variables. Note also that the denominator in (4.57) is a second degree polynomial in k^{II}. We wish to approximate it by a first degree polynomial, but in order to do so we must first turn its coefficients dimensionless. We can then write (4.57) as:

$$C(\vec{q}^{\,(\mathrm{I})}+\vec{k}^{(\mathrm{III})},\,\vec{k}^{(\mathrm{III})}) = iA\frac{\sin\theta_{k^{\mathrm{III}}}\;\varphi(\Delta p\,\vec{q}^{\,(\mathrm{I})}+\hbar k_0\,\vec{k}^{(\mathrm{III})})}{-\frac{\hbar\omega_0^2}{m\Gamma c^2}\left(k^{(\mathrm{III})}\right)^2+k^{\mathrm{III}}\left[\frac{2\omega_0}{\Gamma}\left(1-\frac{q^{\mathrm{I}}\,\Delta p\,\cos\gamma_1}{mc}\right)\right]-\frac{2\omega_0}{\Gamma}+i}\,, \tag{4.58}$$

where $\vec{q}^{\,(\mathrm{I})}=\frac{\vec{q}}{\Delta p}$ and $\vec{k}^{(\mathrm{III})}=\frac{\vec{k}^{(\mathrm{II})}}{\hbar k_0}=\frac{c\vec{k}^{(\mathrm{II})}}{\hbar\omega_0}$ are our new (dimensionless) variables. We can now

discard the quadratic term if:

$$\left|\frac{2\omega_0}{\Gamma}\left(1-\frac{q^{\mathrm{I}}\,\Delta p\,\cos\gamma_1}{mc}\right)\right| \gg \frac{\hbar\omega_0^2}{m\Gamma c^2},$$

or, equivalently:

$$\left|1-\frac{q^{\mathrm{I}}\,\Delta p\,\cos\gamma_1}{mc}\right| \gg \frac{\hbar\omega_0}{2mc^2} \approx 10^{-10}, \tag{4.59}$$

a condition that may break when:

$$\frac{q^{\mathrm{I}}\,\Delta p\,\cos\gamma_1}{mc} \approx 1, \tag{4.60}$$

or:

$$q\cos\gamma_1 \approx mc \approx 10^{-17}\,\mathrm{kg}\cdot\frac{\mathrm{m}}{\mathrm{s}}, \tag{4.61}$$

which would be within relativistic regimes, which is not our case. Note that we used the fact that $q^{\mathrm{I}}\,\Delta p = q$. In the non-relativistic regime we approximate (4.58) as:

$$\begin{aligned}
C(\vec{q}^{\,(\mathrm{I})}+\vec{k}^{\,(\mathrm{III})},\,\vec{k}^{\,(\mathrm{III})}) &\approx iA\frac{\sin\theta_{k^{\mathrm{III}}}\;\varphi(\Delta p\,\vec{q}^{\,(\mathrm{I})}+\hbar k_0\,\vec{k}^{\,(\mathrm{III})})}{k^{\mathrm{III}}\left[\frac{2\omega_0}{\Gamma}\left(1-\frac{q^{\mathrm{I}}\,\Delta p\,\cos\gamma_1}{mc}\right)\right]-\frac{2\omega_0}{\Gamma}+i} \\
&= iA\,\frac{\Gamma}{2\omega_0\left(1-\frac{q^{\mathrm{I}}\,\Delta p\,\cos\gamma_1}{mc}\right)}\frac{\sin\theta_{k^{\mathrm{III}}}\;\varphi(\Delta p\,\vec{q}^{\,(\mathrm{I})}+\hbar k_0\,\vec{k}^{\,(\mathrm{III})})}{k^{\mathrm{III}}-\underbrace{\frac{1}{\left(1-\frac{q^{\mathrm{I}}\,\Delta p\,\cos\gamma_1}{mc}\right)}}_{k^{\mathrm{III}^0}}+\underbrace{\frac{\Gamma}{2\omega_0\left(1-\frac{q^{\mathrm{I}}\,\Delta p\,\cos\gamma_1}{mc}\right)}}_{\gamma}i} \\
&= iA\gamma\frac{\sin\theta_{k^{\mathrm{III}}}\;\varphi(\Delta p\,\vec{q}^{\,(\mathrm{I})}+\hbar k_0\,\vec{k}^{\,(\mathrm{III})})}{k^{\mathrm{III}}-k^{\mathrm{III}^0}+\gamma i} \\
&= iA\gamma\sin\theta_{k^{\mathrm{III}}}\;\varphi(\Delta p\,\vec{q}^{\,(\mathrm{I})}+\hbar k_0\,\vec{k}^{\,(\mathrm{III})})\times \\
&\times\left(\frac{k^{\mathrm{III}}-k^{\mathrm{III}^0}}{(k^{\mathrm{III}}-k^{\mathrm{III}^0})^2+\gamma^2}-i\frac{\gamma}{(k^{\mathrm{III}}-k^{\mathrm{III}^0})^2+\gamma^2}\right) \\
&= iA\pi\sin\theta_{k^{\mathrm{III}}}\;\varphi(\Delta p\,\vec{q}^{\,(\mathrm{I})}+\hbar k_0\,\vec{k}^{\,(\mathrm{III})})(k^{\mathrm{III}}-k^{\mathrm{III}^0})\;\times\frac{\gamma}{\pi(k^{\mathrm{III}}-k^{\mathrm{III}^0})^2+\pi\gamma^2}+ \\
&+ A\gamma\pi\sin\theta_{k^{\mathrm{III}}}\;\varphi(\Delta p\,\vec{q}^{\,(\mathrm{I})}+\hbar k_0\,\vec{k}^{\,(\mathrm{III})})\;\times\underbrace{\frac{\gamma}{\pi(k^{\mathrm{III}}-k^{\mathrm{III}^0})^2+\pi\gamma^2}}_{L(k^{\mathrm{III}^0},\gamma,k^{\mathrm{III}})} \\
&= A\pi\sin\theta_{k^{\mathrm{III}}}\;\varphi(\Delta p\,\vec{q}^{\,(\mathrm{I})}+\hbar k_0\,\vec{k}^{\,(\mathrm{III})})L(k^{\mathrm{III}^0},\gamma,k^{\mathrm{III}})\left[\gamma\;+i(k^{\mathrm{III}}-k^{\mathrm{III}^0})\right],
\end{aligned} \tag{4.62}$$

where $L(k^{\mathrm{III}^0},\gamma,k^{\mathrm{III}})$ stands for a Lorentzian (Cauchy) distribution with location parameter (peak at) $k^{\mathrm{III}^0}=\left(1-\frac{q^{\mathrm{I}}\,\Delta p\,\cos\gamma_1}{mc}\right)^{-1}$ and scale parameter (width) $\gamma=\frac{\Gamma}{2\omega_0}k^{\mathrm{III}^0}$ in the variable k^{III}. Note that so far we have not considered the specific shape of $\varphi(\vec{q}+\vec{k})$, but by equation

(4.54) we note that the amplitude we have been calculating is only non-negligible for $q \in (0, n\,\Delta p)$ where n is a number of order 1. This, in turn, means that $q^{\mathrm{I}} \in (0, n)$ and therefore to consider a small Δp is completely equivalent to consider small q. We can now rewrite our amplitude in terms of our original variables:

$$C(\vec{q}+\hbar\vec{k},\vec{k}) = A\pi \sin\theta_k \; \varphi(\vec{q}+\hbar\vec{k}) L(k^0,\gamma,k)\left[\gamma + i(k-k^0)\right], \tag{4.63}$$

where up to first order in q we get:

$$k^0 = \frac{\omega_0}{c}\left(1+\frac{q\,\cos\gamma_1}{mc}\right) \quad \text{and} \quad \gamma = \frac{\Gamma}{2c}\left(1+\frac{q\,\cos\gamma_1}{mc}\right). \tag{4.64}$$

This yields $\gamma \approx 10^{-2}\,\mathrm{m}^{-1}$ for the $\mathrm{Cs}-\mathrm{D}_2$ line. If we now write $\varphi(\vec{q}+\hbar\vec{k})$ in terms of only wavenumber variables, that is, $\varphi(\hbar\vec{q}'+\hbar\vec{k})$, this generates a Gaussian distribution in the variable q' with a standard deviation $\Delta q' = \frac{\Delta p}{\hbar} \approx 10^6 - 10^{11}\,\mathrm{m}^{-1}$ for the Δp range we consider. This means that our Lorentzian distribution is much narrower than our Gaussian distribution when we look at them in comparable units. With that in mind, it is straightforward to assume that $\varphi(\vec{q}+\hbar\vec{k})$ does not vary a lot when we consider k near the peak of our Lorentzian distribution. In fact, we should be able to assume $\varphi(\vec{q}+\hbar\vec{k}) \approx \varphi(\vec{q}+\hbar\vec{k^0})$, where $\vec{k^0}$ is a vector on the sphere centered at the origin with radius $k^0 = \frac{\omega_0}{c}$, that is, a vector of length k^0. This simplifies the considered amplitude to:

$$C(\vec{q}+\hbar\vec{k},\vec{k}) = A\pi \sin\theta_k \; \varphi(\vec{q}+\hbar\vec{k^0}) L(k^0,\gamma,k)\left[\gamma + i(k-k^0)\right]. \tag{4.65}$$

4.3.2 Small Δp approximation.

In this subsection we aim to obtain a simplified expression suitable to describe the high entanglement regime associated with small atomic momentum uncertainties. Note that for very small Δp, $k^0 = \frac{\omega_0}{c}$ and therefore, it should be a good approximation for the left part of the graph. If $k^0 = \frac{\omega_0}{c}$, then $\gamma = \frac{\Gamma}{2c}$. This in turn means that the Lorentzian distribution is now

a function of *only* $\vec{k}$. Therefore, the amplitude now reads:

$$
\begin{aligned}
C(\vec{q}+\hbar\vec{k},\vec{k}) &= \underbrace{A\pi \sin\theta_k L(k^0,\gamma,k)\left[\gamma\ + i(k-k^0)\right]}_{f_1(\vec{k})}\ \varphi(\vec{q}+\hbar\vec{k^0}) \\
&= f_1(\vec{k})\left(\frac{1}{\pi\Delta p^2}\right)^{\frac{3}{4}} e^{-\frac{\mathrm{q}^2}{2\Delta \mathrm{p}^2}-\frac{\mathrm{q}\hbar\left(\frac{\omega_0}{\mathrm{c}}\right)\cos\gamma_1}{\Delta \mathrm{p}^2}-\frac{\hbar^2\left(\frac{\omega_0}{\mathrm{c}}\right)^2}{2\Delta \mathrm{p}^2}} \\
&= f_1(\vec{k})\ \underbrace{\left(\frac{1}{\pi\Delta p^2}\right)^{\frac{3}{4}} e^{-\frac{\mathrm{q}^2}{2\Delta \mathrm{p}^2}-\frac{\hbar^2\left(\frac{\omega_0}{\mathrm{c}}\right)^2}{2\Delta \mathrm{p}^2}}}_{g_1(\vec{q})}\ e^{-\frac{\mathrm{q}\hbar\left(\frac{\omega_0}{\mathrm{c}}\right)\cos\gamma_1}{\Delta \mathrm{p}^2}} \\
&= f_1(\vec{k})\, g_1(\vec{q})\ e^{-\frac{\mathrm{q}\hbar\left(\frac{\omega_0}{\mathrm{c}}\right)\cos\gamma_1}{\Delta \mathrm{p}^2}}. \qquad (4.66)
\end{aligned}
$$

Therefore, the non-separability of the state comes from the term $e^{-\frac{\mathrm{q}\hbar\left(\frac{\omega_0}{\mathrm{c}}\right)\cos\gamma_1}{\Delta \mathrm{p}^2}}$, encoded directly into the angular variables of the system through the $\cos\gamma_1$ term. Note that as $\Delta\mathrm{p}$ increases, the exponential term goes to 1, bringing the state to a separable (non-entangled) state. We illustrate this behavior and show the validity of (4.66) by calculating the Schmidt rank for the cesium D_2 line (see Fig. 14). We use eq.(4.65), which gives the corresponding solution for the considered range of effective energies (scattered points) and eq.(4.66) (solid green line), which agrees with (4.65) in the small Δp limit. We refer to the small Δp limit as the *Recoil entanglement* regime for reasons that will become clearer when we discuss physically the entanglement regimes.

4.3.3 Large Δp approximation.

When we consider the large Δp regime, we can no longer approximate k^0 and γ as mere parameters that do not depend on any of the momentum variables. In fact, we need to use (4.64) in its full effect. This means that now our Lorentzian distribution carries the entanglement of the system. To show that no non-separability survives in the Gaussian distribution,

we can turn to (4.65) once again to write:

$$
\begin{aligned}
C(\vec{q}+\hbar\vec{k},\vec{k}) &= A\,\pi\sin\theta_k L(k^0,\gamma,k)\left[\gamma\ + i(k-k^0)\right]\ \varphi(\vec{q}+\hbar\vec{k^0}) \\
&= A\,\pi\sin\theta_k L(k^0,\gamma,k)\left[\gamma\ + i(k-k^0)\right]\ \varphi(\vec{q}+\hbar\vec{k^0}) \\
&= A\,\pi\sin\theta_k L(k^0,\gamma,k)\left[\gamma\ + i(k-k^0)\right]\times \\
&\times\, e^{-\frac{\mathrm{q}^2}{2\Delta\mathrm{p}^2}-\frac{\mathrm{q}\hbar\left(\frac{\omega_0}{\mathrm{c}}\right)\cos\gamma_1}{\Delta\mathrm{p}^2}-\frac{\mathrm{q}^2\hbar\left(\frac{\omega_0}{\mathrm{c}}\right)\cos^2\gamma_1}{\mathrm{mc}\Delta\mathrm{p}^2}-\frac{\hbar^2\left(\frac{\omega_0}{\mathrm{c}}\right)^2}{2\Delta\mathrm{p}^2}-\frac{\hbar^2\left(\frac{\omega_0}{c}\right)^2q^2\cos^2\gamma_1}{2(mc)^2\Delta p^2}-\frac{\hbar^2\left(\frac{\omega_0}{c}\right)^2q\cos\gamma_1}{mc\Delta p^2}} \\
&\approx A\,\pi\sin\theta_k L(k^0,\gamma,k)\left[\gamma\ + i(k-k^0)\right]e^{-\frac{\mathrm{q}^2}{2\Delta\mathrm{p}^2}} \\
&= f_2(\vec{k})g_2(\vec{p})L(k^0,\gamma,k)\left[\gamma\ + i(k-k^0)\right], \qquad (4.67)
\end{aligned}
$$

where we defined $f_2(\vec{k}) = A\,\pi\sin\theta_k$ and $g_2(\vec{p}) = e^{-\frac{\mathrm{q}^2}{2\Delta\mathrm{p}^2}}$ (see Appendix A for further details in the simplification of the exponential term). Therefore, what now controls the separability of the state is the Lorentzian distribution, which as we have already seen, becomes a function of *only* $\vec{k}$ when Δp decreases. We should then observe a separable state for small Δp and an entangled state for increasing values of Δp. Figure 14 illustrates this behavior through the solid red line, following the scattered points for large values of Δp and presenting a separable state for small values of Δp. From now on, we call it the *Doppler regime* of entanglement, for reasons that will become clearer when we present a physical discussion of both regimes. Note that these discussions are all valid for spectral lines that split the entanglement regimes quite well, such as the $\mathrm{Cs}-\mathrm{D}_2$ line, and therefore we focus on them for further discussions.

Now, since for both amplitudes (small and large Δp approximations) the calculated purity asymptotically goes to 1 in the complementary regime, we can define the product purity as: $P_p = P_s \times P_l$, where P_s is the purity calculated using the small Δp approximation [eq.(4.66)] and P_l is the purity calculated using the large Δp approximation [eq.(4.67)]. As we can see from Fig. 13, the product purity gives a general behavior close to the actual purity, and therefore, we can use the simplified expressions we obtained to calculate P_s and P_l and then compute the product for a simplified way to obtain the full purity.

Figure 14 – Schmidt rank as a function of $\varepsilon_e/\varepsilon_R$ for the $\mathrm{Cs}-\mathrm{D}_2$ Line. The solid green line represents the purity calculated from the small Δp approximation [eq.(4.66)], while the solid red line represents the purity calculated from the large Δp approximation [eq.(4.67)]. The middle vertical line represents a minimum of entanglement where $\varepsilon_e = \varepsilon_D$. The shaded areas describe the range of ε_e where we obtain each entanglement regime, that is, $\varepsilon_e \leq \varepsilon_R$ for the Recoil entanglement regime and $\varepsilon_e \geq 4\varepsilon_D^2/\varepsilon_R$ for the Doppler entanglement regime.

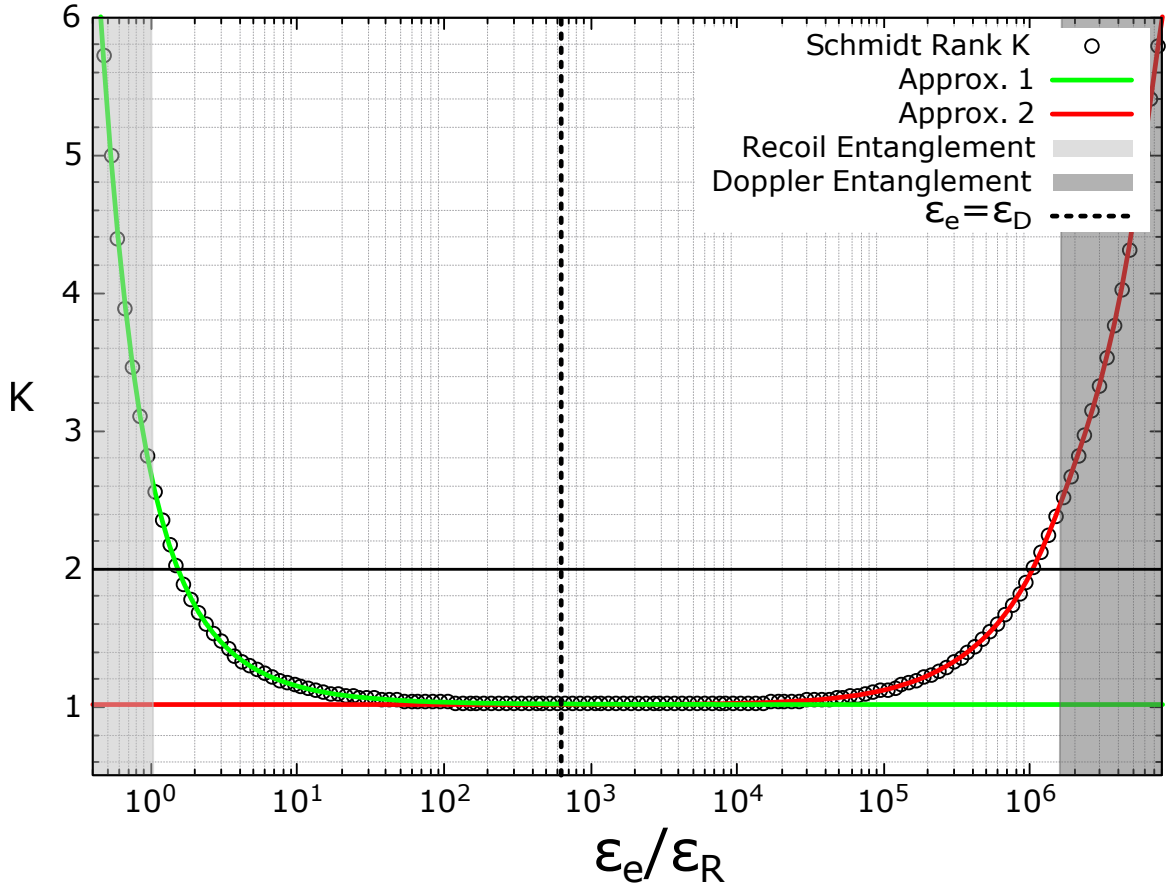

Source: The author.

4.4 PHYSICAL CONSIDERATIONS REGARDING THE ENTANGLEMENT REGIMES

In this section we aim to provide physical intuition about the high entanglement regimes we found. Moreover, we intend to obtain a roughly accurate threshold for the high entanglement regimes (we use $K \geq 2$ as an indicator of high entanglement, due to the fact that for the discrete case, this is the lowest Schmidt rank for entangled states). The physical reasoning that will permeate this section is that as the effect of one subsystem upon the other becomes more and more measurable, more correlations are created in the system, leading to entanglement.

4.4.1 Recoil entanglement

For the small Δp regime, the Recoil entanglement regime, we are dealing with an atom with a well defined initial momentum, $\vec{p_i} \approx 0$. This means that the spontaneous decay process behaves as a classical disintegration process, where one part of the system goes in a given direction while the other part goes in the opposite direction. While the momentum modulus of the atom or photon is well known (explicitly, $p_f \approx \hbar\omega_0/c$ with an uncertainty of $\hbar\Gamma/c$), the direction in which this process occurs is completely undetermined due to the isotropic nature of spontaneous emission. Using eq.(4.51), this yields a state of the form:

$$|\psi\rangle \approx \int \mathrm{d}^3k \; C(0,\vec{k}) \left|-\hbar\vec{k}\right\rangle_{at} \left|\vec{k}\right\rangle_{ph} , \tag{4.68}$$

which is a continuous non-separable state analogous to a (maximally entangled) Bell state. Note that: $k \in (k_0 - \Gamma/2c, k_0 + \Gamma/2c)$, which means that k does not vary a lot, while the angular variables range in the usual intervals. This means that the entanglement is in fact mostly encoded in the angular variables of the system.

Finally, this discussion elucidates the fact that the Recoil entanglement arises in the regime where recoil effects are more relevant, that is, when the recoil due to the photon emission is big enough to change measurably the atomic initial momentum. Therefore, a natural threshold for the Recoil entanglement is:

$$\varepsilon_e \lesssim \varepsilon_R, \tag{4.69}$$

which as we can see from the light gray shaded area in Fig. 14 gives a reasonable threshold for the Recoil entanglement regime, as $K \geq 2$. For effective energies greater than the recoil energy of the considered spectral line, we should not observe any entanglement due to this mechanism, where Fig. 14 corroborates this statement.

We can understand the increase in the Schmidt rank as we decrease ε_e as follows: consider first a sphere of radius $\hbar\frac{\omega_o}{c}$, and therefore, surface area of $4\pi \cdot \hbar^2\frac{\omega_o^2}{c^2}$. Consider now a small circle living on the surface of the previous sphere with radius Δp, and spanning an area of $\pi\Delta p^2$. We argue that the Schmidt rank can be understood as counting the number of small circles that can live in the surface of the big sphere, that is:

$$K \approx \frac{4\pi \cdot \hbar^2\frac{\omega_o^2}{c^2}}{\pi\Delta p^2} = 2\frac{\varepsilon_R}{\varepsilon_e} . \tag{4.70}$$

Note that the counting we performed gives roughly the number of independent atomic scattering modes that fit in a sphere of noise with a radius comparable to the momentum

recoil suffered by the atom. We can compare the estimate (4.70) to the actual calculated Schmidt rank using Fig. 15 and noting that the green solid line, representing the ratio of areas we defined, follows closely the scattered points for $K > 2$. Note that we define $K = 1$ when: $2\,\varepsilon_R/\varepsilon_e \leq 1$.

Figure 15 – Comparison of the Schmidt rank calculated from estimates (4.70) (solid green line) and (4.75) (solid red line) with the actual Schmidt rank. Both estimates work better in the Recoil and Doppler entanglement regimes respectively.

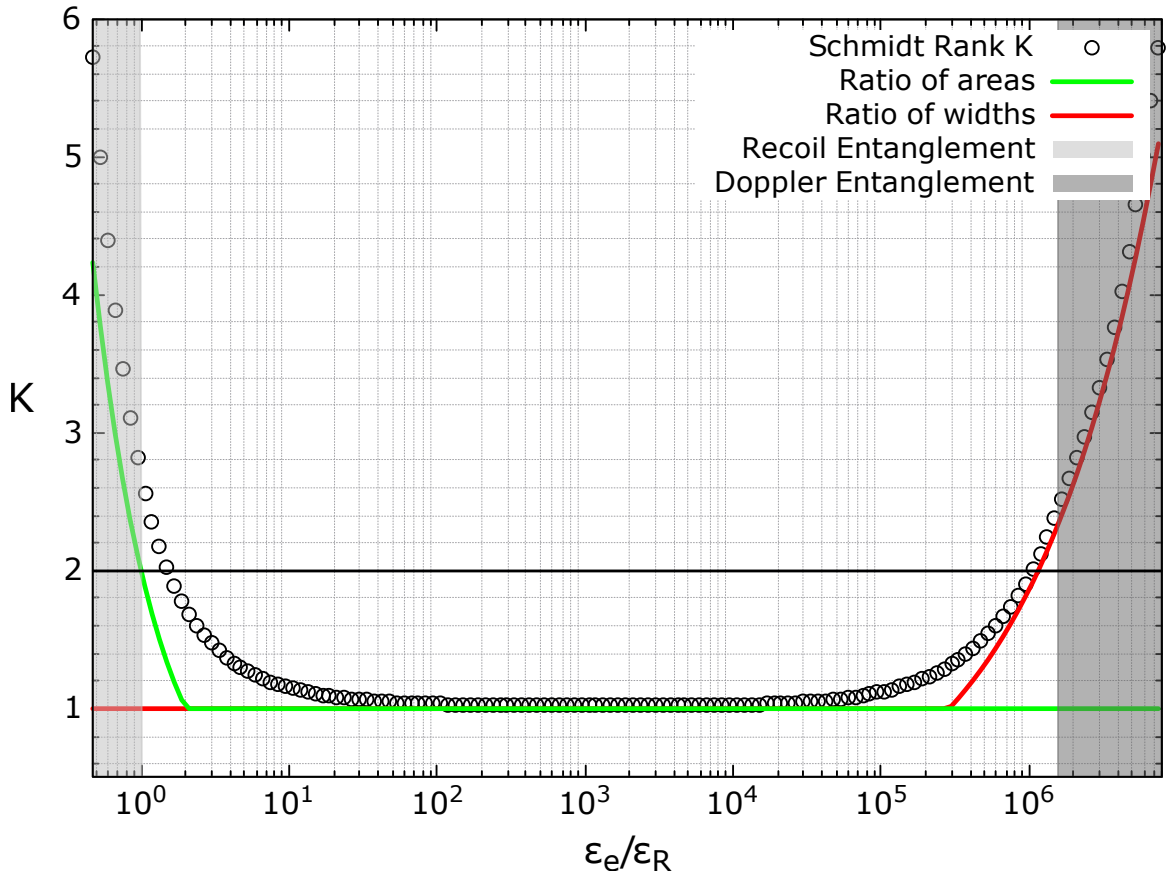

Source: The author.

4.4.2 Doppler entanglement

In the Doppler entanglement regime, we turn back to equation (4.64), to note that the effect of the recoil of the atom over the photon's central frequency is a blueshift or redshift depending on the emission direction in relation to the atom's final momentum direction:

$$\omega^0 - \omega_0 = \left(\frac{\omega_0}{mc}\right) \cdot q_{||}\,, \tag{4.71}$$

where $\omega^0 = k^0/c$ is the new entangled-induced emitted photon's central frequency and $q_{||} = q\,\cos\gamma_1$ is the component of the atom's final momentum in the direction of the emitted photon. Therefore, the central frequency of the emitted photon can be blueshifted if $q_{||} > 0$, or redshifted if $q_{||} < 0$, that is, if the final momentum of the atom is aligned parallel to the direction of the emitted photon or anti-parallel to it.

We should then expect an increase in entanglement as the shift in frequency becomes greater than the natural linewidth Γ. Considering that the components that participate the most in the effect are of the order of Δp, that is, $q_{||} \approx \Delta p$, we can write the condition for entanglement as:

$$\left(\frac{\omega_0}{mc}\right)\Delta p \geq \Gamma\,, \tag{4.72}$$

or equivalently, solving for Δp and writing the solution in terms of ε_e, ε_R, and ε_D, we obtain the Doppler threshold:

$$\varepsilon_e \geq 4\left(\frac{\varepsilon_D}{\varepsilon_R}\right)\varepsilon_D = k_B T_{DE}\,, \tag{4.73}$$

which defines the *Doppler entanglement temperature*. As we can see from Fig. 14, the shaded dark gray area in the right part of the graph [which illustrates the threshold (4.73)] represents well the region where $K \geq 2$. An analog view of this effect is the following: we can understand the threshold (4.73) as the minimum effective energy such that the (homogeneous) Doppler broadening induced by it is greater than the natural linewidth of the spectral line. Explicitly:

$$\Gamma_e = \sqrt{\frac{\varepsilon_e}{mc^2}}\,\omega_0 \geq \Gamma, \tag{4.74}$$

where we define the *effective natural linewidth*, Γ_e, and now, eq.(4.74) can be rewritten as eq.(4.73). Note that we use the term *homogeneous* to emphasize the fact that we are working with a single atom and making parallels with an atomic ensemble at an effective temperature T_e.

We can then understand the increase in the Schmidt rank as a quantification of how many Γ's fit in a given Γ_e. More accurately, since the Gaussian and Lorentzian distribution are of different natures, we compare the Full-Width at Half Maximum (FWHM) of the Doppler induced spectrum $\sqrt{8\log 2}\,\Gamma_e$ to Γ, and argue that:

$$K = \sqrt{8\log 2}\,\frac{\Gamma_e}{\Gamma} = \sqrt{\frac{8\log 2\,\omega_0^2}{\Gamma^2 mc^2}}\cdot\sqrt{\varepsilon_e} \sim \varepsilon_e^{\frac{1}{2}}\,. \tag{4.75}$$

In fact, as we can see from Fig. 15, the red solid line, representing the ratio of widths we just defined, follows along the calculated Schmidt rank specially as K increases from 2, that is, in the Doppler regime. Note that we define $K = 1$ when: $\sqrt{8 \log 2}\, \Gamma_e < \Gamma$.

Finally, we can summarize the thresholds we obtained in Fig. 16 and look at the results shown in Fig. 13 in a analogous manner: note that each spectral line we considered presents a different value of $\varepsilon_D/\varepsilon_R$, which we represent as the vertical lines in Fig. 16. We showed that the interplay between Doppler and Recoil energies plays a crucial role in the observed entanglement behavior, and following along a given spectral line shown in Fig. 16 we can observe the transitions from Recoil entanglement to a low entanglement plateau to Doppler entanglement as is the case for the $\mathrm{Cs} - \mathrm{D}_2$ line, or as in the Strontium narrow line case, we can see that the system does not leave any region of high entanglement, staying highly entangled at all considered values of ε_e. In fact, we can note for the Strontium narrow line that, for certain values of ε_e, the effects of the Recoil and Doppler regimes of entanglement overlap, creating a type of *mixed entanglement regime* where no source of entanglement can be separated from the other.

Figure 16 – Phase diagram elucidating all observed high entanglement regimes and low entanglement regions. The vertical lines represent different spectral lines (color coded with Fig. 13, from left to right: Sr - narrow line, Li - narrow line, K - narrow line, Li - D_2 line, K - D_2 line and Cs - D_2 line) labelled by different values of $\varepsilon_D/\varepsilon_R$.

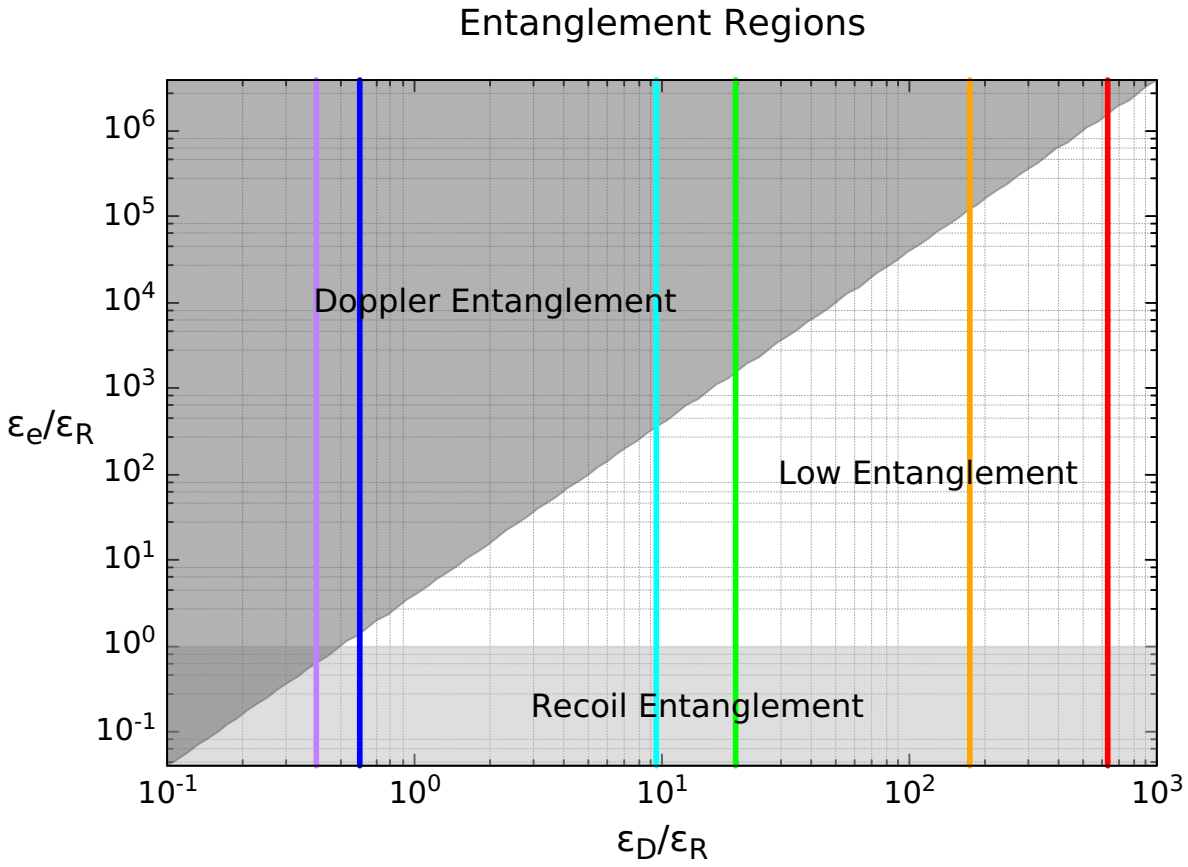

Source: The author.

4.5 PHYSICAL IMPLICATIONS OF THE HIGH ENTANGLEMENT REGIMES

In this section, we briefly discuss one of the implications of the presence of regions of high and low entanglement. Namely, we aim to discuss about the discrimination of two paradigmatic states that arise in our discussion: states with final atomic and photonic momenta parallel to each other ($q_{||} > 0$) and states where the final atomic momentum and photonic momentum are anti-parallel to each other ($q_{||} < 0$).

Physically, these two states seem very different from each other and naively we may assume that a measurement on the atom and photon at the same time should yield precisely with which quantum state we are dealing. Quantum mechanics fails to be that simple and atomic/photonic momentum uncertainties cause the outcomes of measurements to not carry enough information to discriminate these two states.

Though we do not implement or discuss any particular quantum discrimination protocol, we shall understand the indistinguishability between these two states as the overlap between their wave-functions $C(\vec{q},\vec{k})$. In fact, what we observe in Fig. 17 is that the two considered quantum states present less overlap in their wave-functions for values of ε_e corresponding to regions of high entanglement, while for regions of low entanglement, these two quantum states become less distinguishable.

Namely, in Fig. 17 we investigate measurements performed upon the photonic or atomic subsystems: in panels a and b we observe the probability of measuring some frequency for the photon given that the atom is in a certain momentum state (we assume here $q_{||} \approx \Delta p$), while in panels c and d we compute the probability of finding the atom in some momentum state given that we measure a given frequency for the photon (which we assume to be ω_0).

For the $\mathrm{Cs}-\mathrm{D}_2$ line (panels a and c of Fig. 17) we can see that before the Doppler regime of entanglement, measuring the photon's frequency (panel a), the blueshifted ($q_{||} > 0$) and redshifted ($q_{||} < 0$) wave-functions overlap completely, whereas when we get to the Doppler regime of entanglement these two wave-functions split from each other and we can see that, for example, a measurement of a blueshift in the central frequency of the emitted photon yields that we are dealing with a $q_{||} > 0$ state. From panel c, we observe that a measurement on the atomic subsystem does not provide any distinguishability of the given quantum states (note the complete overlap) until we arrive at the Recoil entanglement regime, where the wave-functions split from each other. In the intermediate region, that is, in the low entanglement region, no matter which subsystem you look at, no distinction between the states is observed.

The situation is even more appalling when we consider the Strontium narrow line (panels b and d of Fig. 17): in the considered region of ε_e we can always perform a measurement upon one of the subsystems to obtain information about in which quantum state the other subsystem is. This is a symptom of what we already observed: the atom and photon involved in the Strontium narrow line decay are highly entangled in the whole considered region of ε_e.

Finally, we conclude that the presence of entanglement in the system enhances our chances at discriminating physically distinct quantum states that arise in the process of spontaneous emission. Note that we are not breaking any fundamental rules of quantum mechanics: the complete distinction between two quantum states is only achieved for orthogonal states (null overlapping of wave-functions). Entanglement then is only a consequence of the generation of more and more orthogonal states, which is directly related to the increase in the Schmidt rank.

Figure 17 – Heat map of the probability density function, $|C(\vec{q},\vec{k})|^2$, as a function of $\varepsilon_e/\varepsilon_R$ for different atomic spectral lines: $\mathrm{Cs}-\mathrm{D}_2$ line in panels a) and c) and Strontium narrow line in panels b) and d). a) Heat map of $|C(\vec{q},\vec{k})|^2$ with a fixed value of $q=\Delta p$ for $q\cos\gamma_1 = q > 0$ (in blue) and $q\cos\gamma_1 = -q < 0$ (in red) for the $\mathrm{Cs}-\mathrm{D}_2$ line, b) heat map of $|C(\vec{q},\vec{k})|^2$ with a fixed value of $q=\Delta p$ for $q\cos\gamma_1 = q > 0$ (in blue) and $q\cos\gamma_1 = -q < 0$ (in red) for the Strontium narrow line, c) heat map of $|C(\vec{q},\vec{k})|^2$ with a fixed value of $\omega_k=\omega_0$ for $q\cos\gamma_1 = q > 0$ (in blue) and $q\cos\gamma_1 = -q < 0$ (in red) for the $\mathrm{Cs}-\mathrm{D}_2$ line, d) heat map of $|C(\vec{q},\vec{k})|^2$ with a fixed value of $\omega_k=\omega_0$ for $q\cos\gamma_1 = q > 0$ (in blue) and $q\cos\gamma_1 = -q < 0$ (in red) for the Strontium narrow line

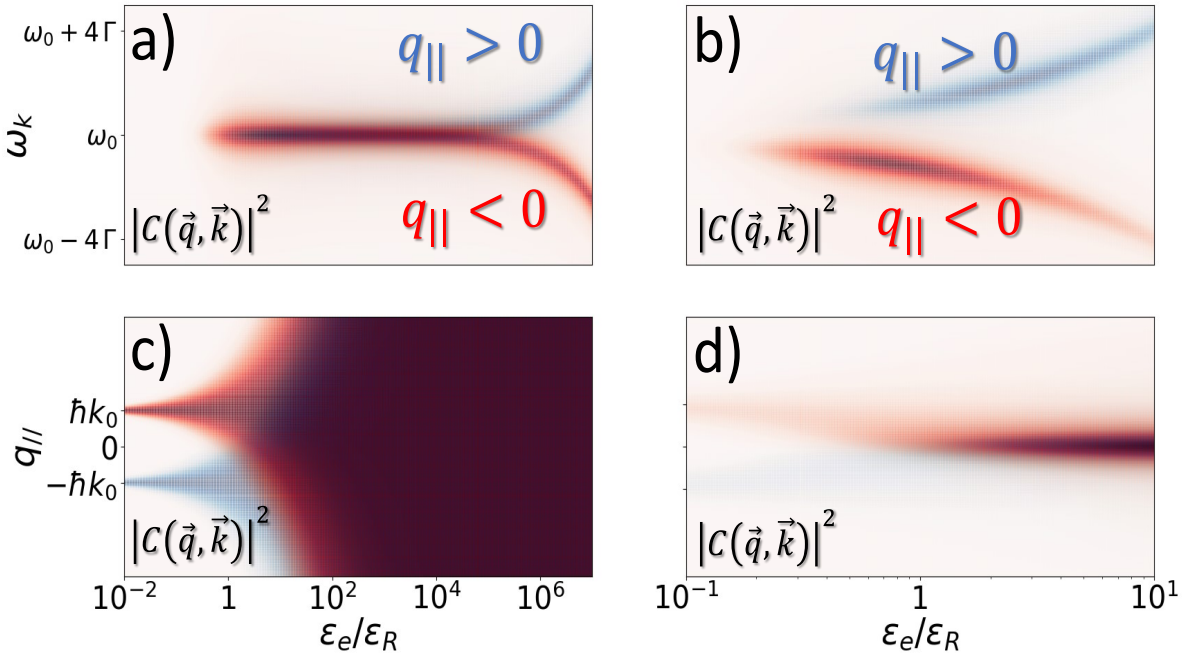

Source: The author.

5 CONCLUSION AND PERSPECTIVES

In this thesis, we developed some of the main theoretical tools required for the modelling of quantum memories based on continuous degrees of freedom. Namely, we used the density matrix (in continuous and mixed variables) formalism to model atom-photon systems in the semi-classical and fully quantum pictures, as well as we investigated the storage of information in the external degrees of freedom of an atomic ensemble and quantified the entanglement encoded in the momentum variables of an atom-photon system after the process of spontaneous decay, which presented regimes of high and low entanglement dependent on the initial atomic momentum dispersion. These techniques are fundamental in the modelling of continuous variables quantum memories and further understanding of distribution of entanglement over a quantum network.

Specifically, in chapter 3 we presented a theoretical model from first principles for a RIR based atomic memory and provided experimental results to corroborate it. Our theory puts the probe transmitted signal in equal footing to the FFWM signal. This is first directly illustrated via the calculations for the temporal evolutions and lineshapes during the reading process, which showed the same structure and amplitude for both signals. Furthermore, the theory predicted that both probe transmission and FFWM are connected to non-volatile memories, as previously observed only for the transmitted signal. This means that the stored in information can be retrieved without its simultaneous destruction. These signals were then in fact experimentally observed with good agreement with the core theoretical predictions. For the writing and reading phase, both (probe and FFWM) experimental spectra showed the same structures predicted by the model. The global comparison between theory and experiment was then carried out in more detail through the time evolution of the linewidths experimentally observed and theoretically predicted for the structures in the writing and reading phases. This comparison showed a good qualitative agreement between experimental data and theoretical predictions, even though some differences could still be noticed. The fact that the theory shows the FFWM and transmission signals as originating from the same phenomenon, at the same order of perturbation, suggests the use of this pair of signals as a source of quantum correlations.

Recently, Moreira *et. al.* reported the observation of the analogous to the non-volatile memory for the spontaneous scattering of light from an ensemble of two-level atoms at the

single photon level (MOREIRA et al., 2021). Araujo *et. al.* also reported the observation of non-classical correlations in the continuous generation of photon pairs in the backward four-wave-mixing excitation of an ensemble of two-level atoms (ARAUJO; MARINHO; FELINTO, 2022), an effect theoretically proposed in 2007 (DU et al., 2007). Thus, the present work point out to the possibility of extending these previous results to explore the correlations in the probe transmission and FFWM at the single photon level with memory.

In chapter 4, we reviewed the problem of spontaneous emission using the formalism developed by (WEISSKOPF; WIGNER, 1930) and (RZAZEWSKI; ZAKOWICZ, 1992), considering external atomic degrees of freedom, and quantified the entanglement encoded in the continuous variables of the system through a calculation of the purity of the reduced atomic state.

By doing so, we observed regimes of high entanglement usually separated by a low entanglement region, though depending on the considered spectral line this region may express itself as a plateau, a peak of purity higher than $P_a = 0.5$ (yielding a Schmidt rank lower than $K = 2$) or a peak that does not cross the $P_a = 0.5$ threshold (not characterizing a true low entanglement region).

Due to their nature, we defined the Recoil and Doppler regimes of entanglement and obtained thresholds in ε_e which need to be crossed in order to achieve these entanglement regimes. We also defined a third regime of mixed entanglement where both regimes are active and yields atom-photon systems that are always highly entangled. We observed that, physically, recoil effects play crucial role in the Recoil entanglement regime, while homogeneous Doppler shifts play a crucial role in the Doppler regime of entanglement, that is, these effects are responsible for the creation of quantum correlations in the atom-photon system. We also presented physical considerations that could describe the increase of the Schmidt rank supported by estimates that agree qualitatively with the calculated Schmidt ranks.

Finally, we investigated the role of entanglement in the discrimination of two physically distinct quantum states and observed that the presence of entanglement in the system allows us to better distinguish between different quantum states that arise naturally in the process of spontaneous decay. This result can be useful for quantum discrimination protocols as well as for quantum imaging.

Further generalizations of our model and method of quantification of entanglement are in order. Namely, extending the investigation to an atomic ensemble in thermal equilibrium with a reservoir at temperature T spontaneously emitting a single photon (and therefore creating a Dicke state) should provide a theoretical model that is easier to implement experimentally.

Note that this extension allows a further generalization regarding the spontaneous emission of n photons, generating in principle multipartite entanglement, which would lead to the necessity of a more robust entanglement quantification. Though more complex, the problem of m atoms spontaneously emitting n photons is also of importance in the construction of quantum protocols.

REFERENCES

AGARWAL, G. S. *Phys. Rev. A*, v. 4, p. 1778–1781, 1971.

ALMEIDA, A. J. F. de; MAYNARD, M.-A.; BANERJEE, C.; FELINTO, D.; TABOSA, F. G. J. W. R. *Phys. Rev. A*, v. 94, p. 063834, 2016.

ARAUJO, M. O.; MARINHO, L. S.; FELINTO, D. *Phys. Rev. Lett.*, v. 128, p. 083601, 2022.

BENNETT, C. H.; BRASSARD, G. In: *International conference on computers, systems and signal processing*. [S.l.: s.n.], 1984. p. 175–179.

BJERRUM, A. J. E.; BRASK, J. B.; NEERGAARD-NIELSEN, J. S.; ANDERSEN, U. L. *Phys. Rev. A*, v. 107, p. 042606, 2023.

BLINOV, B. B.; MOEHRING, D. L.; DUAN, L.-M.; MONROE, C. *Nature*, v. 428, p. 153–157, 2004.

BOCK, M.; EICH, P.; KUCERA, S.; KREIS, M.; LENHARD, A.; BECHER, C.; ESCHNER, J. *Nature Communications*, v. 9, p. 1998, 2018.

BONIFACIO, R.; DESALVO, L. *Nucl. Instrum. Methods Phys. Res.*, A341, p. 360, 1994.

BONIFACIO, R.; PREPARATA, G. *Phys. Rev. A*, v. 2, p. 336–347, 1970.

BROWN, K. R.; KIM, J.; MONROE, C. *npj Quantum Information*, v. 2, p. 16034, 2016.

BRZOZOWSKA, M.; BRZOZOWSKI, T. M.; ZACHOROWSKI, J.; GAWLIK, W. *Phys. Rev. A*, v. 73, p. 063414, 2006.

CAPELLA, J. C. C.; MELO, A. M. G. de; LOPEZ, J. P.; TABOSA, J. W. R.; FELINTO, D. Atomic memory based on recoil-induced resonances. *Phys. Rev. A*, v. 106, p. 013101, Jul 2022.

CARIOLARO, G. *Quantum communications*. [S.l.]: Springer, 2015.

CHAN, K. W.; LAW, C. K.; EBERLY, J. H. *Phys. Rev. Lett.*, v. 88, p. 4, 2002.

CHAN, K. W.; LAW, C. K.; EBERLY, J. H. *Phys. Rev. A*, v. 68, p. 022110, 2003.

CHEN, S.; CHEN, Y.-A.; ZHAO, B.; YUAN, Z.-S.; SCHMIEDMAYER, J.; PAN, J.-W. *Phys. Rev. Lett.*, v. 99, p. 180505, 2007.

CIRAC, J. I.; ZOLLER, P.; KIMBLE, H. J.; MABUCHI, H. *Phys. Rev. Lett.*, v. 78, p. 3221, 1997.

COURTOIS, J.-Y.; GRYNBERG, G.; LOUNIS, B.; VERKERK, P. *Phys Rev. Letters*, v. 72, p. 3017, 1994.

CROCKER, C.; LICHTMAN, M.; SOSNOVA, K.; CARTER, A.; SCARANO, S.; MONROE, C. *Opt. Express*, v. 27, p. 28143–28149, 2019.

CRUZ, L. S.; FELINTO, D.; GÓMEZ, J. G. A.; MARTINELLI, M.; VALENTE, P.; LEZAMA, A.; NUSSENZVEIG, P. *The European Physical Journal D*, v. 41, p. 531–539, 2007.

DEBNATH, S.; LINKE, N. M.; FIGGATT, C.; LANDSMAN, K. A.; WRIGHT, K.; MONROE, C. *Nature*, v. 536, p. 63–66, 2016.

DHARA, P.; LINKE, N. M.; WAKS, E.; GUHA, S.; SESHADREESAN, K. P. *Phys. Rev. A*, v. 105, p. 022623, 2022.

DIEKS, D. *Physics Letters A*, v. 92, p. 271–272, 1982.

DIRAC, P. A. M. *Proc. R. Soc. Lond. A*, v. 114, p. 243–265, 1927.

DONG, R.; LASSEN, M.; HEERSINK, J.; MARQUARDT, C.; FILIP, R.; LEUCHS, G.; ANDERSEN, U. L. *Nature Physics*, v. 4, n. 12, p. 919–923, 2008.

DU, S.; WEN, J.; RUBIN, M. H.; YIN, G. Y. *Phys. Rev. Lett.*, v. 98, p. 053601, 2007.

DUAN, L. M.; LUKIN, M. D.; CIRAC, J. I.; ZOLLER, P. *Nature (London)*, v. 414, p. 413, 2001.

EBERLY, J. H.; CHAN, K. W.; LAW, C. K. Schmidt-mode analysis of entanglement for quantum information studies. In: SHUMOVSKY, A. S.; RUPASOV, V. I. (Ed.). *Quantum Communication and Information Technologies*. [S.l.]: Springer Netherlands, 2003. p. 1–12.

EINSTEIN, A. *The collected papers of Albert Einstein: On the quantum theory of Radiation*. [S.l.]: Princeton University Press, 1917.

EKERT, A. K. Quantum cryptography based on bell's theorem. *Phys. Rev. Lett.*, v. 67, p. 661–663, 1991.

ESGUERRA, L.; MESSNER, L.; ROBERTSON, E.; EWALD, N. V.; gAN, M. Gündo; WOLTERS, J. *Phys. Rev. A*, v. 107, p. 042607, 2023.

FEDOROV, M. V.; EFREMOV, M. A.; KAZAKOV, A. E.; CHAN, K. W.; LAW, C. K.; EBERLY, J. H. *Phys. Rev. A*, v. 72, p. 032110, 2005.

FISCHER, M. C.; DUDAREV, A. M.; GUTIERREZ-MEDINA, B.; RAIZEN, M. G. *J. Opt B: Quantum Semiclass. Opt.*, v. 3, p. 279, 2001.

FURUSAWA, A.; SøRENSEN, J. L.; BRAUNSTEIN, S. L.; FUCHS, C. A.; KIMBLE, H. J.; POLZIK, E. S. *Science*, v. 282, n. 5389, p. 706–709, 1998.

GABRIELSE, G.; DEHMELT, H. *Phys. Rev. Lett.*, v. 55, p. 67–70, Jul 1985.

GHAFOOR, F.; ZHU, S.-Y.; ZUBAIRY, M. S. *Phys. Rev. A*, v. 62, p. 013811, 2000.

GHIRARDI, G. In: *Advances in Quantum Mechanics*. [S.l.]: IntechOpen, 2013.

GORDON, K.; DESAVAGE, S.; DUNCAN, D.; WELCH, G. R.; DAVIS, J. P.; NARDUCCI, F. A. *J. Mod. Opt.*, v. 57, p. 1849, 2010.

GROBE, R.; RZAZEWSKI, K.; EBERLY, J. H. *Journal of Physics B: Atomic, Molecular and Optical Physics*, v. 27, p. L503, 1994.

GROSSHANS, F.; ASSCHE, G. V.; WENGER, J.; BROURI, R.; CERF, N. J.; GRANGIER, P. *Nature*, v. 421, p. 238–241, 2003.

GUIBAL, S.; TRICHŽ, C.; VERKERK, S. G. P.; GRYNBERG, G. *Opt. Commun*, v. 131, p. 61, 1996.

GUO, J.; BERMAN, P. R. *Phys Rev. A*, v. 47, p. 4128, 1993.

GUO, J.; BERMAN, P. R.; DUBETSKY, B.; GRYNBERG, G. *Phys Rev. A*, v. 46, p. 1426, 1992.

GUO, W. *Phys. Rev. A*, v. 77, p. 062111, 2008.

HAMMERER, K.; SØRENSEN, A. S.; POLZIK, E. S. *Rev. Mod. Phys.*, v. 82, p. 1041–1093, 2010.

HE, Z.; ZHANG, Y.; TONG, X.; LI, L.; WANG, L. V. *Nature Communications*, v. 14, p. 2441, 2023.

HENSON, B. M.; THOMAS, K. F.; MEHDI, Z.; BURNETT, T. G.; ROSS, J. A.; HODGMAN, S. S.; TRUSCOTT, A. G. *Opt. Express*, v. 30, p. 13252–13262, 2022.

HOFFMAN, K.; KUNZE, R. *Linear Algebra*. [S.l.]: Pearson, 1971. 271-272 p.

HORAK, P.; GHERI, K. M. *Phys. Rev. A*, v. 53, p. R1970–R1973, 1996.

HOSSEINI, M.; SPARKES, B. M.; HÉTET, G.; LONGDELL, J. J.; LAM, P. K.; BUCHLER, B. C. *Nature*, v. 461, p. 241–245, 2009.

JENSEN, K.; WASILEWSKI, W.; KRAUTER, H.; FERNHOLZ, T.; NIELSEN, B. M.; OWARI, M.; PLENIO, M. B.; SERAFINI, A.; WOLF, M. M.; POLZIK, E. S. *Nature Physics*, v. 7, p. 13–16, 2011.

KIMBLE, H. J. *Nature*, v. 453, p. 1023–1030, 2008.

KLEPPNER, D. *Phys. Rev. Lett.*, v. 47, p. 233–236, 1981.

KOZUMA, M.; IMAI, Y.; NAKAGAWA, K.; OHTSU, M. *Phys. Rev. A*, v. 52, p. R3421, 1995.

KRUSE, D.; CUBE, C. von; ZIMMERMANN, C.; COURTEILLE, P. *Phys. Rev. Lett.*, v. 91, p. 183601, 2003.

KRUTYANSKIY, V.; MERANER, M.; SCHUPP, J.; KRCMARSKY, V.; HAINZER, H.; LANYON, B. P. *npj Quantum Information*, v. 5, p. 72, 2019.

KURTSIEFER, C.; DROSS, O.; VOIGT, D.; EKSTROM, C. R.; PFAU, T.; MLYNEK, J. *Phys. Rev. A*, v. 55, p. 4, R2539, 1997.

LAGO-RIVERA, D.; RAKONJAC, J. V.; GRANDI, S.; RIEDMATTEN, H. d. *Nature Communications*, v. 14, p. 1889, 2023.

LANDAU, L. D.; LIFSHITZ, E. M. *Quantum mechanics: non-relativistic theory*. [S.l.]: Pergamon Press, 1989.

LEENT, T. van; BOCK, M.; GARTHOFF, R.; REDEKER, K.; ZHANG, W.; BAUER, T.; ROSENFELD, W.; BECHER, C.; WEINFURTER, H. *Phys. Rev. Lett.*, v. 124, p. 010510, 2020.

LEENT, T. van et al. *Nature*, v. 607, p. 69–73, 2022.

LOPEZ, J. P.; ALMEIDA, A. J. F. de; FELINTO, D.; TABOSA, J. W. R. *Opt. Lett.*, v. 42, p. 4474, 2017.

LOPEZ, J. P.; MELO, A. M. G. de; FELINTO, D.; TABOSA, J. W. R. *Phys. Rev. A*, v. 100, p. 023839, 2019.

LOPEZ, J. P.; MELO, A. M. G. de; TABOSA, J. W. R. *Opt. Lett.*, v. 45, p. 3490, 2020.

LVOVSKY, A. I.; SANDERS, B. C.; TITTEL, W. *Nature Photonics*, v. 3, p. 706–714, 2009.

MA, L.; LEI, X.; YAN, J.; LI, R.; CHAI, T.; YAN, Z.; JIA, X.; XIE, C.; PENG, K. *Nature Communications*, v. 13, p. 2368, 2022.

MAUNZ, P.; OLMSCHENK, S.; HAYES, D.; MATSUKEVICH, D. N.; DUAN, L.-M.; MONROE, C. *Phys. Rev. Lett.*, v. 102, p. 250502, 2009.

MEACHER, D. R.; BOIRON, D.; METCALF, H.; SALOMON, C.; GRYNBERG, G. *Phys. Rev. A.*, v. 50, p. R1992, 1994.

MONROE, C.; KIM, J. *Science*, v. 339, p. 1164–1169, 2013.

MONROE, C.; RAUSSENDORF, R.; RUTHVEN, A.; BROWN, K. R.; MAUNZ, P.; DUAN, L.-M.; KIM, J. *Phys. Rev. A*, v. 89, p. 022317, 2014.

MOREAU, P.-A.; TONINELLI, E.; GREGORY, T.; PADGETT, M. J. *Nature Reviews Physics*, v. 1, p. 367–380, 2019.

MOREIRA, R. S. N.; CAVALCANTI, P. J.; MU NOZ-MARTÍNEZ, L. F.; MORALES, J. E. O.; SALDANHA, P. L.; TABOSA, J. W. R.; FELINTO, D. *Opt. Commun.*, v. 495, p. 127075, 2021.

NIELSEN, M. A.; CHUANG, I. L. *Quantum computation and quantum information*. [S.l.]: Cambridge University Press, 2000.

NUNN, J.; REIM, K.; LEE, K. C.; LORENZ, V. O.; SUSSMAN, B. J.; WALMSLEY, I. A.; JAKSCH, D. *Phys. Rev. Lett.*, v. 101, p. 260502, 2008.

OLMSCHENK, S.; MATSUKEVICH, D. N.; MAUNZ, P.; HAYES, D.; DUAN, L.-M.; MONROE, C. *Science*, v. 323, p. 486–489, 2009.

OURJOUMTSEV, A.; JEONG, H.; TUALLE-BROURI, R.; GRANGIER, P. *Nature*, v. 448, n. 7155, p. 784–786, 2007.

PARK, J. L. *Foundations of Physics*, v. 1, p. 23–33, 1970.

PASPALAKIS, E.; KNIGHT, P. L. *Phys. Rev. Lett.*, v. 81, p. 293–296, 1998.

PAULETTI, T.; GARCIA, M.; CANELLA, G. A.; FRANçA, V. V. *Linear entropy fails to predict entanglement behavior in low-density fermionic systems*. 2023.

PFAU, T.; SPALTER, S.; KURTSIEFER, C.; EKSTROM, C. R.; MLYNEK, J. *Phys. Rev. Lett.*, v. 73, p. 1223, 1994.

PIRANDOLA, S.; LAURENZA, R.; OTTAVIANI, C.; BANCHI, L. *Nature Communications*, v. 8, p. 15043, 2017.

PLENIO, M. B.; VIRMANI, S. *Quantum Info. Comput.*, v. 7, p. 1–51, 2007.

POPESCU, S.; ROHRLICH, D. *Phys. Rev. A*, v. 56, p. R3319–R3321, 1997.

ROSENFELD, W.; HOCKE, F.; HENKEL, F.; KRUG, M.; VOLZ, J.; WEBER, M.; WEINFURTER, H. *Phys. Rev. Lett.*, v. 101, p. 260403, 2008.

ROSSMANN, W. *Lie Groups: An Introduction through Linear Groups*. [S.l.]: Oxford University Press, 2006.

RZAZEWSKI, K.; ZAKOWICZ, W. *J. Phys. B*, v. 25, p. L319, 1992.

SANTRA, S.; MURALIDHARAN, S.; LICHTMAN, M.; JIANG, L.; MONROE, C.; MALINOVSKY, V. S. *New J. Phys.*, v. 21, p. 073002, 2019.

SCHMIDT, E. *Mathematische Annalen*, v. 63, p. 433, 1906.

SHEN, S.; YUAN, C.; ZHANG, Z.; YU, H.; ZHANG, R.; YANG, C.; LI, H.; WANG, Z.; WANG, Y.; DENG, G.; SONG, H.; YOU, L.; FAN, Y.; GUO, G.; ZHOU, Q. *Nature*, v. 12, p. 115, 2023.

SHERSON, J. F.; KRAUTER, H.; OLSSON, R. K.; JULSGAARD, B.; HAMMERER, K.; CIRAC, I.; POLZIK, E. S. *Nature*, v. 443, p. 557–560, 2006.

SHI, Y.-Q.; CONG, L.; ECKLE, H.-P. *Phys. Rev. A*, v. 105, p. 062450, 2022.

SHOR, P. In: *Proceedings 35th Annual Symposium on Foundations of Computer Science*. [S.l.: s.n.], 1994. p. 124–134.

STECK, D. A. Cesium d line data. 2003.

STEPHENSON, L. J.; NADLINGER, D. P.; NICHOL, B. C.; AN, S.; DRMOTA, P.; BALLANCE, T. G.; THIRUMALAI, K.; GOODWIN, J. F.; LUCAS, D. M.; BALLANCE, C. J. *Phys Rev. Lett.*, v. 124, p. 110501, 2020.

STOOP, H.; żEWSKI, K. Rza̧. *Phys. Rev. A*, v. 52, p. 1494–1499, 1995.

STORZ, S.; SCHÄR, J.; KULIKOV, A.; MAGNARD, P.; KURPIERS, P.; LÜTOLF, J.; WALTER, T.; COPETUDO, A.; REUER, K.; AKIN, A.; BESSE, J.-C.; GABUREAC, M.; NORRIS, G. J.; ROSARIO, A.; MARTIN, F.; MARTINEZ, J.; AMAYA, W.; MITCHELL, M. W.; ABELLAN, C.; BANCAL, J.-D.; SANGOUARD, N.; ROYER, B.; BLAIS, A.; WALLRAFF, A. *Nature*, v. 617, p. 265–270, 2023.

TAKAHASHI, H.; NEERGAARD-NIELSEN, J. S.; TAKEUCHI, M.; TAKEOKA, M.; HAYASAKA, K.; FURUSAWA, A.; SASAKI, M. *Nature Photonics*, v. 4, n. 3, p. 178–181, 2010.

TAKEOKA, M.; GUHA, S.; WILDE, M. M. *Nature Communications*, v. 5, p. 5235, 2014.

TOMASZ, N.; BRZOZOWSKI P., M. B.; ZACHOROWSKI, J.; GAWLIK, W. *Act Phys. Hung*, B26, p. 95–119, 2006.

VENGALATTORE, M.; PRENTISS, M. *Phys. Rev. A*, v. 52, p. R3421, 2005.

VOLZ, J.; WEBER, M.; SCHLENK, D.; ROSENFELD, W.; VRANA, J.; SAUCKE, K.; KURTSIEFER, C.; WEINFURTER, H. *Phys. Rev. Lett.*, v. 96, p. 030404, 2006.

WANG, P.; LUAN, C.-Y.; QIAO, M.; UM, M.; ZHANG, J.; WANG, Y.; YUAN, X.; GU, M.; ZHANG, J.; KIM, K. *Nature Communications*, v. 12, p. 233, 2021.

WANG, S.-Z.; WANG, M.-J.; WEN, Y.-F.; XU, Z.-X.; MA, T.-F.; LI, S.-J.; WANG, H. *Communications Physics*, v. 4, p. 168, 2021.

WANG, W.; DENG, J.; WANG, Y. *J. Opt Soc. Am. B*, v. 32, p. 2441, 2015.

WEISSKOPF, V.; WIGNER, E. *Zeitschrift für Physik*, v. 63, p. 54–73, 1930.

WERNER, R. F. *Phys. Rev. A*, v. 40, p. 4277–4281, 1989.

WOOTERS, W. K. *Quantum Info. Comput.*, v. 1, p. 27–44, 2001.

WOOTTERS, W. K.; ZUREK, W. H. A single quantum cannot be cloned. *Nature*, v. 299, p. 802–803, 1982.

YAN-TING, Z.; DIAN-QIANG, S.; ZHONG-HUA, J.; HONG-SHAN, Z.; LIAN-TUAN, X.; SUO-TANG, C. J. *Phys. B*, v. 24, p. 093701, 2015.

ZAPATERO, V.; LEENT, T. van; ARNON-FRIEDMAN, R.; LIU, W.-Z.; ZHANG, Q.; WEINFURTER, H.; CURTY, M. *Nature*, v. 9, p. 10, 2023.

APPENDIX A - TREATMENT OF THE EXPONENTIAL TERM IN EQ. 4.67

In this appendix, we aim to make the approximation in (4.67) clearer. Throughout this section we will use the fact that $q \simeq \Delta p$, that is, q is a number of the order of Δp, or more explicitly, $\frac{q}{\Delta p} \simeq 1$. We need to elucidate each term of:

$$-\frac{q^2}{2\Delta p^2}-\frac{q\hbar\left(\frac{\omega_0}{c}\right)\cos\gamma_1}{\Delta p^2}-\frac{q^2\hbar\left(\frac{\omega_0}{c}\right)\cos^2\gamma_1}{mc\Delta p^2}-\frac{\hbar^2\left(\frac{\omega_0}{c}\right)^2}{2\Delta p^2}-\frac{\hbar^2\left(\frac{\omega_0}{c}\right)^2 q^2\cos^2\gamma_1}{2(mc)^2\Delta p^2}-\frac{\hbar^2\left(\frac{\omega_0}{c}\right)^2 q\cos\gamma_1}{mc\Delta p^2} \tag{A.1}$$

The first term. This is the easiest term: in fact, $-\frac{\mathrm{q}^2}{2\Delta \mathrm{p}^2}$ is a term of order 1 and it is what survives in the whole sum, therefore it is whom we compare to.

The second term. We approximate: $-\frac{q\hbar\left(\frac{\omega_0}{c}\right)\cos\gamma_1}{\Delta p^2} \approx -\frac{\hbar\left(\frac{\omega_0}{c}\right)}{\Delta p}\cos\gamma_1$, and in the large Δp limit this term is negligible when compared to 1. Note that $\cos\gamma_1$ is a limited function between -1 and 1.

The third term. We approximate: $\frac{q^2\hbar\left(\frac{\omega_0}{c}\right)\cos^2\gamma_1}{mc\Delta p^2} \approx \frac{\hbar\left(\frac{\omega_0}{c}\right)}{mc}\cos^2\gamma_1$ and since $\hbar\left(\frac{\omega_0}{c}\right) \approx 10^{-28}\,\mathrm{kg}\cdot\frac{\mathrm{m}}{\mathrm{s}} \ll mc \approx 10^{-17}\,\mathrm{kg}\cdot\frac{\mathrm{m}}{\mathrm{s}}$, for the $\mathrm{Cs}-\mathrm{D}_2$ line (which we use as a guide), this term is again negligible when compared to 1.

The fourth term. The term: $-\frac{\hbar^2\left(\frac{\omega_0}{c}\right)^2}{2\Delta p^2}$ is negligible in the large Δp limit when compared to 1.

The fifth term. We approximate: $-\frac{\hbar^2\left(\frac{\omega_0}{c}\right)^2 q^2\cos^2\gamma_1}{2(mc)^2\Delta p^2} \approx \frac{1}{2}\left[\frac{h\left(\frac{\omega_0}{c}\right)}{mc}\right]^2\cos^2\gamma_1$ and since $\hbar\left(\frac{\omega_0}{c}\right) \approx 10^{-28}\,\mathrm{kg}\cdot\frac{\mathrm{m}}{\mathrm{s}} \ll mc \approx 10^{-17}\,\mathrm{kg}\cdot\frac{\mathrm{m}}{\mathrm{s}}$, for the $\mathrm{Cs}-\mathrm{D}_2$ line, this term is again negligible when compared to 1.

The sixth term. We note: $-\frac{\hbar^2\left(\frac{\omega_0}{c}\right)^2 q\cos\gamma_1}{mc\Delta p^2} = -\left[\frac{\hbar\left(\frac{\omega_0}{c}\right)}{\Delta p}\right]^2\cdot\frac{q\cos\gamma_1}{mc} \ll 1$ since we are in the large Δp limit, and $q\cos\gamma_1 \ll mc$, which is the non-relativistic approximation we have been taking in consideration this whole time.